Computational Design of Auxetic Shells

Mina Konaković Luković

Thèse n. 9662 2019
présenté le 19 Juin 2019
à la Faculté Informatique et Communications
laboratoire d'Informatique Graphique et Géométrique
programme doctoral en Informatique et Communications
École Polytechnique Fédérale de Lausanne

pour l'obtention du grade de Docteur ès Sciences
par

Mina Konaković Luković

acceptée sur proposition du jury:

Prof. Pierre Dillenbourg, président du jury
Prof. Mark Pauly, directeur de thèse
Prof. Wenzel Jakob, rapporteur
Prof. Keenan Crane, rapporteur
Prof. Niloy Mitra, rapporteur

Lausanne, EPFL, 2019

To my family...

Acknowledgements

I would like to express my deepest gratitude to my Ph.D. advisor Mark Pauly. Thanks for introducing me to the incredible field of digital fabrication, for teaching me how to conduct high-quality research, for challenging me to move boundaries, and sending me around the world to meet new people and develop new skills. Thanks for being supportive of my ambitions and ideas, and encouraging me to pursue an academic career.

I am grateful to Keenan Crane for hosting me at CMU for two summers, for long discussions on (discrete) differential geometry and optimization, and for teaching me various technical, as well as the non-technical skills. Thanks for insisting on good taste and being an endless source of inspiration.

I am thankful to Sofien Boaziz and Bailin Deng for guiding me through my first year when I knew nothing about computer graphics, tools and research topics I was working on.

My research and my achievements were significantly influenced by my collaborators — Keenan Crane, Sofien Bouaziz, Bailin Deng, Julian Panetta, Christopher Robeller, Mira Dedijer, Yves Weinand, Daniel Piker, Florin Isvoranu, Etienne Bouleau. I am grateful for their passion, inspiration, hard work, and innovative ideas.

I would like to thank Danny Kaufman for being an extraordinary mentor during my internship in Adobe Research. Thanks to Vova Kim and Amanda Ghassai for insightful discussions, and other Adobe Research scientists, interns, and stuff for a wonderful summer in Seattle.

I would like to thank the rest of my thesis committee, Pierre Dillenbourg, Wenzel Jakob, and Niloy Mitra, for all their help.

During my Ph.D. studies, I had a chance to meet and share my workplace with numerous exceptional people. I thank all the LGG members for sharing the incredible moments: Sofien Bouaziz, Christopher Brandt, Tim Chen, Minh Dang, Anders Holden Deleuran, Bailin Deng, Mario Deuss, Alexandru-Eugen Ichim, Florin Isvoranu, Stefan Lienhard, Liane Makatura, Julian Panetta, Peng Song, Yuliy Schwartzburg, Andrea Tagliasacchi, Romain Testuz, Andrea Tkach, Ziqi Wang. Thanks to Sabine Süsstrunk and IVRL members, Sami Arpa, Nikos Arvanitopoulos, Bin Jin, Zahra Sadeghipoor, Marjan Shahpaski, for the great first semester of my Ph.D. I am thankful to Geometry Collective people, especially Etienne Corman, Nick Sharp, Wode Ni, and Rohan Sawhney, for two unforgettable summers at CMU. I am grateful to Madeleine Robert for all the help, long, cheerful talks, and making the administrative problems seem impossibly

simple. Thanks to incredible researchers and stuff from the NCCR Digital fabrication. The main part of my Ph.D. research was funded by the Swiss National Science Foundation, NCCR Digital Fabrication Agreement #51NF40-141853.

A number of friends have made my time at EPFL easier and more enjoyable, huge thanks to them: Tihomir Gvero, Alba Lopez, Helena Peić Tukuljac, Dražen Nadoveza, Predrag Spasojević, Gaspard Zoss, Merlin Nimier-David, Bin Jin. Special thanks to my best friend Mina Spasić for bringing the vital dose of fun and happiness all over the world.

I am eternally grateful to my amazing family for their unconditional love and support. Thanks to my parents for encouraging me to do whatever I like and helping me with all my crazy ideas. Most of all, I am grateful to my life partner Aleksa and my brother Pavle for their physical and mental support throughout the long days and nights in the office, the incredible journey of obtaining our three diplomas in Switzerland, and sharing all the intense, stressful, but also fun, enjoyable, and memorable moments in the past few years.

Lausanne, 14 May 2019 M. K.L.

Abstract

Recent advances in material science and digital fabrication provide promising opportunities for product design, mechanical and biomedical engineering, robotics, architecture, art, and science. Engineered materials and personalized fabrication are revolutionizing manufacturing culture and having a significant impact on various scientific and industrial works. As new fabrication technologies emerge, effective computational tools are needed to fully exploit the potential of digital fabrication.

This thesis introduces a novel computational method for design and fabrication with *auxetic* materials. The term auxetic refers to solid materials with negative Poisson ratio — when the material is stretched in one direction, it also expands in all other directions. In particular, we study 2D auxetic materials in the form of a triangular linkage which exhibits auxetic behavior at the macro scale. This stretching, in turn, allows the flat material to approximate doubly-curved surfaces, making it attractive for fabrication. We physically realize auxetic materials by introducing a specific pattern of cuts into approximately inextensible material such as sheet metal, plastic, or leather. On a larger scale, we use individual rigid triangular elements and connect them with joints.

First, this thesis focuses on a regular triangular linkage. When deformed into a curved shape, the linkage yields spatially-varying hexagonal openings. However, the global coupling of the linkage elements makes manual, incremental approach unlikely to succeed when trying to approximate a given curved surface. Thus, we leverage conformal geometry to enable complex surface design. In particular, we compute a global conformal map with bounded scale factor to initialize an otherwise intractable non-linear optimization. Constraint-based optimization is used to find the final linkage configuration that closely approximates a target 3D surface.

Furthermore, we develop a computational method for designing novel deployable structures via *programmable* auxetics, i.e., spatially varying triangular linkage optimized to directly and uniquely encode the target 3D surface in the 2D pattern. The target surface is rapidly deployed from a flat initial state via inflation or gravitational loading.

The thesis presents both inverse and forward design tools for interactive surface design with programmable auxetics. This allows the user to efficiently approximate a given shape and directly edit and adapt the auxetic linkage structure to explore the design alternatives. In addition, our solution enables simulation-based form-finding that uses deployment forces for interactive exploration of feasible shapes. The resulting designs can be easily manufactured via digital fabrication technologies such as laser cutting, CNC milling, or 3D printing.

Abstract

Auxetic materials and deployable structures enable scientific, industrial, and consumer applications across a wide variety of scales and usages. We validate our computational methods through a series of physical prototypes and application case studies, ranging from surgical implants, through art pieces, to large-scale architectural structures.

Keywords: digital fabrication, computational design, auxetic materials, smart materials, deployable shells, global optimization, differential geometry, conformal geometry

Zusammenfassung

Jüngste Fortschritte in der Materialwissenschaft und der digitalen Fertigung bieten vielversprechende Möglichkeiten für Produktdesign, Maschinenbau, biomedizinische Verfahrenstechnik, Robotik, Architektur, Kunst und Wissenschaft. Technisierte Materialien und personalisierte Fertigung revolutionieren die Produktionskultur und haben einen erheblichen Einfluss auf verschiedene wissenschaftliche und industrielle Arbeiten. Begleitend zu der Entstehung neuer Fertigungstechnologien sind effektive Berechnungswerkzeuge erforderlich, um das Potenzial der digitalen Fertigung voll auszuschöpfen.

Diese Arbeit stellt eine neuartige Berechnungsmethode für Design und Fertigung mit *auxetischen* Materialien vor. Der Begriff "auxetisch" bezieht sich auf feste Materialien mit negativer Poissonzahl - wird das Material in eine Richtung gedehnt, dehnt es sich auch in alle anderen Richtungen aus. Insbesondere untersuchen wir 2D auxetische Materialien in Form von Dreiecksverbindungen, die ein auxetisches Verhalten auf der Makroskala zeigen. Diese Ausdehnung wiederum ermöglicht es dem flachen Material, sich nicht abwickelbaren Oberflächen anzunähern, was es für die Fertigung attraktiv macht. Wir realisieren auxetische Materialien, indem wir ein bestimmtes Schnittmuster auf fast starre Materialien wie Blech, Kunststoff oder Leder anwenden. Für größere Fertigungen verwenden wir einzelne starre Dreieckselemente, verbunden durch Bindeglieder.

Zunächst konzentriert sich diese Arbeit auf regelmäßige Dreiecksverbindungen. Unter Deformation in eine gekrümmte Form entstehen räumlich variierende hexagonale Öffnungen in der Verbindung. Die globale Kopplung der Verbindungselemente macht die erfolgreiche Approximation einer bestimmten gekrümmten Oberfläche durch einen manuellen, inkrementellen Ansatz unwahrscheinlich. Daher nutzen wir konforme Geometrie, um eine komplexe Oberflächengestaltung zu ermöglichen. Wir berechnen eine global konforme Abbildung mit begrenztem konformem Faktor, um eine ansonsten renitente nichtlineare Optimierung zu initialisieren. Optimierung unter Nebenbedingungen wird verwendet, um eine Verbindungskonfiguration zu finden, die einer 3D-Zielfläche nahe kommt.

Darüber hinaus entwickeln wir ein Berechnungsverfahren zur Gestaltung neuartiger entfaltbarer Strukturen mittels *programmierbarer* Auxetik, d.h. einer räumlich variierenden Dreiecksverbindung, die optimiert ist, die 3D Zielfläche direkt und eindeutig im 2D Muster zu kodieren. Die Zielfläche kann aus einem flachen Ausgangszustand durch Aufblasen oder der Einwirkung von Schwerkraft rasch entfaltet werden.

Diese Arbeit präsentiert sowohl inverse als auch direkte Design Werkzeuge für interaktives Oberflächendesign mit programmierbarer Auxetik. Dies ermöglicht es dem Benutzer, eine

bestimmte Form effizient zu approximieren und die auxetische Verbindungsstruktur direkt zu bearbeiten und anzupassen, um Alternativen für das Design zu untersuchen. Darüber hinaus ermöglicht unsere Lösung eine simulationsbasierte Formfindung, bei der Entfaltungskräfte zur interaktiven Sichtung realisierbarer Formen eingesetzt werden. Die daraus resultierenden Entwürfe können problemlos über digitale Fertigungstechnologien wie Laserschneiden, CNC Fräsen oder 3D-Druckern hergestellt werden.
Auxetische Materialien und entfaltbare Strukturen ermöglichen wissenschaftliche, industrielle und verbraucherorientierte Anwendungen in unterschiedlichster Größenordnung und Nutzungsabsicht. Wir validieren unsere Berechnungsmethoden durch eine Reihe von gefertigten Prototypen und Anwendungsbeispielen, die von chirurgischen Implantaten über Kunstwerke bis hin zu großformatigen architektonischen Konstruktionen reichen.

Stichwörter: digitale Fertigung, generative Gestaltung, auxetische Materialien, intelligente Werkstoffe, entfaltbare Strukturen, globale Optimierung, Differentialgeoemtrie, konforme Geometrie

Contents

List of Figures

1 Introduction

The emerging field of digital fabrication delivers versatile application opportunities in architecture, art, material science, medicine, robotics, and computer science [Gibson et al. 2015; Caneparo 2016]. With the development of new fabrication technologies, such as efficient and accurate 3D printers and laser cutters, the demand for personalized fabrication is rapidly growing. In recent years, 3D printing is increasingly used to create new materials with custom properties and performance by controlling their microstructure [Tang and Zhao 2016; Ngo et al. 2018]. On the software side, however, this technology is still in the early development phase and effective computational tools are needed that link creative design exploration to material realization.

It is a common case in architecture and design that the initially designed surface is not physically realizable. Therefore, it is necessary to approximate a desired design surface with a closest surface that is suitable for fabrication. However, this is often a very difficult task. After architects design a model, in order to proceed with manufacturing, engineers need to find a compromise between striking designs and physical constrains. Rationalization is often harder than the 3D modeling of a surface and makes realisation of complex freeform structures very expensive. This gap between the design freedom and the production was the main reason for mathematicians and computer scientists to initiate the interdisciplinary field of Architectural Geometry [Pottmann et al. 2015].

A design process for fabrication typically requires balancing multiple objectives that are often in conflict. Finding the right trade-off between appearance, functionality, stability, durability, price, etc. is challenging. In some cases, no single solution exists that satisfies all objectives at the same time. That is where the use of advanced computational methods becomes essential.

Computational tools not only facilitate design exploration and make the production pipeline from modeling to manufacturing more time- and cost-efficient, but also help discover and enable designs not possible before. By incorporating optimization algorithms within computational design tools, it is possible to design within the space of feasible shapes and instantly explore manufacturable design alternatives. One direction of research in Architectural Ge-

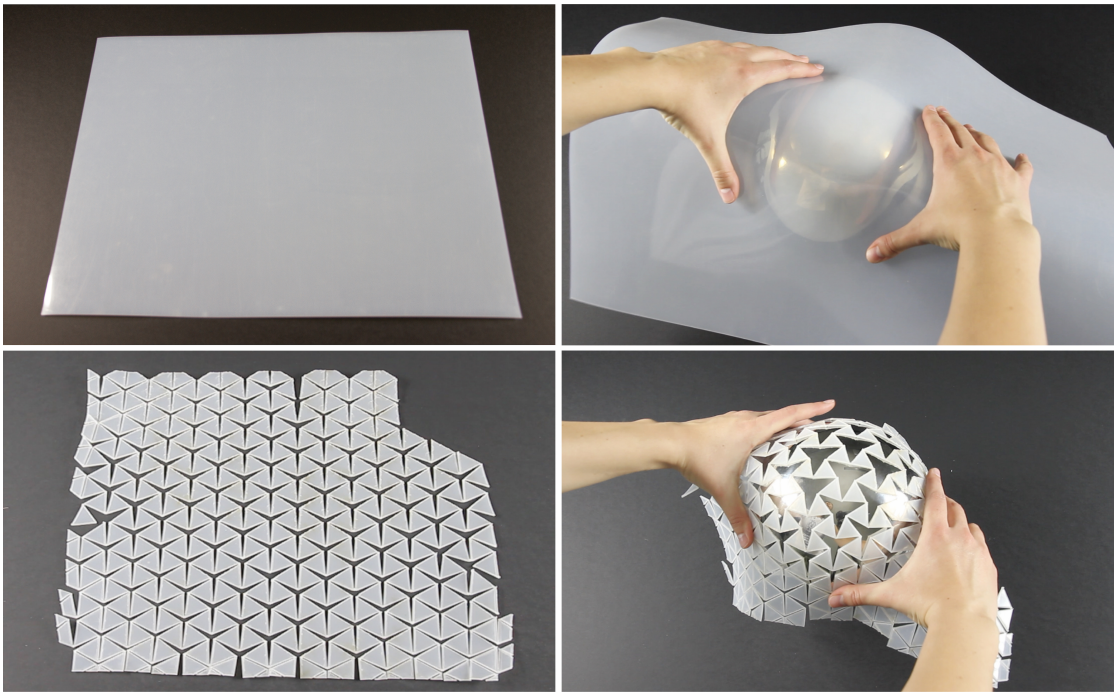

Figure 1.1 – The thin flat plastic sheet shown at top left is an example of a developable material that can bend, but not stretch or shear. Hence, it can only bend along one direction at each point and form a cylindrical or conical shape. It cannot wrap around a simple doubly-curved surface such as a sphere (top right). However, inserting a regular pattern of cuts into the same material turns this inextensible developable plastic into an auxetic material (bottom left) that can locally expand. This enables the material to wrap around a sphere (bottom right) and approximate free-form shapes.

ometry is based on developing interactive tools for problem-specific form-finding design. However, to this date, there is still no general framework to address many open problems in fabrication.

A series of computational methods focus on working with *developable* surfaces and *developable* materials [Pottmann et al. 2015; Liu et al. 2006; Kilian et al. 2008; Tang et al. 2016; Stein et al. 2018]. A surface is called developable if it can be flattened into a plane without stretching or shearing. More formally, it is a planar or single-curved surface, with zero Gaussian curvature at each point. Developable surfaces can be approximated by flat materials that can bend freely, but not stretch, such as metal sheets, paper, or thin plastic. They can also be panelled with single-curved glass or wood elements. Developable surfaces are popular in the architecture, shipbuilding, car and aerospace industries due to their cost-effectiveness in manufacturing 3D objects from flat parts.

While there is a rich set of striking developable designs, they are still limited to zero Gaussian curvature shapes. Even a simple doubly-curved surfaces such as a sphere cannot be closely

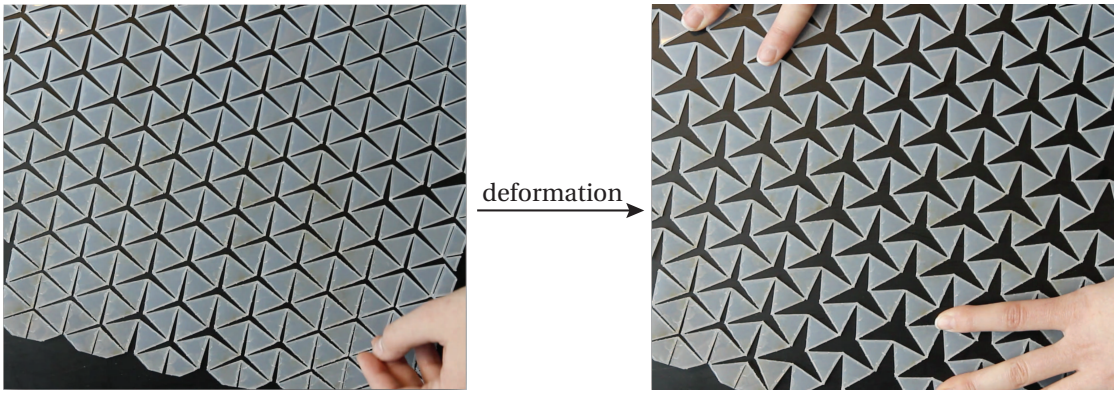

Figure 1.2 – When stretched, auxetic material expands approximately isotropically by rotating the triangle elements relative to their neighbors. The material increases its area in all directions, exhibiting a behavior typical for materials with negative Poisson ratio.

approximated by a single sheet of developable material without making additional cuts (Figure 1.1).

On the other hand, introducing a regular pattern of slits into inextensible, but flexible sheet material makes a developable sheet behave like an *auxetic* material that can locally expand in an approximately uniform way. This modified deformation behavior allows the material to assume doubly-curved shapes (such as a sphere) using only flat pieces (Figure 1.1), making it attractive for fabrication.

Auxetic Materials

Auxetic materials are solid materials with negative Poisson ratio [E. Evans and Alderson 2000]. In practice, this means that when the material is stretched in one direction, it also expands in all other directions. This behavior is a result of the material's internal structure and its deformation under loading. These structures can be both 2- and 3-dimensional, and be on a microscopic and macroscopic level. Some examples of auxetic materials include Gore-tex, auxetic polyurethane foam, tendons, cork, certain types of fabrics and paper, etc. They can also be engineered with controled properties for specific usage in the form of origami-inspired patterns and metamaterials. A recent survey on auxetics can be find in [Saxena et al. 2016]. These materials have a wide range of application fields. They have been used in electronically actuated materials, footwear, fashion, art pieces, automotive industry, medical devices, and architecture (some examples are shown in Figure 2.1). However, these applications have typically been limited to very simple geometries (e.g., planar or spherical) due to the lack of sophisticated design tools.

We develop a computational method for interactive 3D design and rationalization of complex freeform shapes via auxetic materials. We first focus on auxetic materials based on a kinematic linkage composed of equilateral triangles arranged in a regular lattice. The regular triangular

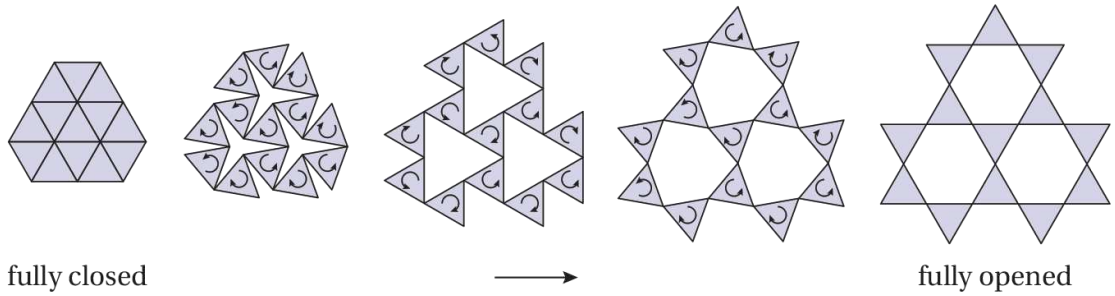

Figure 1.3 – Our auxetic linkage is defined as a tri-hexagonal pattern. A uniform linkage can transition in the plane between a fully closed state (left) and a fully opened state (right) by rotating triangles around their connecting vertices. This expansion increases total area by a factor of four, which corresponds to a scaling of length by a factor two.

linkage yields hexagonal openings of spatially-varying shape and size when deformed (see Figure 1.2). The triangular elements can rotate relative to their neighbors, allowing the material to uniformly stretch up to a certain point (see Figure 1.3). When the linkage is maximally stretched, the triangles and hexagons form a trihexagonal pattern, also know as the *Kagome lattice* (see Figure 1.4). In this configuration, the surface area of the material including the openings is four times larger than in the fully closed configuration.

An incremental process of exploring designs by moving linkage elements one by one is inefficient and unpredictable. Linkage elements are globally coupled — moving elements on one side of the material can affect the triangles on the other part of the material. Moreover, it is nearly impossible to manually foresee how to cut and align the material to achieve global pattern continuity across the seams. Simply wrapping a piece of material around a target object is unlikely to produce an acceptable result (see Figure 3.2 for example). Hence, we use

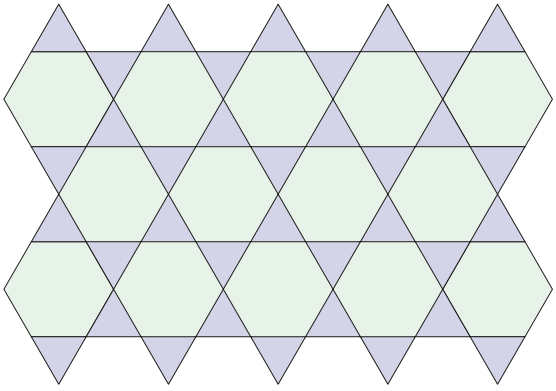

Figure 1.4 – The Kagome lattice is one of eleven uniform tilings of the Euclidean plane consisting of only regular polygons. The name "Kagome" originally comes from a traditional Japanese woven bamboo patterns. The term Kagome lattice first appeared in physics and it is also used to refer to the crystal structures of certain minerals.

constraint-based optimization to assist in the design process. Several requirements need to be satisfied at the same time, such as preserving the rigidity of the linkage elements, avoiding self-collisions and keeping the linkage close to the target surface. This leads to a non-linear optimization system that needs a careful initialization. If the initial guess is too far from the solution, the solver might get stuck in an undesirable local minimum. Initialization is often the most challenging part of the computational rationalization algorithms [Pottmann et al. 2015]. A key insight of our approach is that we can leverage theory and algorithms from conformal geometry to facilitate the auxetic design process.

Conformal Geometry

When the triangular linkage is deformed, it forms approximately isotropic openings whose shape smoothly varies across the surface (Figure 1.2). It indicates that locally the surface scales nearly uniformly without significant shearing. This provides a direct link to conformal geometry.

Conformal mapping is a transformation that allows local rotation and uniform scaling, but not shearing. In other words, a conformal mapping $f : M_0 \rightarrow M$ between two surfaces preserves angles between any two vectors, but not their lengths. The figure below shows one example of a conformal map f, where a disk from $\mathbb{R}^2$ is mapped to a surface in $\mathbb{R}^3$. Note that the squares locally preserve 90 degree angles and only the edge lengths uniformly scale.

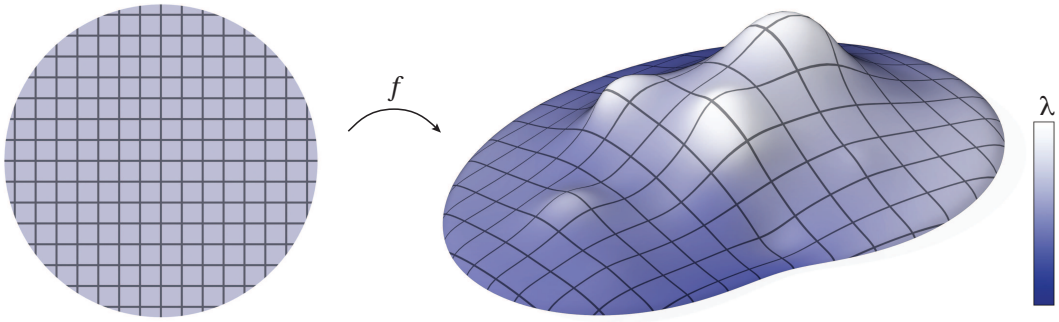

We can characterize a conformal map by a local scaling factor λ, that indicates the local change in lengths. More formally, $\lambda := |df(X)|/|X|$, where df denotes the Jacobian or differential of f. Since our goal is to model curved objects from flat materials, we need to establish a relationship between the local stretching of the material and the curvature of the target surfaces. In conformal mapping, this connection is given by the *Yamabe equation* $\Delta u = K_0 - e^u K$, where Δ denotes the Laplacian on M_0, $u = \log(\lambda)$, and K_0, K are initial and the target Gaussian curvature, respectively [Aubin 2013, Chapter 5]. This equation tells us that the amount by which the material scales to go from a flat to a curved configuration is related to the Gaussian curvature of the target surface. Note that, for example, for a mapping from a plane to a

developable surface where both Gaussian curvatures K_0 and K are zero, u must be a harmonic function. More general functions allow realization of double-curved surfaces.

Deployable Structures

Deployable structures are shape-shifting mechanisms that can transition between two or more geometric configurations. Often conceived to minimize space requirements for storage or transport, deployable structures are used, for example, for antennas or solar panels in satellites, as coronary stents in medical applications, as consumer products (e.g. umbrellas), or in architectural designs (e.g. retractable bridges or relocatable, temporary event spaces). However, most of these examples have simple geometries and rely on strong symmetries. Deploying more general curved surfaces is challenging due to the complexity in jointly designing initial and target configurations while satisfying the constraints imposed by the deployment mechanism [Gantes 2001].

Programmable Auxetic Materials

In recent years, programmable materials have become a popular research topic in digital fabrication due to their ability to change physical properties, self-deploy, and transition between the programmed shapes. The materials are fabricated in one state (often flat for manufacturing convenience) and the deployment is then generally triggered by external stimuli, such as a change in temperature with thermoviscoelastic base material [Wagner et al. 2017], by swelling of hydrogels [Raviv et al. 2014], or external mechanical forces [Chen et al. 2017; Celli et al. 2018], to assume a complex curved shape.

Auxetic materials with a perfectly regular pattern of slits are reconfigurable and encode no information about the target shape. With the same piece of material, one can approximate an infinite family of doubly-curved surfaces. While this can be an advantage in some applications, it can also require a complicated fabrication process to place each linkage triangle to their target positions. We address this limitation with spatially graded auxetic materials where a 3D shape is directly encoded into a 2D material. By spatially varying the triangle sizes, we control the maximal expansion factor at each point, which in turn provides control over the curvature of the target 3D shape. By applying appropriate forces, we program the material to transition between a flat state and a target curved shape. We show that the maximal expansion is successfully achieved through deployment via inflation or gravitational loading. Our programmable auxetics are novel deployable structures that can approximate a large class of doubly-curved surfaces. Their potential applications are in various fields, ranging from small-scale medical stents to large-scale architectural structures.

1.1 Contributions

A summary of main contributions of this thesis is listed below.

- In the same way that isometry is fundamental in developable surface modeling, we show how conformal geometry can be used to understand and design auxetic materials.
- We present a computational method for design and fabrication with regular auxetic linkages. The method can closely approximate given doubly-curved surfaces and handle non-trivial topology and non-local dependencies inherent in auxetic linkage.
- We introduce a generalization to programmable auxetics. Its spatially graded auxetic linkages have a target 3D shape directly encoded into the 2D pattern and are suitable for deployment via inflation or gravitational loading.
- We provide a formal classification and analysis of doubly-curved shapes realizable through inflation and gravitational loading.
- We propose an optimization algorithm for solving an inverse design problem with programmable auxetics. Given a target 3D surface, our method computes a 2D spatially graded auxetic linkage that closely approximates the target surface when deployed.
- We develop a forward design tool for programmable auxetics. Our approach enables simulation-based form-finding, and provides optimization-based direct manipulation tools for efficient exploration of design alternatives.

1.2 Publications

This thesis mainly covers the following peer-reviewed publications:

- Mina Konaković, Keenan Crane, Bailin Deng, Sofien Bouaziz, Daniel Piker, and Mark Pauly. Beyond Developable: Computational Design and Fabrication with Auxetic Materials. *ACM Transactions on Graphics (Proceedings of SIGGRAPH), 2016*.
- Mina Konaković-Luković, Julian Panetta, Keenan Crane, and Mark Pauly. Rapid Deployment of Curved Surfaces via Programmable Auxetics. *ACM Transactions on Graphics (Proceedings of SIGGRAPH), 2018*.
- Mina Konaković-Luković, Pavle Konaković, and Mark Pauly. Computational Design of Deployable Auxetic Shells. *Advances in Architectural Geometry, 2018*.

In addition, the following publications were published during the same time period but are not explicitly addressed in this thesis:

- Christopher Robeller, Mina Konaković, Mira Dedijer, Mark Pauly, and Yves Weinand. A Double-layered Timber Plate Shell – Computational Methods for Assembly, Prefabrication and Structural Design. *Advances in Architectural Geometry, 2016*.

- Christopher Robeller, Mina Konaković, Mira Dedijer, Mark Pauly, and Yves Weinand. Double-layered timber plate shell. *International Journal of Space Structures, 2017*.

- Julian Panetta, Mina Konaković-Luković, Florin Isvoranu, Etienne Bouleau, and Mark Pauly. X-Shells: A new class of deployable beam structures. *ACM Transactions on Graphics (Proceedings of SIGGRAPH), 2019*.

Abstracts of the last three mentioned papers are listed in the Appendix E.

1.3 Overview

We present a computational method for design and fabrication with regular and programmable auxetic materials. The remainder of the thesis is organized as follows:

- In Chapter 2 we provide an extensive review of the related work in material design and surface rationalization. We further discuss deployable structures and their applications. Finally, we give an overview of literature related to conformal geometry.

- Chapter 3 focuses on regular auxetic linkages. This chapter introduces conformal geometry for auxetic design and discusses feasible shapes from regular auxetic linkages. A constraint-based optimization approach is used to approximate a target 3D surface with a linkage and incorporate design and fabrication requirements. Conformal maps serve to initialize an otherwise intractable non-linear optimization. As the material can uniformly stretch up to a certain extent, conformal maps with bounded scale factors need to be used. Insertion of cone singularities reduces the local scaling factor in the transformation from 2D to 3D. We further discuss the types of cone singularities suitable for regular auxetic linkages. We demonstrate a rich set of complex shapes that our method can achieve through a series of design studies and physical prototypes. This work opens up new fabrication opportunities in various scientific and industrial works; additionally, it inspires new fundamental problems in discrete differential geometry.

- In Chapter 4 we introduce programmable auxetics. These spatially graded auxetic linkages are designed to encode a target 3D surface into a 2D pattern layout. They are

fabricated flat and rapidly deployed by either inflation or gravitational loading. Chapter 4 presents a detailed description of the material design and properties. Section 4.2 provides a formal classification of feasible shapes and analysis of deployment via inflation and gravity. In particular, we show that only surfaces of positive mean curvature everywhere and a limited area distortion are realizable. In case the target surface does not satisfy these requirements, an algorithm is proposed for surface modification towards a similar feasible shape. In addition, we discuss the connection between balloons and conformal embeddings. Section 4.4 presents a surface approximation algorithm which computes a 2D material layout that uniquely encodes the given 3D surface. To validate our approach, we implement a physics-based simulation of the inflation and gravity deployment, and we build several physical prototypes. We conduct a number of application case studies to highlight the potential use across domains ranging from small-scale heart stents to large-scale architectural domes.

- Chapter 5 extends the computational method for programmable auxetics from Chapter 4. While the post-rationalization process in Section 4.4 that finds a deployable auxetic linkage for a given input surface is an important design tool, it offers limited support for evaluating design alternatives or engaging in material- and construction-aware exploration. By using only the global optimization from Section 4.4, it can be difficult to anticipate the resulting functional and aesthetic properties of the auxetic linkage. Chapter 5 presents a computation-assisted design system that enables efficient design space exploration of deployable auxetic structures and gives the designer full control of the final deployed surface geometry. In addition, our approach provides tools for simulation-based form-finding, where the designed surfaces are interactively computed using the deployment mechanism as a form-finding force. We demonstrate the potential of our solution in the context of various architectural applications.

- Finally, Chapter 6 summarizes the main contributions of this thesis and includes a discussion of future work. We outline potential research directions and open problems in differential and discrete differential geometry, computation, architecture, materials science, and digital fabrication.

2 Related Works

Novel fabrication technologies and advances in material science are revolutionizing manufacturing culture and having a significant impact on various scientific fields. Computational tools that link creative design exploration to physical realization play a crucial role in these emerging technologies. A number of prior works focus on building such computational tools to capture the fabrication requirements in the form of geometric constraints and enable designs which were not possible before. Computer graphics and related disciplines have recently seen increasing interest in computational design for digital fabrication. For a general overview we refer to recent surveys [Pottmann et al. 2015; Bermano et al. 2017; Bickel et al. 2018; Attene et al. 2018]. Here we focus the discussion on prior art that is most closely related to the work of this thesis.

2.1 Material Design and Surface Rationalization

Material-aware Computational Design

Various computational tools assist the design of 3D shapes that are realized using specific physical materials. Typically, these materials impose fabrication or assembly requirements that are incorporated as geometric constraints. For example, Igarashi et al. [2012] model 3D beadwork as polygonal meshes with near-uniform edge length, while Garg et al. [2014] use Chebyshev nets to capture the deformation behavior of interwoven, inextensible wires. Similar tools have been applied to other construction techniques, including curved folding [Kilian et al. 2008; Tang et al. 2016], reciprocal frames [Song et al. 2013], inflatable structures [Skouras et al. 2014], Zometool [Zimmer and Kobbelt 2014], wire wrapping [Iarussi et al. 2015], flexible rod meshes [Pérez et al. 2015], LEGO [Testuz et al. 2013; Luo et al. 2015], and intersecting planar pieces [Hildebrand et al. 2012; Schwartzburg and Pauly 2013; Cignoni et al. 2014]. Successful examples of using geometric representations for abstracting fabrication and material constraints also include tools for modeling developable surfaces targeting materials such as paper, thin wood or metal [Solomon et al. 2012; Pottmann et al. 2015; Tang et al. 2016; Stein et al. 2018; Rabinovich et al. 2018], and conical and circular meshes for architectural facades

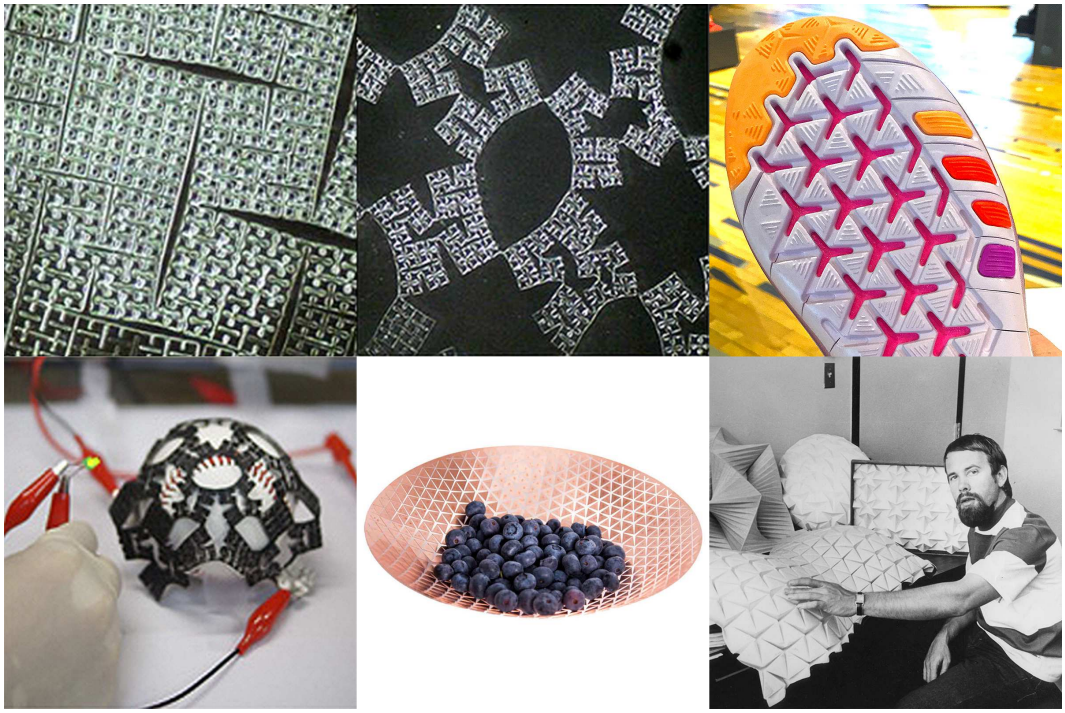

Figure 2.1 – (Top to bottom, left to right:) Regular patterns have been used to emulate auxetic behavior in microscopic materials, footwear, electronically actuated materials, simple design applications, and origami (image courtesy of Yigil Cho et al., fundmental.berlin, and Eric Gjerde)[1]. However, these applications have been limited to very simple geometries (e.g., planar or spherical) due to the lack of sophisticated design tools.

[Liu et al. 2006]. The work presented in this thesis extends this line of inquiry, focusing on a new class of material behavior obtained by cutting otherwise inextensible sheets. We therefore encounter a unique set of geometric constraints, demanding a new computational approach.

Origami

The cut pattern we study in Chapter 3 of this thesis has been used by Ron Resch in the context of origami design [Resch 1973] (see Figure 2.1, bottom right). Tachi [2010] further studied this pattern and introduced various extensions for origami design [Tachi 2013b]. Building on earlier work on freeform origami, he presents an optimization method to realize double-curved origami surfaces by solving a series of constraints derived from the specific origami folding method. Note that this construction is inherently more constrained than the pattern we study due to the absence of gaps in the pattern.

[1] The Resch portrait is provided by Eric Gjerde under license *CC BY-NC 2.0*; the footwear photo was released by the authors under a Creative Commons Public Domain Dedication; other images are used with permission from David J. Srolovitz and fundamental.berlin.

Material Science

Physical realizations of the cutting pattern we use in Chapter 3 also appear in design objects (Figure 2.1, bottom middle). In this specific piece a circular shape with fixed boundary can be manually deformed into simple shapes such as a bowl. Kim et al. [2012] create a new self-actuating material by photo-patterning polymer films that exhibits approximately conformal deformation behavior under temperature changes. They show simulation results where initially flat material assumes simple shapes such as spherical caps, cones, or basic minimal surfaces. Cho et al. [2014] and Gatt et al. [2015] report that hierarchical cut patterns similar to our linkages can drastically increase the expandability of thin sheet materials. Moreover, Cho et al. show in their simulation that such cut patterns allow the material to be wrapped onto simple 3D shapes such as spheres and cubes using a conformal deformation. Rafsanjani and Pasini [2016a] demonstrate the use of auxetic materials to achieve reversible reconfiguration between two stable arrangements of geometric patterns. Our work not only provides geometrical insights into these phenomena, but also shows that through a carefully designed optimization we can realize a much broader class of surface shapes with auxetic materials.

Computational Material Design

Several previous works have designed custom materials to achieve high-level deformation goals. Bickel et al. [2010] stack layers of various nonlinear base materials to produce a desired force-displacement curve. Ion et al. [2016] use carefully designed metamaterials to 3D print mechanisms that can perform mechanical functions. They show examples such as a door latch, a pair of pliers, a switch, and a pantograph. Coulais et al. [2016] discuss the potential of aperiodic and shape-shifting textured mechanical metamaterials for prosthetics, haptic devices, and wearables. These materials are programmed to morph to a complex 3D shape when uniaxially compressed. Microstructure design works [Panetta et al. 2015; Schumacher et al. 2015; Zhu et al. 2017] construct small-scale structures from one or two printing materials to emulate a large space of linearly elastic materials. These works focus on designing deformable materials that typically undergo small stretches and return to their rest configurations when unloaded, making them less suitable as deployment mechanisms.

Inverse Elastic Shape Design

Another common goal is to optimize deformable objects' rest shapes so that they assume desired equilibrium shapes under load. The inverse elastic shape design algorithms of Chen et al. [2014] and Pérez et al. [2015] design flexible objects achieving specified poses under gravity or user-defined forces. These works do not attempt to find compact rest configurations amenable to efficient fabrication, transport, and deployment. One exception is Skouras et al. [2012], which designs rubber balloons that inflate to desired target shapes. However, fabricating custom rubber balloons involves a complicated multi-step molding process best

suited for small-scale target shapes. Additionally, the inflation must be carefully controlled to avoid under- or over-inflating. In contrast, the programmable auxetic material we present in Chapters 4 and 5 has a flat initial state that facilitates simple fabrication at a wide range of scales. Our deployment method is also more robust, since the final state is precisely singled out by construction – the target is reached when the material cannot expand any further.

Auxetic Materials

Auxetic surface materials are an essential ingredient of this thesis: auxetic linkages permit otherwise inextensible flat sheets of material to uniformly stretch as needed to deform into doubly curved surfaces. We refer the reader to [Saxena et al. 2016] for a survey on auxetic patterns, their unique mechanical properties, and their potential applications to diverse engineering and medical problems.

Uniform auxetic materials have been studied in Naboni and Sortori Pezzi [2016] to design bending-active grid shells. Friedrich et al. [2018] seek to encode the target surface by limiting the pointwise maximal stretch factors. Rather than designing a fully opened linkage on the target surface, the authors outline a heuristic to construct a partially opened pattern in the plane.

Multi-stable auxetic patterns [Rafsanjani and Pasini 2016b] are another potential avenue for encoding maximal stretch factors in a material: they expand from their rest configuration and settle into stable equilibrium at one or more stretched configurations. We leave investigation on how to modify these patterns to encode curved surfaces as future work.

Polyhedral Patterns

When deployed, our programmable auxetic linkage's equilateral triangles and hexagonal openings tile the target surface with a tri-hex pattern. A common task in architectural geometry is to rationalize curved input surfaces using planar polyhedral patterns. Schiftner et al. [2009a] and Jiang et al. [2015] both introduce algorithms that can approximate input surfaces with tri-hex patterns as a special case. Vaxman et al. [2017] propose a form-finding tool for general combinatorial patterns and show applications to tri-hex meshes. These works focus on symmetry, planarity, and other pattern quality requirements, making no attempt to ensure the tri-hex pattern can be flattened into a planar configuration by closing the hexagons, which is essential in our approach.

2.2 Deployable Structures

Actuated Shape-shifting Structures

The engineering and graphics communities have both sought to design mechanisms that transition between discrete configurations or trace out continuous deformation paths when actuated. By embedding a rigid fiber lattice in flexible silicon, Connolly et al. [2017] design tubes that accurately reproduce bending and twisting motions when inflated. Ma et al. [2017] generalize this idea, segmenting objects into chambers that, when inflated to certain pressures, drive the shape into a sequence of desired poses. Also using pneumatic actuation, Overvelde et al. [2016] present an origami-inspired metamaterial that dramatically changes shape, and Ou et al. [2016] design flat sheets that fold into complex origami shapes. Raviv et al. [2014] design structures that can bend, stretch, and fold when exposed to water. Liu et al. [2017] study how a pre-strained elastomer sheet patterned with ink can self-fold when heated by a lamp. Deployable structures are also used for various building components. For example, Hannequart et al. [2018] investigate the use of shape memory alloys for deformable facade shading devices.

Deployment-aware Design

Other works have focused on designing objects that rapidly expand into nearly rigid target shapes. Skouras et al. [2014] construct inflatable structures by fusing together sheets of nearly inextensible material. Because each panel inflates into a nearly developable surface, many small panels are potentially needed to closely approximate a smooth, wrinkle-free doubly-curved surface. Zheng et al. [2016] design compact scissor linkage assemblies that, when stretched, uniformly expand into coarse approximations of 3D shapes. Their method ensures a collision-free expansion path for sparse wireframe designs. Kilian et al. [2017] propose a method for curved folded surfaces that transition from planar sheets to freeform shapes actuated by a network of strings, making the actuation process an integral part of the structure. Rigid-foldable origami can also be used to design deployable shells at architectural scale [Tachi 2013a]. Dudte et al. [2016] perform basic research into approximating singly- and doubly-curved surfaces with generalized Miura folds. Their origami patterns have a single degree of freedom parametrizing their path from the flat configuration to the target shape. For doubly curved surfaces, the construction is bi-stable, leading to an especially simple deployment process. However, the design algorithm produces flat configurations with over twice the surface area of the target.

Elastic Gridshells

The concept of kinematic deployment is well studied in architecture. For large-scale structures, elastic grid shells are probably the most prominent example. Composed of interconnected elastic beams, an elastic grid shell achieves its desired target shape by active bending, [Lienhard

2014; Du Peloux 2017]. Common methods of erection include lifting with cranes or various types of scaffolding or mechanical formwork. During erection, a gridshell often has to go through high-energy configurations until it settles in the final shape when the boundary is fixed. To increase safety and reduce the time and cost of manufacturing and erecting an elastic gridshell, Quinn and Gengnagel [2014]; Liuti et al. [2017] study erection with pneumatic formwork. Form-finding for elastic grid shells is also an active topic in material science; see, for example, the recent work of [Baek et al. 2017].

Actuated Form-prescribed Geometry

Recent work [Guseinov et al. 2017; Pérez et al. 2017] follows a similar rationale as the method in Chapter 4 of encoding a 3D target surface in a flat sheet of material. In these methods, the activation mechanism is directly integrated into the material in the form of a pre-tensioned elastic membrane. Upon release, the membrane contracts and forces the pre-shaped rigid elements into their global target configuration. This approach achieves impressive results, but has several drawbacks. (i) Pre-stretched materials are limited in scale. (ii) Fabrication is more complex, since it requires compositing multiple materials. (iii) Shaping by contraction means that the flat surface is larger in area than the target surface, reducing potential packing benefits. (iv) Closed surfaces are more difficult to realize (only disk-topology surfaces have been shown).

Our approach is scale-invariant, does not require multi-material compositing (our inflation balloons need not be attached to the auxetic linkage), leads to compact flat-packed sheets, and can handle shapes of arbitrary topology.

2.3 Conformal Mapping

We briefly review the literature on computing angle-preserving or *conformal* maps, which play a crucial role in our algorithms—for a more extensive discussion, see Gu and Yau [2008]. In computer graphics, conformal maps are often associated with texture mapping [Lévy et al. 2002]; more broadly they play a role in a diverse array of computational applications including simulation [Bazant and Crowdy 2005], shape analysis [Ben-Chen and Gotsman 2008; Lipman and Funkhouser 2009], surface fairing [Crane et al. 2013], shape editing [Crane et al. 2011; Vaxman et al. 2015], and layout of sensor networks [Li et al. 2013]. In architectural geometry, conformal maps have been used for designing circle and sphere packings [Schiftner et al. 2009b] and paneling layouts [Röhrig et al. 2014] on freeform surfaces.

A variety of strategies have been proposed to numerically approximate conformal maps based on different characterizations in the smooth setting. These include piecewise linear discretization of the Cauchy-Riemann equations [Lévy et al. 2002; Desbrun et al. 2002], conformal gradient fields [Gu and Yau 2003], circle packings [Stephenson 2003; Guo 2011], circle patterns [Kharevych et al. 2006], spin transformations [Crane et al. 2011], and local Möbius

transformations [Vaxman et al. 2015]. Most relevant to our setting are methods based on conformal scaling of the metric [Springborn et al. 2008; Ben-Chen et al. 2008], which provide additional flexibility via the insertion of *cone singularities* (Section 3.2.2). We also use the recent method of Sawhney and Crane [2017] to compute a conformal flattening of a surface. Soliman et al. [2018] introduced an algorithm for optimal placement of cone cingularities. *Quasiconformal* methods allow for maps with bounded angle distortion [Weber et al. 2012; Lipman 2012]. In contrast, we seek maps with *scale factors* bounded to a predefined range. None of the work above directly enforces such bounds. Aflalo et al. [2013] optimize conformal maps to make scaling as uniform as possible, providing a theoretical bound on the resulting scale factor. However, this bound can be much larger than our feasible range, making the method unsuitable for our problem.

3 Computational Design and Fabrication with Regular Auxetic Materials

This chapter presents a computational method for interactive 3D design and rationalization of surfaces via *auxetic* materials, i.e., flat flexible material that can stretch uniformly up to a certain extent. A key motivation for studying such a material is that one can approximate doubly-curved surfaces (such as the sphere) using only flat pieces, making it attractive for fabrication. We physically realize surfaces by introducing cuts into approximately inextensible material such as sheet metal, plastic, or leather. The cutting pattern is modeled as a regular triangular linkage that yields hexagonal openings of spatially-varying radius when stretched. In the same way that isometry is essential to modeling developable surfaces, we leverage *conformal* geometry to understand auxetic design. We use conformal mapping with bounded scale factor to initialize an otherwise intractable non-linear optimization. We demonstrate that this global approach can handle non-trivial topology and non-local dependencies inherent in auxetic material. Design studies and physical prototypes are used to illustrate a wide range of possible applications.

3.1 Introduction

In this chapter we study approximation of surfaces by near-inextensible material (such as sheet metal or plastic) cut along a regular pattern of thin slits (see Figure 3.1). Elements formed through this cutting process allowing the surface to stretch uniformly up to a certain limit. This stretching in turn allows the surface to exhibit non-zero Gaussian curvature, thus enriching the space of possible shapes relative to traditional developable design. As introduced in Chapter 1, we call such patterns *regular auxetic linkages*.

For computational design, we use constraint-based optimization to find configurations that closely approximate a target surface. A key insight is that one can leverage theory and algorithms from conformal geometry to facilitate the design process. In particular, conformal maps with *bounded scale factor* provide highly effective initialization for our non-linear solver—

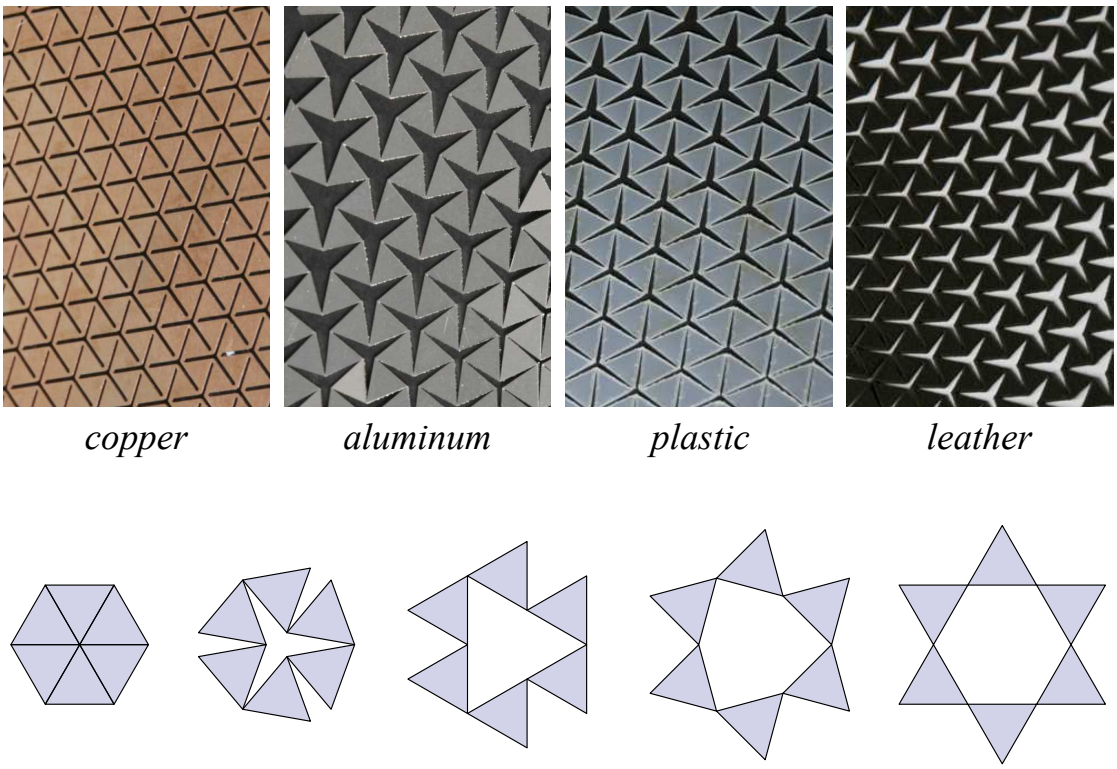

Figure 3.1 – Top: Samples of materials used in our experiments. The leftmost photo shows the undeformed configuration. Bottom: Geometric abstraction using a triangular linkage. A single unit of the linkage deforms to form a regular hexagon opening in the maximally extended configuration.

initialization is often the most difficult step in computational rationalization [Pottmann et al. 2015]. Global optimization also helps address challenging design decisions–for instance, prediction of the 2D region that most easily approximates a target shape in 3D (see for example Figure 3.12). Here, global rigidity makes a manual, incremental design approach ineffective, i.e., simply wrapping a piece of material around a target object is unlikely to succeed (see Figure 3.2), since the shape of the boundary strongly influences the space of feasible configurations (Appendix A). Moreover, it is nearly impossible to predict (by hand) how material should be cut and oriented to achieve global continuity across seams. Computation also aids the constrained exploration of *cone singularities*, essential for surfaces with large Gaussian curvature.

Through a series of design studies and physical prototypes we demonstrate that our solution encompasses a rich class of shapes, with attractive material and functional properties. This approach opens up new design opportunities in diverse fields, including biomechanics, engineering, consumer goods, and architecture; it also inspires new fundamental questions in discrete differential geometry.

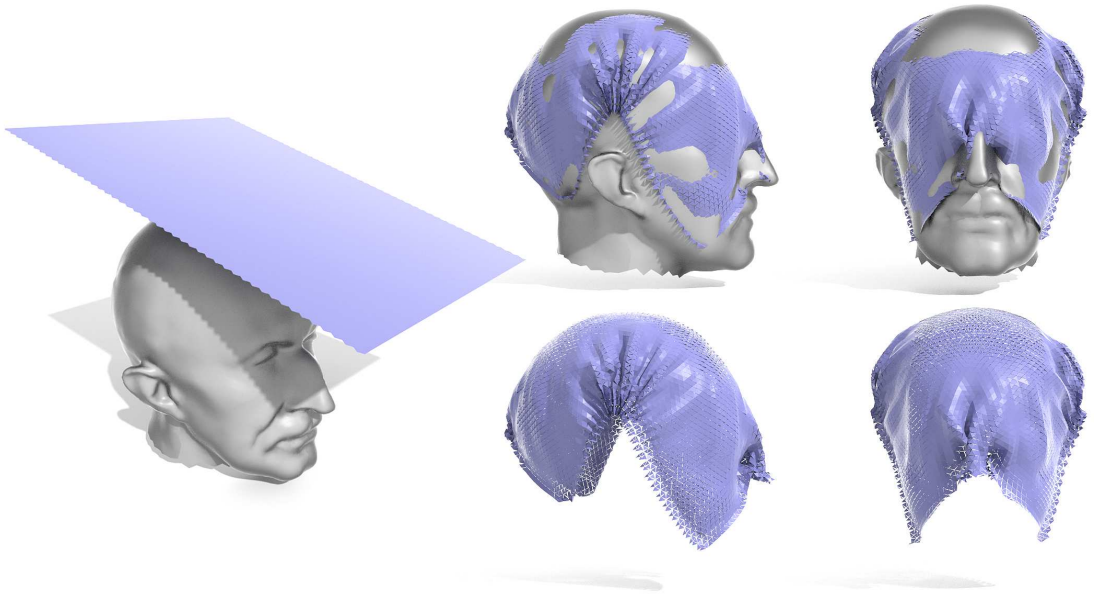

Figure 3.2 – Optimizing auxetic linkages from arbitrary initial shapes can lead to undesirable local minima. Left: initializing a linkage as a flat rectangular patch for the rationalization of Max Planck. Right: undesirable foldovers and wrinkles in the optimized linkage.

3.2 Regular Auxetic Linkages

To obtain a regular auxetic linkage, we experiment with cutting triangular patterns into different material samples (see Figure 3.1). We observed that under deformation, the triangles remain close to rigid. The deformation is concentrated at the hinge points connecting the triangles as these offer the least resistance to the exerted forces. We also noted that the openings that form remain roughly isotropic and that their shape varies smoothly over the surface. This suggests that locally the surface scales approximately uniformly without noticable shearing.

The linkage triangle rotations are coupled. For example, in an infinite planar lattice, one can see through a counting argument that there is only a single degree of freedom in the entire linkage that allows for a global uniform scaling. If a planar linkage has a boundary, however, we obtain one degree of freedom per degree-2 boundary vertex (see also Section 3.2.3 and Appendix A for more details).

Our observation of locally uniform scaling under deformation of the linkage surface provides a direct link to conformal geometry. More specifically, we can exploit the theory and algorithms of conformal maps to find a globally consistent initialization for a subsequent non-linear optimization that maps a closed 2D linkage to a given 3D design surface.

3.2.1 Conformal Geometry

One attractive feature of conformal geometry is that the curvature of a surface is easily expressed using the logarithmic factor (whereas in general, the expression can be rather complicated). We take advantage of this relationship to help reason about our design process.

In particular, let $\Omega \subset \mathbb{R}^2$ be any region in the complex plane, and consider a map $f : \Omega \to \mathbb{R}^3$ that gives Ω some new (e.g., curved) geometry. Let df denote the Jacobian or *differential* of f, expressing how a vector in $\mathbb{R}^2$ gets transformed by f as we go into $\mathbb{R}^3$. If the inner products $X \cdot Y$ and $df(X) \cdot df(Y)$ differ only up to a positive rescaling λ^2 at each point, then we say that f is *conformal*. Geometrically, then, we know that conformal maps must preserve *angles*, since angles can be expressed in terms of the inner product. The fact that λ is *positive* ensures that it never passes through zero, i.e., angles are always well-defined.

Often it will be convenient to express the conformal scale factor $\lambda : \Omega \to \mathbb{R}^+$ as $\lambda = e^{\phi}$, since now ϕ can be *any* function $\phi : \Omega \to \mathbb{R}$ (i.e., not just a positive one); ϕ is called the *logarithmic scale factor*, since $\phi = \log(\lambda)$. From here, the *Gaussian curvature* K of the target surface $f(\Omega)$ can be expressed as

$$K = \frac{\Delta\phi}{e^{2\phi}} = \Delta_f \phi, \tag{3.1}$$

where Δ denotes the Laplace operator in the plane [Ben-Chen et al. 2008], and Δ_f denotes the Laplace-Beltrami operator on the new surface. Notice that for conformal maps from the plane to itself ($K = 0$), ϕ is a harmonic function, i.e. $\Delta\phi = 0$.

Bounded Scaling

In principle, the Riemann mapping theorem guarantees that every surface of disk topology can be realized via a conformal map f. For auxetic design, however, we must restrict our search to conformal maps where the scale factor λ is bounded between 1 and some constant $\sigma > 1$. (Note that this condition is different from *quasi-conformality*, which puts bounds on *angle* distortion.) These bounds on the conformal factor imply that not every surface can be approximated (at least, not without additional *cone singularities*—see Section 3.2.2).

An idealized version of our linkage can at most double in size ($\sigma = 2$). To see why, consider Figure 3.1, bottom: each vertex in the closed configuration becomes an empty hexagon in the fully extended configuration. Hence, if the area of each triangle is 1, then we go from a total area of F to $F + 6V$, where V and F are the number of vertices and faces in the pattern, respectively. But since the ratio of faces to vertices in the closed pattern is $2 : 1$, the final area is $2V + 6V = 8V$ for an expansion factor of $8V/2V = 4$ in area, or $\sqrt{4} = 2$ in length. For physical realizations, σ must be strictly smaller than the ideal value since the material undergoes significant deformations at hinge points which can lead to material failure. For materials tested in our experiments, appropriate values of σ were determined empirically (see Section 4.5).

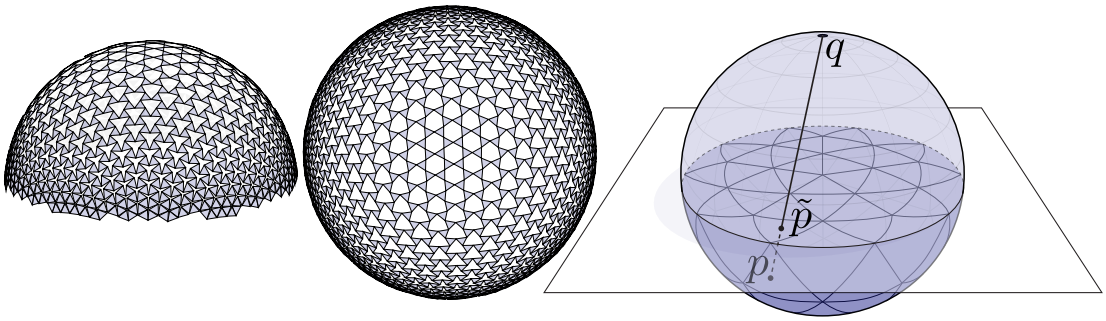

Figure 3.3 – Conformal mapping of the sphere using the stereographic projection sketched on the right. Since our linkage pattern restricts the conformal factor to be less or equal to two, at most a half-sphere can be realized with a single regular patch of auxetic material. Note how the surface is completely closed at the boundary and maximally stretched in the center.

These restrictions lead to a natural question: are auxetic materials with bounded scale factor flexible enough to approximate interesting geometry? To provide some intuition about this question, we consider two simple examples below.

Surjectivity. A conformal parameterization of the sphere S^2 can be obtained via *stereographic projection* [Feeman 2002]: each point $p \in S^2$ is projected to a point $\tilde{p}$ on the equatorial plane by finding the intersection with a segment that connects p to the north pole q. The area element induced by f is $d\tilde{A} := 4/(1+|\tilde{p}|^2)^2\, dA$, where dA is the usual area on the plane. This means that the length scale factor is 2 at the origin, shrinks to 1 at the equator, and for points outside the unit disk it shrinks further, to arbitrarily small values. Moreover, stereographic projection is the conformal parameterization of the hemisphere with *least* area distortion, because it is an isometry along the boundary [Springborn et al. 2008, Appendix E]. Therefore, a single auxetic patch can cover *at most* half of the sphere when the maximal conformal factor is bounded by 2, i.e. local area increase is bounded by a factor 4 (see Figure 3.3).

Integrability. Independent of the scale bound, there is also a question of *integrability*: is it possible to approximate surfaces that close up seamlessly? Following [Sullivan 2011], we consider a family of conformal embeddings of the torus $f_s(u,v) : [0,s] \times [0,1] \to R^3$ given by

$$f_s(u,v) = \frac{t+1}{2\pi(t-\cos(2\pi v))} \begin{pmatrix} s\cos(2\pi u/s) \\ s\sin(2\pi u/s) \\ \sin(2\pi v) \end{pmatrix},$$

where $t = \sqrt{s^2+1} = R/r$ is the ratio of major radius R to minor radius r. A simple calculation reveals that this mapping has minimal scaling factor of one, and maximal scaling factor given by $\sigma = \frac{t+1}{t-1}$. Since our tiling pattern restricts σ to be below two, this leads to the constraint $t > 3$

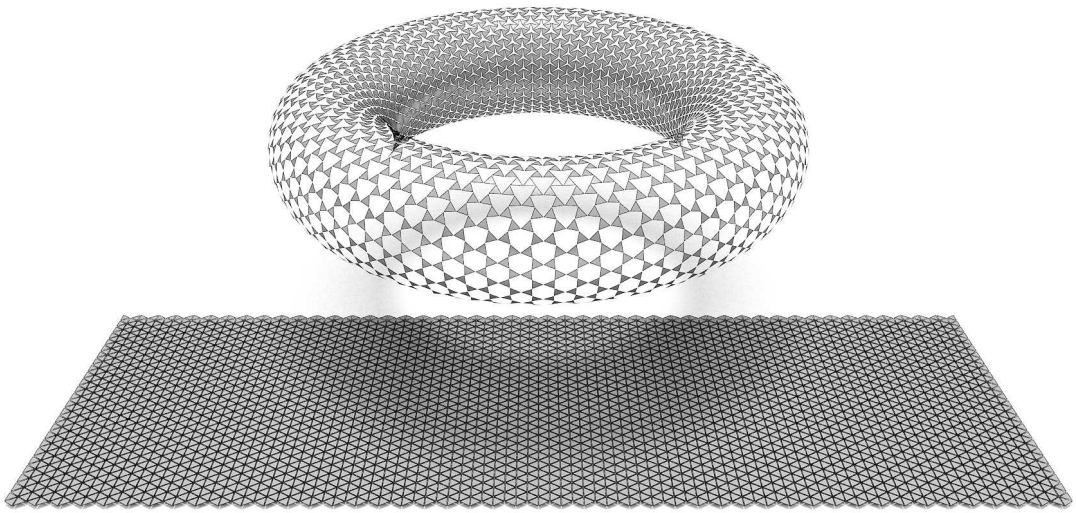

Figure 3.4 – The regular linkage we study can even be used to construct closed surfaces with nontrivial topology. Here a torus with rectangular conformal type floats over its initial (closed) tiling, given by the fundamental domain; the aspect ratio of this rectangle maximizes the relative scaling that can be achieved with our linkage.

(see Figure 3.4). This restriction again motivates the need for cone singularities, which provide additional flexibility.

3.2.2 Cone Singularities for Regular Auxetics

A surface has a *cone metric* if it can be perfectly flattened away from a collection of isolated points called *cone singularities*—examples include the paper cups used for snow cones (one cone) and cone coffee filters (two cones). Cutting from the boundary to each cone point yields a surface that can be flattened without any stretching. In recent years, cone singularities have been adopted as a tool for conformal surface parameterization: rather than mapping directly to the plane, one computes a conformal map to a cone metric, which can then be trivially flattened (via cutting) [Kharevych et al. 2006; Springborn et al. 2008; Ben-Chen et al. 2008; Sawhney and Crane 2017; Soliman et al. 2018]. The key benefit of concentrating curvature at cones is that area distortion is *also* concentrated near cones (see Equation (3.1)). For texture mapping, controlled area distortion improves signal fidelity; for auxetic design, it is crucial for approximating surfaces with large Gaussian curvature. However, we face additional challenges due to the discrete, rigid nature of our linkage (Figure 3.5).

In our linkage, cone singularities correspond to vertices of irregular degree. Recall that the *angle defect* at a vertex in a standard triangle mesh is 2π minus the sum of incident angles; a vertex can be flattened only if this value is equal to zero. In general, the angle defect is equal to the integrated *Gaussian curvature* in a small neighborhood around the vertex. Suppose, then, that we generalize our closed pattern from a regular grid to an equilateral triangle mesh where

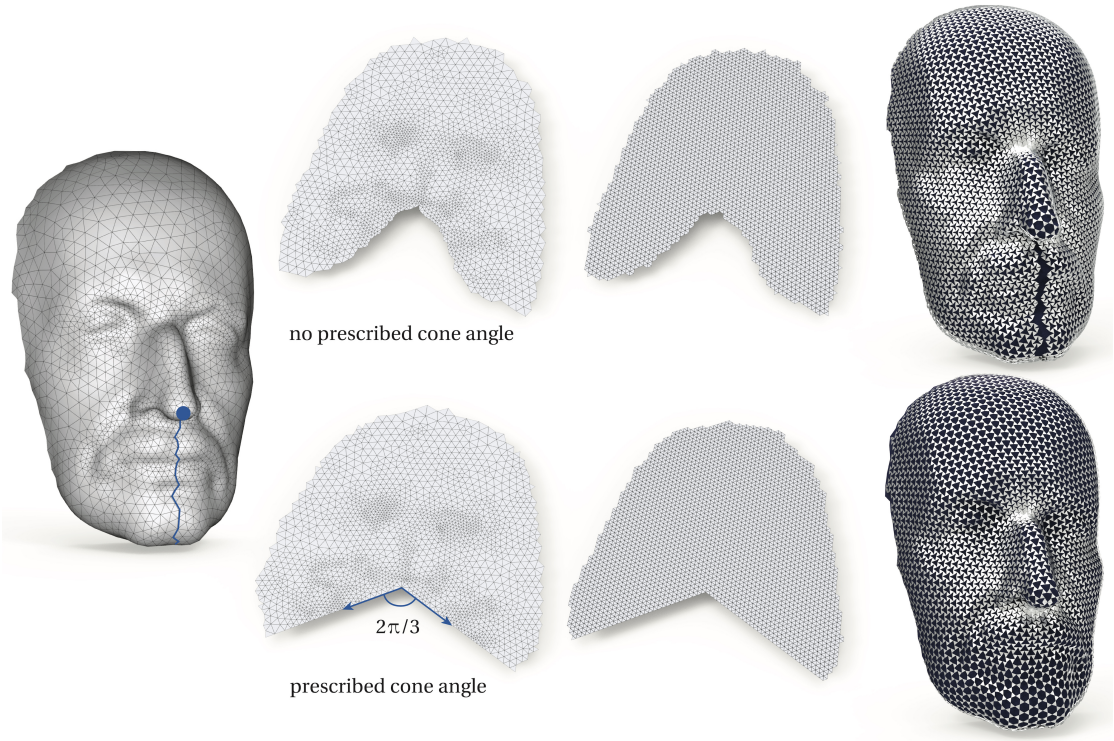

Figure 3.5 – Cone singularities are used for surfaces with large Gaussian curvature to lower the conformal scaling factor to our feasible range. Here a cone singularity is introduced at the tip of the nose and the surface is cut to the bottom. However, without prescribing a cone angle (top row), a regular tiling cannot align with the 2D conformal layout and seamlessly close in 3D. We compute a conformal map with a prescribed cone angle (bottom row) to ensure the continuity across the final linkage pattern.

every vertex has even degree. At each vertex, the corresponding open pattern is obtained by cutting along every other edge *almost* to the opposite vertex (see Figure 3.6). Globally, these cuts are made in such a way that no edge is cut twice; note that there are always two possible cutting patterns. Since every triangle is equilateral, and every vertex has even degree, the angle defect at each vertex is $2\pi - 2k\pi/3$ for some integer $k \geq 0$. Typically we find that cones of curvature $\pm 2\pi/3$ are the most useful, since cones with larger (negative) curvature will induce more severe area distortion.

Although irregular vertices globally reduce area distortion (moving us toward the bound $\lambda < \sigma$ from Section 3.2.1), they also incur large area distortion in the immediate vicinity of the cone. In the smooth setting, in fact, the scale factor goes to *infinity*, since ϕ locally looks like a harmonic Green's function $\frac{1}{2\pi}\log r$, where r is the distance from the cone; in the discrete setting the situation is not quite as dire, since this area distortion is distributed over a finite region. However, high curvature at cones still presents some difficulty. For example, Figure 3.7 shows an illustration where a subdivided octahedral linkage cannot be deformed into a round sphere without either creating spikes or self-intersections. A practical remedy is to remove

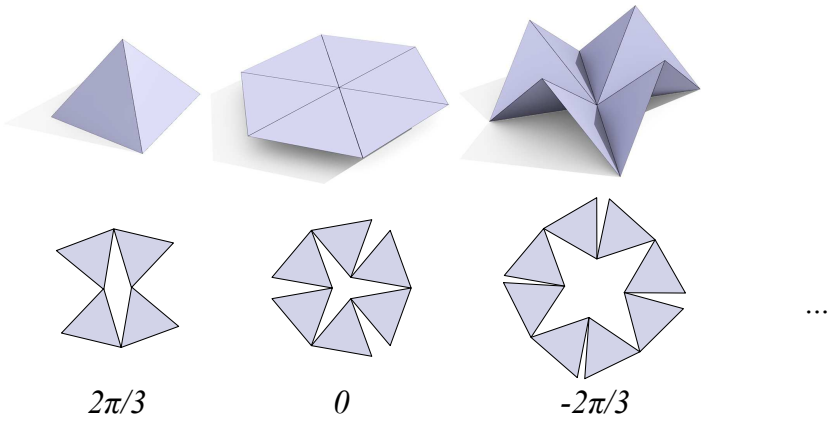

Figure 3.6 – Incorporating irregular vertices or *cone singularities* into our linkage pattern allows us to better approximate surfaces with large Gaussian curvature. Since each vertex must have even degree, the possible cone angles come in quanta of $2\pi/3$. *Top:* closed configuration. *Bottom:* corresponding open pattern.

triangles near the cone, creating additional openings in the surface at the cost of leaving some triangles "dangling," i.e., connected to only two neighbors. Despite these limitations, cone singularities significantly increase the space of shapes that are well-approximated by a single patch of material (see also Section 4.5).

Figure 3.8 validates the necessity of cone singularities in auxetic linkage design. For the target bump surface, conformal parameterization without singularities results in out-of-bound scale factors around the tip of the bump. Starting from such parameterization, the optimized linkage either deviates from the target surface or has non-uniform edge length. In contrast, introducing a cone singularity at the tip enables close approximation of the target surface, while satisfying all the constraints (see Section 3.3 for details).

3.2.3 Discrete Conformal Geometry

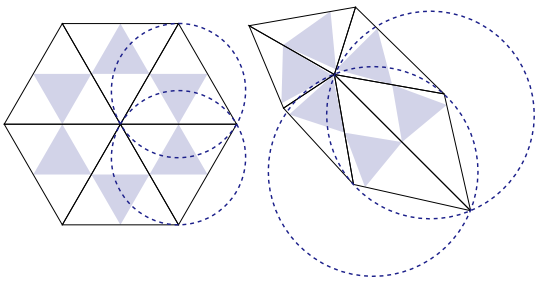

Although conformal geometry provides us with a great deal of intuition, we have thus far shown no rigorous, formal connection between our linkage and existing conformal theory. Naturally one would like to connect this discrete linkage to discrete theories such as *circle patterns* [Kharevych et al. 2006] or *discrete conformal equivalence* [Springborn et al. 2008]; so far, however, such a connection remains elusive. For instance, if one inscribes our linkage in a triangulation, one can easily construct configurations where this triangulation has neither the same length cross ratios nor the same angle sums as an equilateral grid (see inset). One can, however, establish one key fact that is strongly suggestive of a conformal theory, namely that the configuration of a finite planar

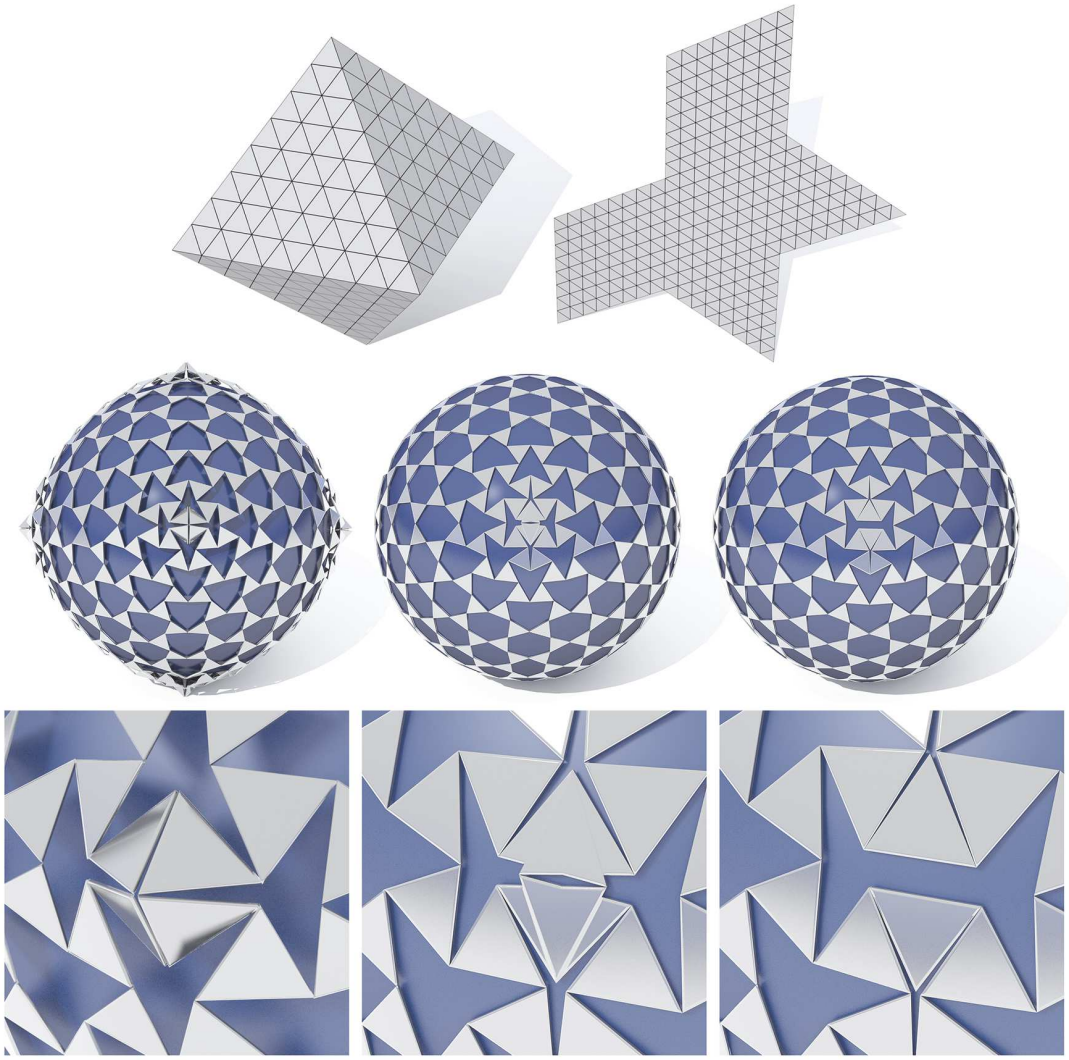

Figure 3.7 – The discrete, rigid nature of auxetic linkages introduces additional challenges for cone singularities. Here, six singularities on the octahedron (of curvature $2\pi/3$) cannot be flattened to match the curvature of the sphere without violating our maximal stretching criterion elsewhere on the surface. Hence we obtain high-curvature spikes (left) or self-intersections (middle) that can be avoided by deleting triangles (right) at the expense of creating dangling triangles only connected to two neighbors.

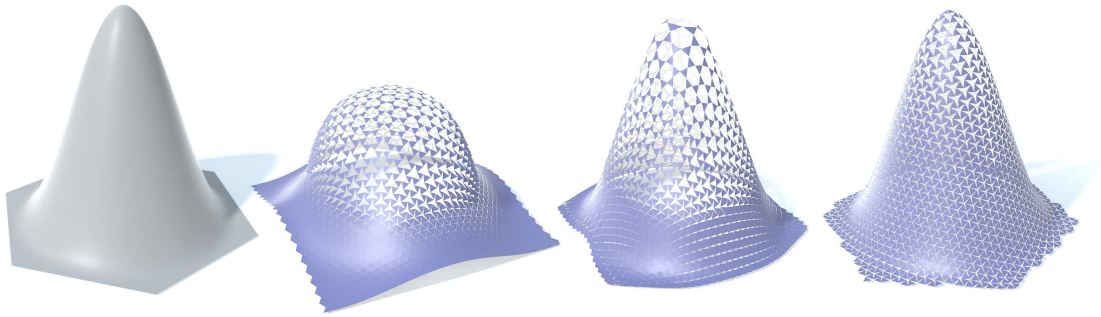

Figure 3.8 – Without singularities, rationalizing a bump with large curvature (left) results in either large deviation from the target surface (center left) or nonrigid distortion of triangles (center right). Adding a cone singularity at the tip allows one to closely approximate the target surface while satisfying fabrication constraints (right).

linkage is determined by *real* degrees of freedom at the boundary (see Appendix A). This situation corresponds to Cauchy-Riemann, where one cannot prescribe the full boundary values of a conformal map, but rather only one of its two real components. This fact places our linkage between rigid mechanisms like scissor-jointed structures, which have only one global degree of freedom, and far more flexible discrete harmonic maps, which have one *vector*-valued degree of freedom per boundary vertex. Understanding the geometric meaning of these boundary values, and indeed, further connections to conformal geometry is an enticing direction for future study. A particularly compelling feature of auxetic linkages is that each unit can rotate either clockwise or counter-clockwise, potentially capturing the behavior of both holomorphic and *antiholomorphic* functions.

3.3 Surface Rationalization

The central problem that we address in this chapter is surface rationalization, i.e., how to approximate a given 3D design surface with the linkage-based auxetic material introduced above. The highly non-local nature of the problem resulting from the spatial coupling of triangles imposed by our specific linkage topology, calls for a global approach using numerical optimization. At the same time, it is essential to keep the designer in the loop, as many high-level aesthetic decisions about the specific surface layout require user guidance. We therefore propose an interactive, optimization-supported rationalization approach described in the remainder of this section.

3.3.1 Interactive Workflow

Based on the connection between auxetic linkages and conformal maps outlined above, we introduce the following workflow for rationalization: We first create a conformal mapping of the 3D input surface to the 2D plane based on the method described in [Springborn et al.

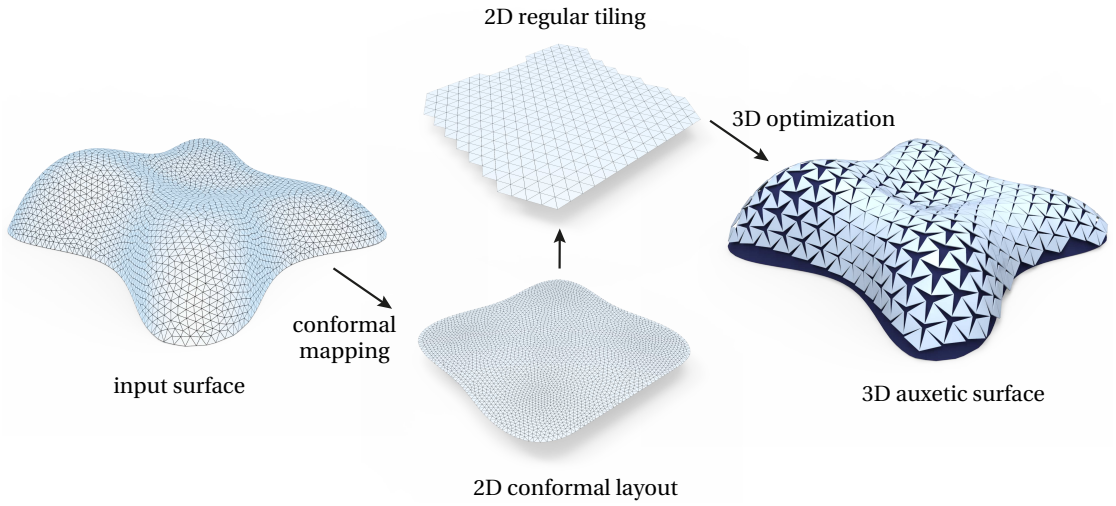

Figure 3.9 – Computational design workflow. By controlling the properties of a global conformal map and alignment of the 2D regular tiling with that map, the designer iteratively refines the 3D auxetic surface. Here we show and example with no cone singularities, as the scale factor is sufficiently small.

2008][1] (see Figure 3.9). Since this mapping has a strong influence on the visual appearance of the final surface, we provide full control over the specific properties of the conformal map. In particular, the designer indicates the desired locations of cone singularities and marks the cutting path necessary to map the surface to a 2D patch with disk topology.

During editing, we visualize the conformal factor on the surface so that the designer can introduce additional singularities to ensure that the scale factor is below the bound mandated by the limited material extensibility. Given the conformal map, the designer selects the global orientation of the regular tiling grid, which is then clipped appropriately and lifted onto the 3D design surface. The initial linkage configuration is then obtained by inscribing linkage triangles into the conformally lifted regular tiling grid (see Appendix B).

Due to the discrete nature of our linkage, the conformally lifted pattern typically does not satisfy the rigidity constraints of triangles exactly. Furthermore, neighboring triangles can potentially inter-penetrate. We therefore apply a global optimization to satisfy all constraints as described below.

The optimization also provides us with more flexibility when creating the conformal map. If the bounds on the scaling factor are violated within a confined region, the optimization can typically recover a valid solution. In general, we apply several iterations between adapting the conform map and global optimization.

[1] available in the software tool *Varylab* at www.varylab.com

3.3.2 Numerical Optimization

The conformal map provides us with 3D positions on the design surface for each linkage vertex. The resulting lifted linkage needs to be further optimized to satisfy the following requirements: 1) all triangles are rigid, i.e. have the same edge length prescribed by the user; 2) the triangles do not collide with each other; 3) the vertices remain close to the input design surface. To meet these objectives we minimze an objective function with respect to the vertex positions $\mathbf{x}_1, \ldots, \mathbf{x}_n \in \mathbb{R}^3$ (omitted below for notational brevity):

$$E(\mathbf{x}_1, \ldots, \mathbf{x}_n) = w_1 E_{\text{design}} + w_2 E_{\text{rigid}} + w_3 E_{\text{collision}}, \tag{3.2}$$

where E_{design}, E_{rigid}, and $E_{\text{collision}}$ measure the closeness to the design surface, the violation of rigidity constraints, and the violation of non-penetration constraints, respectively. The weights w_1, w_2, w_3 control the trade-off between these objectives.

The energy terms of Equation (3.2) are defined according to the framework proposed by Bouaziz et al. [2012], i.e., using projection operators onto feasible sets. Specifically,

$$E_{\text{design}} = \sum_{i=1}^{n} \| \mathbf{x}_i - P_{\text{design}}(\mathbf{x}_i) \|^2,$$

where $P_{\text{design}}(\mathbf{x}_i)$ is the projection of vertex $\mathbf{x}_i$ onto the input design surface. The rigidity constraint is formulated as

$$E_{\text{rigid}} = \sum_{(i,j) \in \mathscr{E}} \| (\mathbf{x}_i - \mathbf{x}_j) - P_{\text{edge}}(\mathbf{x}_i - \mathbf{x}_j) \|^2,$$

where $\mathscr{E}$ is the index set for all vertex pairs that belong to a common edge; $P_{\text{edge}}(\cdot) : \mathbb{R}^3 \mapsto \mathbb{R}^3$ is the projection operator onto the set of vectors whose norms are equal to the user-specified edge length L: $P_{\text{edge}}(\mathbf{v}) = L\mathbf{v}/\|\mathbf{v}\|$.

For collision avoidance we enforce non-penetration locally between neighboring triangles that share a vertex. Since our initial lifted surface is already close to the solution, the optimization typically leads to only moderate changes of the shape. We therefore do not prevent global collisions to avoid unnecessary computational overhead. Let $\mathbf{v}_1, \mathbf{v}_2, \mathbf{v}_3, \mathbf{v}_4$ be four edge vectors that originate from the same vertex, where $(\mathbf{v}_1, \mathbf{v}_2)$ and $(\mathbf{v}_3, \mathbf{v}_4)$ belong to two triangles, and $\mathbf{v}_2, \mathbf{v}_3$ correspond to their shared edge in the rest shape (see Figure 3.10). We then require that

$$(\mathbf{v}_1 \times \mathbf{v}_2) \cdot (\mathbf{v}_2 \times \mathbf{v}_3) \geq 0, \tag{3.3}$$

$$(\mathbf{v}_4 \times \mathbf{v}_3) \cdot (\mathbf{v}_3 \times \mathbf{v}_2) \geq 0. \tag{3.4}$$

Geometrically, if $\mathbf{v}_1, \mathbf{v}_2$ are linearly independent, then they span a plane P_{12}, and $\mathbf{v}_2$ defines a line that cuts P_{12} into two half-planes; condition $(\mathbf{v}_1 \times \mathbf{v}_2) \cdot (\mathbf{v}_2 \times \mathbf{v}_3) \geq 0$ requires that the

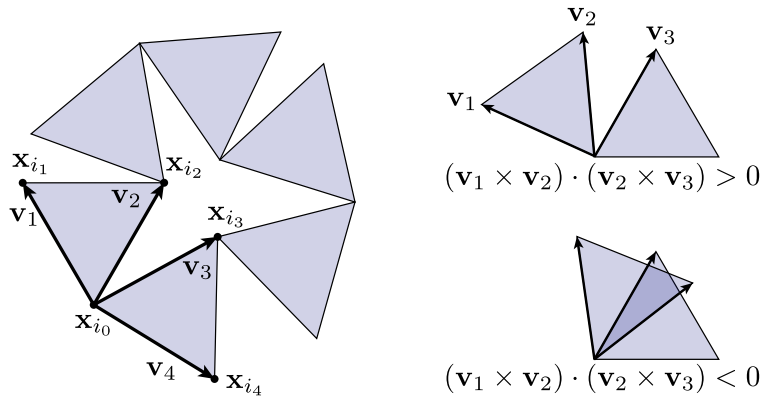

Figure 3.10 – Non-penetration constraint. Viewed from the normal direction of the triangle $\mathbf{v}_1\mathbf{v}_2$ (shown on the right), the condition $(\mathbf{v}_1 \times \mathbf{v}_2) \cdot (\mathbf{v}_2 \times \mathbf{v}_3) \geq 0$ prevents $\mathbf{v}_3$ from projecting into the interior of the triangle $\mathbf{v}_1\mathbf{v}_2$.

projection of $\mathbf{v}_3$ falls onto a half-plane different from $\mathbf{v}_1$. Viewing along the normal of triangle $\mathbf{v}_1\mathbf{v}_2$, this condition prevents $\mathbf{v}_3$ from moving into the triangle $\mathbf{v}_1\mathbf{v}_2$ (see Figure 3.10 right). The same restriction applies to $\mathbf{v}_2$ with respect to triangle $\mathbf{v}_3\mathbf{v}_4$, under the condition $(\mathbf{v}_4 \times \mathbf{v}_3) \cdot (\mathbf{v}_3 \times \mathbf{v}_2) \geq 0$. The two conditions combined avoid penetration between adjacent triangles. Given three vectors $\mathbf{v}_1, \mathbf{v}_2, \mathbf{v}_3$, the projection operator onto the feasible set of (3.3) requires solving a system of quadratic equations, and is expensive to compute. Instead we use an approximate projection operator that minimally moves $\mathbf{v}_2, \mathbf{v}_3$ to linear dependent positions if Condition (3.3) is violated:

$$P_{\text{collision}}([\mathbf{v}_1, \mathbf{v}_2, \mathbf{v}_3]) = \begin{cases} [\mathbf{v}_1, \mathbf{v}_2, \mathbf{v}_3] & \text{if } (\mathbf{v}_1 \times \mathbf{v}_2) \cdot (\mathbf{v}_2 \times \mathbf{v}_3) \geq 0 \\ [\mathbf{v}_1, \mathbf{h}(\mathbf{h} \cdot \mathbf{v}_2), \mathbf{h}(\mathbf{h} \cdot \mathbf{v}_3)] & \text{otherwise} \end{cases},$$

where $\mathbf{h}$ is the left singular vector of matrix $[\mathbf{v}_2, \mathbf{v}_3] \in \mathbb{R}^{3\times 2}$ for the largest singular value. Then the collision objective is defined as

$$\begin{aligned} E_{\text{collision}} = \sum_{\mathcal{T}} \big(& \left\| [\mathbf{x}_{i_1} - \mathbf{x}_{i_0}, \mathbf{x}_{i_2} - \mathbf{x}_{i_0}, \mathbf{x}_{i_3} - \mathbf{x}_{i_0}] - P_{\text{collision}}([\mathbf{x}_{i_1} - \mathbf{x}_{i_0}, \mathbf{x}_{i_2} - \mathbf{x}_{i_0}, \mathbf{x}_{i_3} - \mathbf{x}_{i_0}]) \right\|^2 \\ & + \left\| [\mathbf{x}_{i_4} - \mathbf{x}_{i_0}, \mathbf{x}_{i_3} - \mathbf{x}_{i_0}, \mathbf{x}_{i_2} - \mathbf{x}_{i_0}] - P_{\text{collision}}([\mathbf{x}_{i_4} - \mathbf{x}_{i_0}, \mathbf{x}_{i_3} - \mathbf{x}_{i_0}, \mathbf{x}_{i_2} - \mathbf{x}_{i_0}]) \right\|^2 \big) \end{aligned}$$

where $\mathbf{x}_{i_0}, \mathbf{x}_{i_1}, \mathbf{x}_{i_2}, \mathbf{x}_{i_3}, \mathbf{x}_{i_4}$ are the vertex positions related to the vectors $\mathbf{v}_1, \mathbf{v}_2, \mathbf{v}_3, \mathbf{v}_4$ for a pair of neighboring triangles (see Figure 3.10 left), and $\mathcal{T}$ is the index set of such vertex tuples.

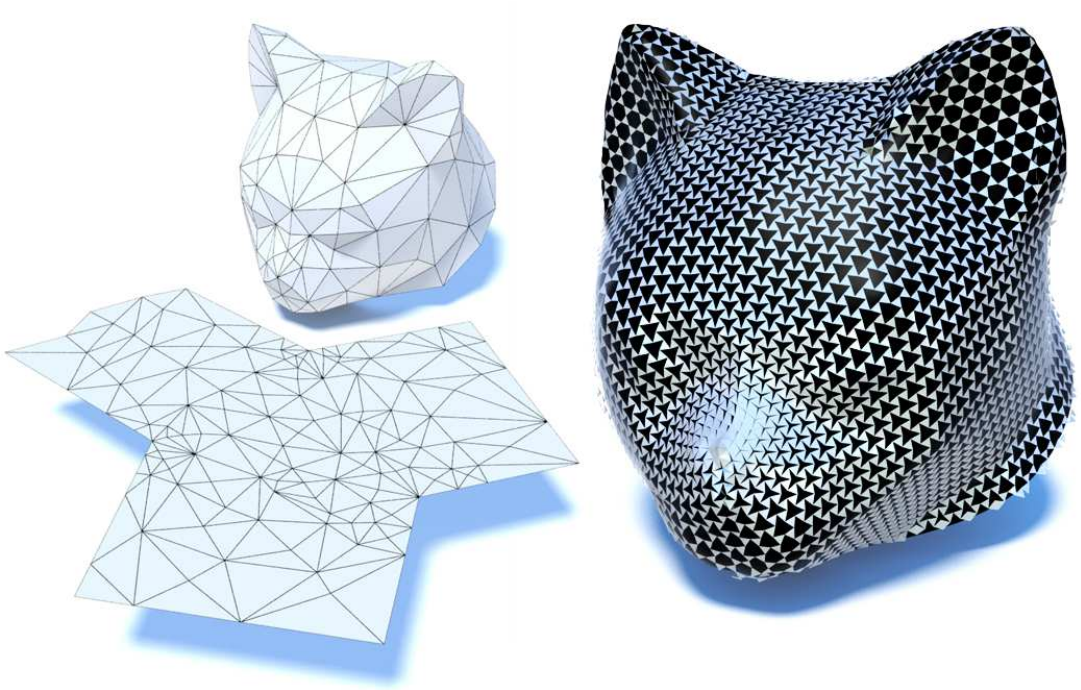

Figure 3.11 – Rationalization of the cat model with singularities of $2\pi/3$ curvature at the nose and both ears.

Implementation details

The target function (3.2) is optimized using alternating minimization with auxiliary variables, as described in detail in [Bouaziz et al. 2012]. We use the open-source implementation of this method described in [Deuss et al. 2015]. The only extension necessary is the implementation of the projection operator for collisions that we provide in Appendix C.

Below we give performance data for the largest of our examples, the Max Planck model of Figure 3.13 with 15k vertices. All our other models have significantly fewer vertices and thus require only a fraction of the computation time. The optimization requires 2.5ms per iteration on a single core of a 2012 Macbook Pro laptop with 2.6GHz when solving for edge length and non-penetration constraints, while fixing the closest points on the design surface to the 3D positions specified by the conformal map. This is useful to get a quick first impression of the surface layout, which might inform the designer that the conformal map needs to be adapted. When solving the full optimization including dynamic closest point computations for the P_{design} projection operator, this number increases to 350ms. We typically run 20-50 iterations for visual feedback to highlight possible constraint violations that then trigger further design iterations. Once the layout is finalized we run an additional 200 iterations to obtain the final linkage surface.

The weights w_2 and w_3 in Equation (3.2) are kept fix at 1 for the entire optimization process. For the surface closeness weight w_1 we follow the relaxation strategy commonly used for non-rigid registration, see e.g. [Li et al. 2009]. We initialize w_1 with 0.001 and gradually increase its value to 0.1 to first resolve the constraints and then let the surface evolve closer towards the input design.

Our optimization problem is non-convex with many local minima, and our numerical solver only finds a local minimum close to the initial shape. Thus it is important to start the solver from a shape that is already close to the desirable solution. Our initialization using conformal maps follows a common strategy of understanding discrete objects from their continuous analogues [Pottmann et al. 2015], which proves to be effective in our experiments. In comparison, running the solver from an arbitrary initial shape often results in an undesirable local minimum (see Figure 3.2).

3.4 Applications and Physical Prototypes

We validate our computational design and rationalization approach with a number of numerical and physical experiments, illustrating the broad applicability of our approach for different materials and usage domains.

Shoe

Figure 3.12 shows a design of a shoe using an auxetic linkage. In contrast to a purely inextensible material, our material can realize this double curved shape with a single piece. At the same time, the pattern provides an interesting esthetic and offers certain functional properties, e.g. ventilation. Creating such a surface without optimization is extremely difficult as it is not clear how one would need to lay out the surface in 2D such that the material would match seamlessly at the cut. This highly non-local constraint is handled implicitly by our initialization based on a global conformal map.

Sculptures

In Figures 3.11 and 3.13 we show rationalizations of the cat model and the Max Planck bust, with several singularities to accommodate the complex double-curved shapes. Note how a rationalization of these surfaces with developable material would require numerous thin strips that would have to be connected along their boundaries in a way that cannot provide tangent continuity across the connections. Auxetic linkages preserve the smooth appearance of the input surface while capturing important geometric features.

Figure 3.12 – The shoe model has been fabricated from a single piece of metallic material using our interactive rationalization method based on conformal geometry and global, non-linear optimization. Thanks to our global approach, the 2D layout of the material can be computed such that no discontinuities occur at the seam. The center zoom shows the region of the seam, where one row of triangles is doubled to allow for easy gluing along the boundaries. The base is 3D printed.

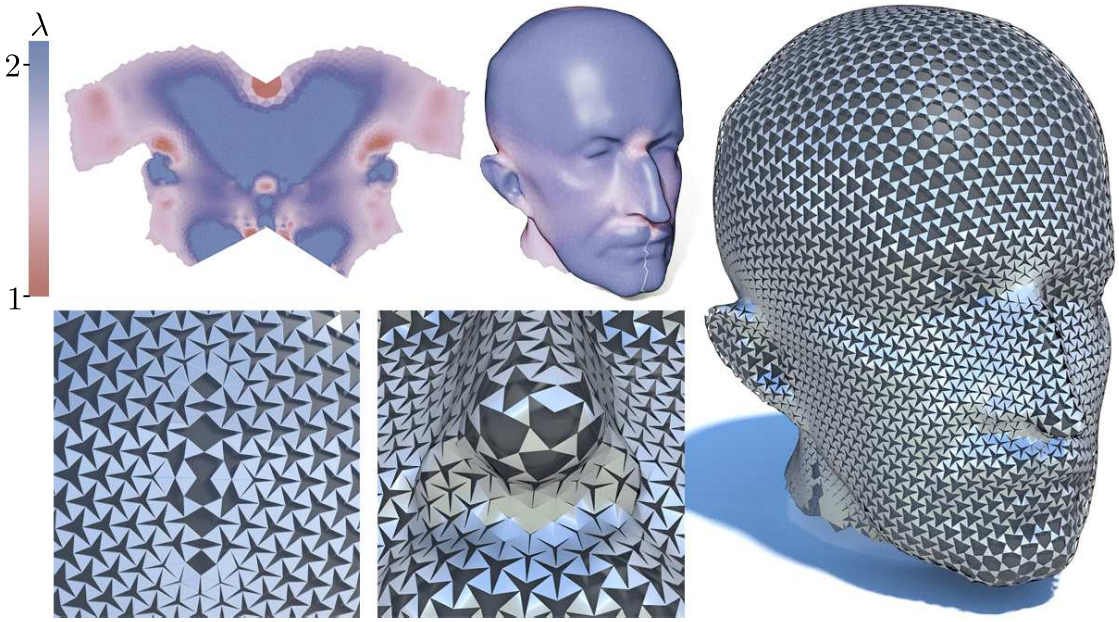

Figure 3.13 – A rationalization of the Max Planck illustrates the limits of what can be approximated with a single patch of auxetic material. One singularity with $2\pi/3$ curvature is at the top of the nose (middle zoom) with a completely closed four-sided polygon. A combination of $2\pi/3$ and $-2\pi/3$ curvature singularities is required to close the top of the head (left zoom). The cut behind the ear could not be closed without violating the bound on the conformal factor, which is visualized on the model and 2D layout.

Face masks

Figure 3.14 shows a physical realization of the Max Planck model cut from a single sheet of perforated copper. While our current fabrication technique produces a single rigid surface, kinematic linkages can also be employed in dynamic settings where an object transitions through different geometric configurations. Figure 3.15 illustrates this shape shifting idea, where the same linkage is used to approximate two different face models. How to mechanically actuate such a transition is an interesting question for future work.

Fashion top

Figure 3.16 shows an application in fashion design, where auxetic material is laser cut from a nearly inextensible leather textile and stretches to conform to the doubly-curved mannequin body. Since optimization ensures a continuous transition across seams, the final dress has no visible discontinuities. The design surface was created by 3D scanning a physical mannequin, highlighting the potential of our approach for personalized fashion design.

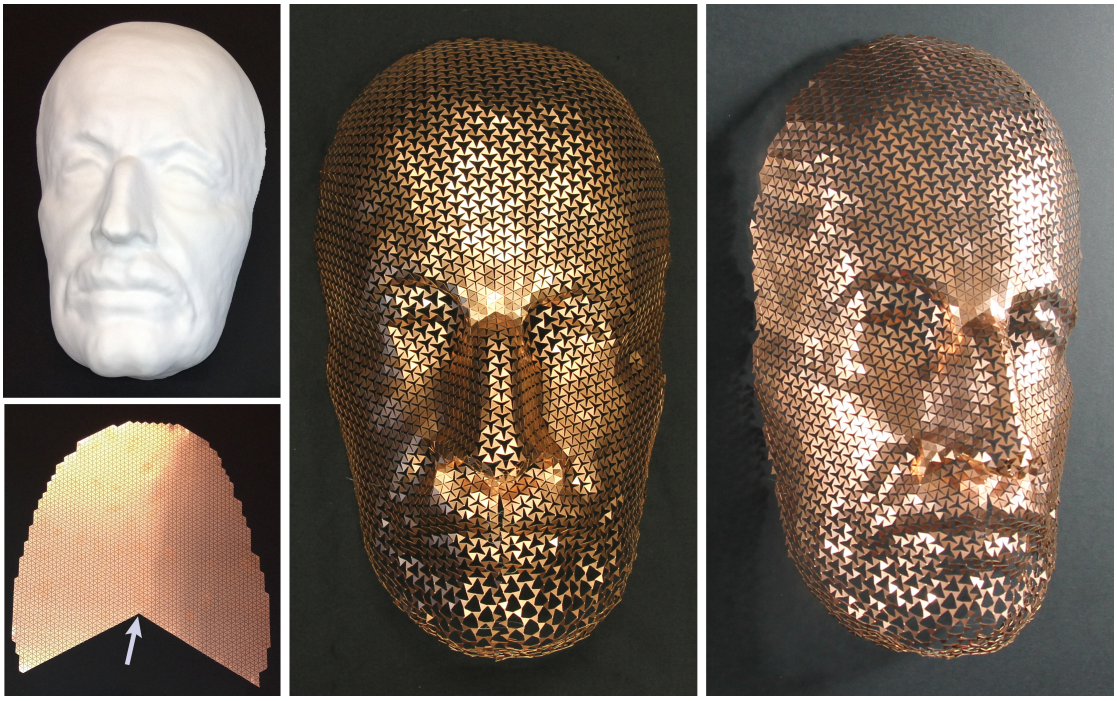

Figure 3.14 – Fabrication of the Max Planck model. Top left: 3D printed reference model used for geometric guidance; Bottom left: flat, undeformed perforated copper sheet. The purple arrow indicates the singular vertex located at the tip of the nose; Middle, Right: two photographs of the final model.

Lamp shade

Beyond rationalization of a given input, techniques from Section 3.3.2 can also be used for interactive design using, e.g., a standard handle-based click-and-drag interface. Constraints on vertex positions replace the surface closeness energy in Equation (3.2), which is augmented with a smoothness term as described in [Bouaziz et al. 2012]. Optimization ensures that edge length and inter-penetration constraints are satisfied, allowing the user to interactively explore the shape space of a given linkage topology. Figure 3.17 shows an auxetic lamp shade, modeled with handle-based manipulation. The form of the object influences the emission of light, leading to interesting shadow patterns.

Facade

Figure 3.18 shows an application in architectural shading system. Shading and lighting systems can take advantage of the reconfigurable nature of regular auxetic linkage. Here we present a free-form facade built from identical triangular elements and connected with a single type of rotational joints for cost-efficient manufacturing. The facade can be computer-operated to optimize the amount of light passing through. The linkage allows local control

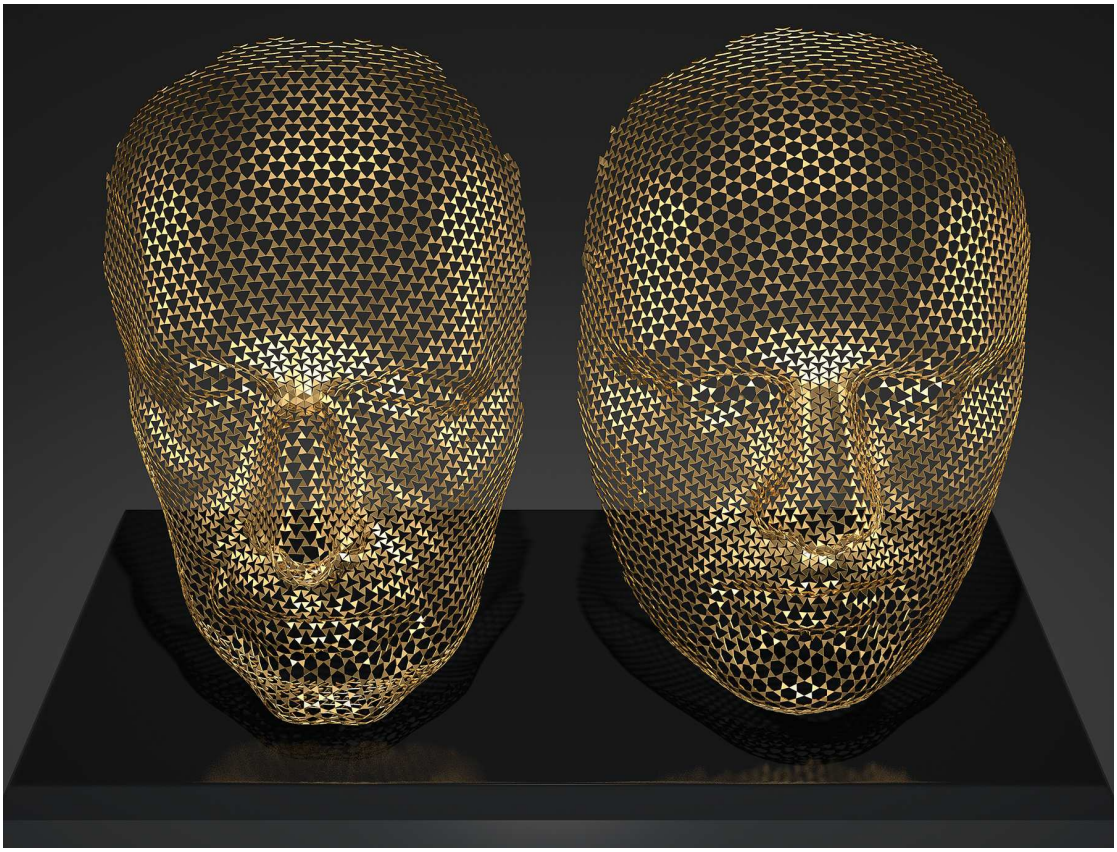

Figure 3.15 – While several design and engineering applications have used the kagome lattice, they have been so far restricted to very simple geometries like the hemisphere. In contrast, we can approximate arbitrary curved surfaces by an auxetic linkage—here we show two configurations of an identical linkage, opening the door to reconfigurable matter.

over the openings, making it convenient for a multi-purpose space.

3.5 Discussion

In recent years, study of isometric maps has led to numerous computational methods for geometric modeling, for example in the domains of origami, curved foldings, or developable surface rationalization. Our work aims to initiate a similarly fruitful discussion for a richer set of surfaces that can be achieved when the material can also locally scale in a uniform way. Our results demonstrate that non-trivial shapes can be rationalized effectively, offering a new class of design surfaces with applications in many domains.

We empirically observed that our abstraction based on linkages of rigid elements well approximates the geometric behavior of the cut surface materials. However, we do not explicitly model the complex physical behavior at the linkage joints. Metals, for example, deform plastically to retain the deformed state, while the plastics we experimented with deform elastically and push

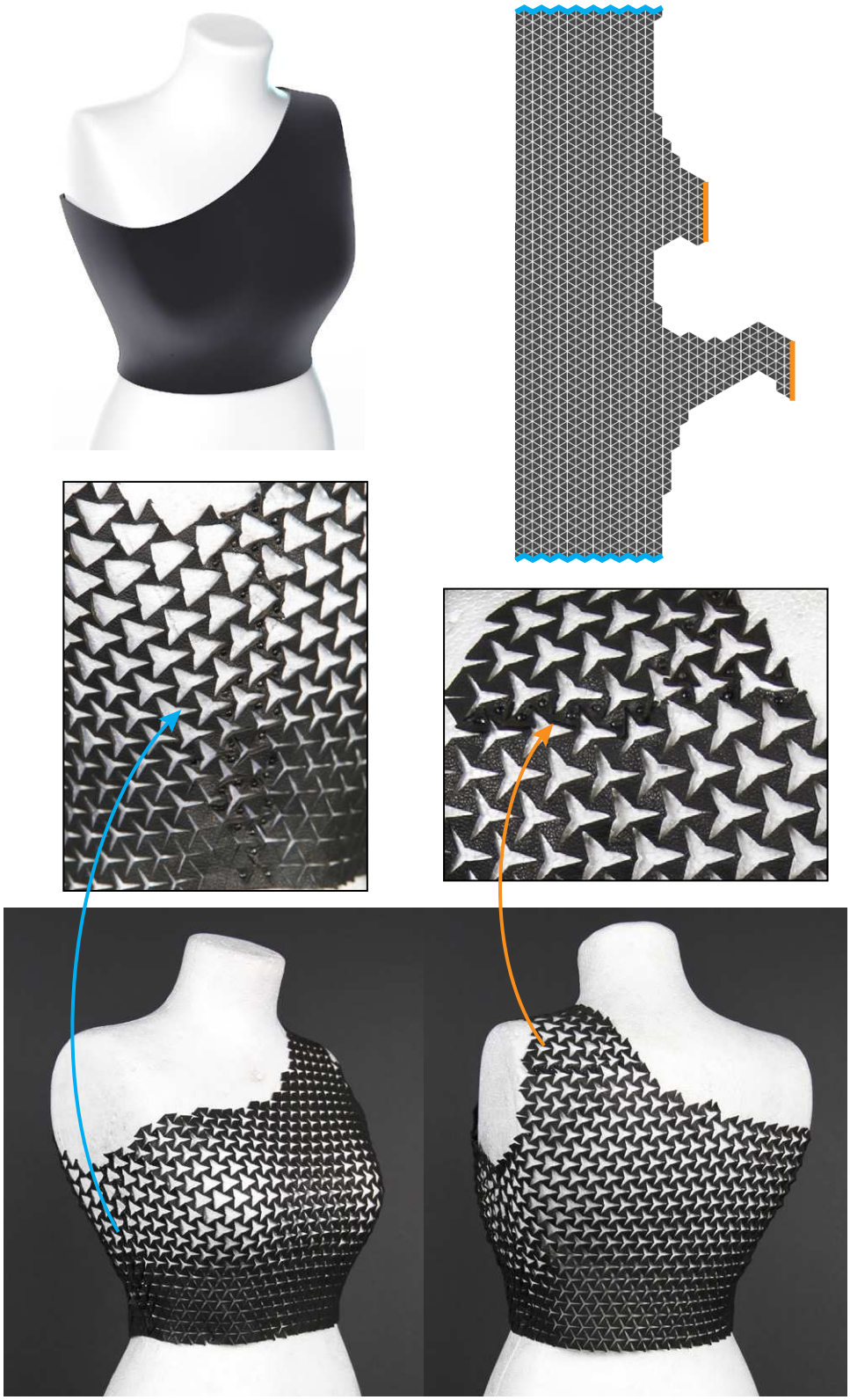

Figure 3.16 – A double-curved top fabricated from approximately inextensible leather. The zooms illustrate the global continuity of the pattern across the seams, which are fixed with pins.

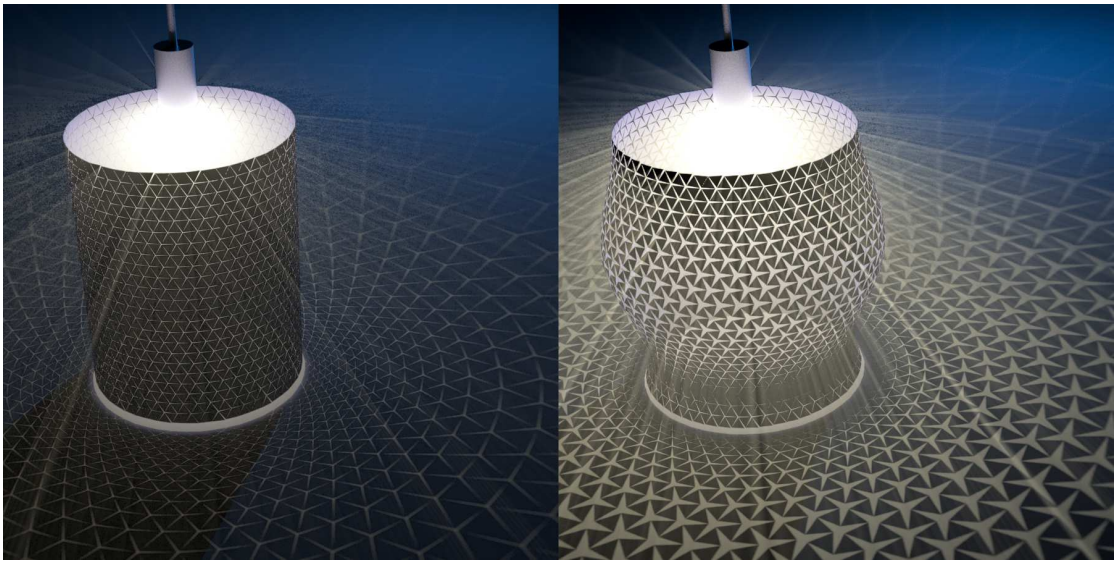

Figure 3.17 – Our auxetic design tools can also be used to explore lighting design—here an "open" and "closed" configuration of the same linkage provide mechanical dimming.

back towards the rest state. In practice, linkage joints cannot be stretched beyond a certain limit without fracturing, which means that for many materials we cannot achieve the maximal scaling factor of the linkage. Suitable bounds need to be determined for each base material as a function of the sheet thickness and the incision depth. Currently, we determine these bounds empirically through experimentation. In general, the concrete physical behavior of each piece strongly depends on the material and the specific geometry. It would be interesting to integrate finite-element simulation into the design process to provide feedback on the structural performance of the physical realization.

For closed designs or surfaces with singularities, we currently do not optimize for the seam, but rely on the user to specify an appropriate path on the surface. While this gives the user full control, finding good cut paths is not always an easy task and additional computational support could be helpful for untrained users. Appearance of seams could be improved by quantizing the target geodesic curvature to agree with the symmetry of our triangular pattern, a la Springborn et al [Springborn et al. 2008, Section 6]; in the future, one might also consider augmented tilings that conform exactly to the boundary.

Examples of Figures 3.17 and 3.18 are emblematic for applications of our method in lighting and shading control, for example, in an architectural context. Given a desired solar energy density profile, the openings and orientation of the surface can be determined through a form finding optimization, taking into account other constraints such as limits on curvature or smoothness of the facade. This is an example of the concept of form follows function (or more precisely, performance). For large scale facades, fabrication would probably follow a panel-based assembly approach, where the fact that all triangles are identical can significantly

Figure 3.18 – A free-form facade constructed from uniform triangular elements connected with rotational joints. Thanks to the reconfigurable nature of the regular auxetic linkage, the facade can be used as a computer-controlled dynamic external shading system.

simplify manufacturing. Related to the passage of light through the material, one can also imagine other transport scenarios, e.g., flow of liquids or granular material, where the openings can be used for flow control.

The particular cutting pattern we study here is just one of many possibilities; other regular tilings have been explored, for example in the sculptural art of Haresh Lalvani. A unified theory of linkage-based auxetic materials is an exciting avenue for future research. For example, a clear notion of discrete conformal equivalence for linkage patterns (with compatible discrete notions of curvature, Laplace operator, etc.) would provide insights into the geometry of linkage surfaces, with potential implications for algorithm design. More generally, the possibility to control the deformation behavior of sheet material by introducing cuts offers new opportunities for material-aware design. Interesting questions arise concerning the physical behavior of such materials. Form-finding algorithms and interactive design tools that optimize for the cutting pattern rather than prescribing it a priori offer a rich space for future research. One such example is presented in the following chapters.

Note

This chapter is mainly based on the following publication:

> Mina Konaković, Keenan Crane, Bailin Deng, Sofien Bouaziz, Daniel Piker, and Mark Pauly. Beyond Developable: Computational Design and Fabrication with Auxetic Materials. *ACM Transactions on Graphics (Proceedings of SIGGRAPH), 2016*.

The candidate contributed most of the scientific developments and implementation of this publication.

4 Computational Design and Deployment of Programmable Auxetics

Deployable structures are physical mechanisms that can easily transition between two or more geometric configurations; such structures enable industrial, scientific, and consumer applications at a wide variety of scales. This chapter develops novel deployable structures that can approximate a large class of doubly-curved surfaces and are easily actuated from a flat initial state via inflation or gravitational loading. The structures are based on two-dimensional rigid mechanical linkages that implicitly encode the curvature of the target shape via a user-programmable pattern that permits locally isotropic scaling under load. We explicitly characterize the shapes that can be realized by such structures—in particular, we show that they can approximate target surfaces of positive mean curvature and bounded scale distortion relative to a given reference domain. Based on this observation, we develop efficient computational design algorithms for approximating a given input geometry. We validate our approach through a series of physical prototypes and application case studies.

4.1 Introduction

Deployable structures are shape-shifting mechanisms that can transition between two or more geometric configurations. They are often convenient for storage or transport due to their ability to minimize the space requirement. Deployable structures are used, for example, for antennas or solar panels in satellites, as coronary stents in medical applications, as consumer products (e.g. umbrellas), or in architectural designs (e.g. retractable bridges or relocatable, temporary event spaces).

Most existing realizations of deployable structures are geometrically simple and often exhibit strong symmetries. Deploying more general curved surfaces is made difficult by the inherent complexity of jointly designing initial and target geometries within the constraints imposed by the deployment mechanism [Gantes 2001].

We propose a new class of deployable structures and associated computational methods that enable rapid deployment of doubly-curved freeform surfaces (see Figure 4.1). Our approach

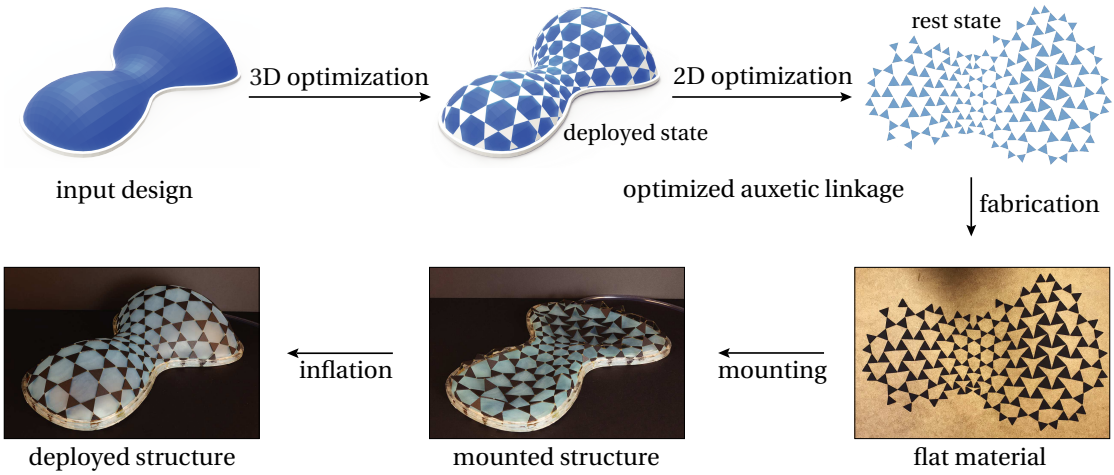

Figure 4.1 – Our algorithm computes a spatially graded triangular auxetic linkage that closely approximates a given surface when deployed to maximal extension via inflation. The fabricated material is laser cut from a single sheet, mounted onto the support frame, and inflated with a generic rubber balloon.

is based on a planar linkage of rigid triangles connected by rotational joints at vertices; this linkage has regular connectivity, but spatially varying scale. In-plane rotation of the triangles induces an approximately isotropic expansion or contraction in area, which allows a mechanical interpretation of the linkage as an auxetic surface metamaterial [Saxena et al. 2016], or a geometric interpretation in terms of conformal maps as in Chapter 3.

By spatially varying the triangle sizes, we effectively control the maximum possible expansion at each point, which in turn provides control over curvature: under maximal extension, nonuniform expansion forces the structure to buckle out of the plane and assume a curved configuration. Here several questions arise: which curvature functions can be encoded in such a pattern? How can we actuate a linkage to achieve maximal expansion? Which surfaces can we hope to realize using this procedure? Several key contributions help to address these questions:

- We introduce *spatially graded* auxetic metamaterials suitable for deployment via inflation or gravitational loading. In particular, we show that these deployment strategies achieve maximal expansion everywhere and provide additional regularization to ensure that the target shape is unique.
- We provide a general analysis of deformation by inflation and gravitational loading to formally classify the set of realizable doubly-curved target shapes.
- We present an optimization algorithm to solve the inverse design problem: Given a desired target geometry, our method finds appropriate scaling parameters and a corresponding layout of the 2D linkage such that the target shape is achieved when the linkage is deployed.

The resulting structures offer a number of benefits: (i) The rest-state is (piece-wise) flat, which facilitates compact storage as well as cost- and time-efficient fabrication techniques (such as laser cutting or milling); (ii) The target geometry is directly encoded in the 2D linkage structure so that no additional support or scaffolding is required to guide deployment; (iii) Our approach is scale-invariant and can be applied to realize a broad and explicitly defined class of doubly-curved surfaces. If a given surface is not within the set of realizable shapes, we apply optimization to find a feasible target surface that is close to the desired design.

The rest of the chapter is organized as follows: Section 4.2 considers geometric models of inflation and gravitational loading, helping to understand the feasible design space. Specifically, we characterize the shapes that can be achieved via inflation or gravitational loading in terms of surfaces of positive mean curvature and conformal deformations with bounded scale factor. Section 4.3 introduces our spatially graded auxetic metamaterial, realized as a rigid triangular linkage. We show how to locally adapt maximal expansion (and hence, target curvature) by varying the scale and orientation of linkage elements in the initial flat state. Section 4.4 describes an optimization algorithm for solving the inverse design problem, *i.e.*, finding suitable parameters for our metamaterial that ensure the target surface is faithfully approximated when actuated. In Section 4.5 we present several case studies and physical prototypes that highlight potential applications across domains ranging from small-scale heart stents to large-scale air-supported domes. We conclude with a discussion of the limitations of our approach, and also identify opportunities for future research (4.6).

4.2 Shape Space

Which shapes can we hope to achieve with our structures? The answer depends jointly on the geometry of the structure, as well as the method used to actuate it. Rather than study this question in terms of the detailed geometry of a specific mechanical linkage, we will first consider an idealized model based on smooth differential geometry. This analysis will then inform the design of discrete mechanical linkages and their physical actuation described in Section 4.3 and the corresponding optimization algorithm discussed in Section 4.4. In particular, we will explicitly characterize the shapes one can hope to achieve via (i) inflation and (ii) gravitational loading; we will also make an interesting connection between inflated balloons and conformal geometry (Section 4.2.2).

4.2.1 Preliminaries

In this section, we consider a closed, compact, and oriented topological surface M with geometry given by a map $f : M \to \mathbb{R}^3$ assigning coordinates to each point of M. The *differential* df of f maps tangent vectors X on M to the corresponding vectors $df(X)$ in $\mathbb{R}^3$; the differential is also sometimes denoted as the *Jacobian* or *deformation gradient*. A map f is an *immersion* if its differential is injective, *i.e.*, if at each point $p \in M$ it maps nonzero vectors to nonzero vectors; since M is compact, it is an *embedding* if f is also injective (loosely speaking: if it has

no self-intersections). Formally, we will require that f is a twice differentiable immersion with bounded curvature.

To any immersed surface we can associate the quantity

$$\text{vol}(f) := \int_M N \cdot f \, dA_f,$$

where N is the outward unit normal and dA_f is the area element induced by f; when f is embedded, $\text{vol}(f)$ is just the enclosed volume. We will also use g and H to denote the metric and mean curvature (*resp.*) induced by f. We use the definition $H = \frac{1}{2}\nabla_f \cdot N$, so, *e.g.*, a sphere has constant *positive* mean curvature. If dA and $d\tilde{A}$ are two area measures on M, we will write $dA \leq d\tilde{A}$ to mean that $dA(U) \leq d\tilde{A}(U)$ for all measurable subsets $U \subset M$. When considering variations of the surface, we will think of f as a time-parameterized family of immersions $f(t)$, and adopt the shorthand $\dot{\phi} := \frac{d}{dt}\phi|_{t=0}$ for any time-varying quantity ϕ.

4.2.2 Inflation

To understand the space of shapes that can be achieved via inflation, we consider an idealized and purely geometric model of rubber balloons. From a mechanical viewpoint, our model would correspond (very roughly) to a thin isotropic elastic membrane with spatially varying maximal expansion.

This model should however be taken with a grain of salt: our goal here is not to formulate a precise mechanical model, but rather to get a sense of the most significant geometric effects exhibited by our discrete mechanism—a more rigorous analysis (*e.g.*, based on homogenization of the small-scale geometry) is beyond the scope of this thesis. Moreover, for computational design, it is often more useful to have a simple and easily computable geometric model than a detailed mechanical model which is accurate but difficult to explore due to heavy computational requirements (*e.g.*, finite element analysis).

We specifically consider the geometry of immersions that (i) locally maximize enclosed volume, and (ii) do not stretch area above a given upper bound. Note that we do not consider questions of *dynamics* (*e.g.*, "can this configuration be reached from a given starting point?"), which are notoriously difficult even without constraints on volume or area. Instead we consider only the simple static question of, "what will be true about a surface that achieves these conditions?" In particular, we make the following observation:

Proposition 1. *Let dA^+ be an area measure on M. Among all immersions $f : M \to \mathbb{R}^3$ such that $dA_f \leq dA^+$, those that locally maximize the enclosed volume* $\text{vol}(f)$ *will (i) have strictly positive mean curvature $H > 0$ and (ii) achieve the upper bound on area ($dA_f = dA^+$).*

Proof. An immersion f locally maximizes volume if and only if every volume-increasing variation of f violates the upper bound on area distortion. Since tangential motion has no

effect on volume, we only need to consider normal variations $\dot{f} := uN$ for some suitably regular function $u : M \to \mathbb{R}$. The corresponding first-order change in volume is

$$\frac{d}{dt}\text{vol}(f)|_{t=0} = \int_M u \, dA_f.$$

A normal variation therefore increases volume if and only if u integrates to a positive value, which means u must be positive on a set of nonzero measure. The change in the area measure is given by

$$d\dot{A}_f = 2uH dA_f.$$

A normal variation uN therefore violates the upper bound on area if and only if both u and H have the same sign at a point $p \in M$ where this bound is achieved ($dA_f(p) = dA^+(p)$). As mentioned above, f locally maximizes volume only if the constraint is violated by *all* volume-increasing variations, which includes all positive and compactly supported bump functions $u_{p,\varepsilon} : M \to \mathbb{R}$ of width $\varepsilon > 0$ centered at points $p \in M$. But since ε can be arbitrarily small, a volume-maximizing immersion must have positive mean curvature and maximal area at every point. □

Roughly speaking, the surfaces that can be realized via inflation in our model are those that have positive mean curvature (see Proposition 1 and Section 4.3.1 for further discussion). In practice, we therefore modify a given target surface to have positive mean curvature, as described in Section 4.2.4.

Conformal Balloons

Suppose we no longer consider volume maximization nor an upper bound on area, but simply ask about the shape of a balloon that tries to minimize the elastic membrane energy when filled with a fixed volume of air. In particular, the *Dirichlet energy* $E_D(f) := \int_M |df|^2 \, dA_0$ models an elastic membrane with zero rest length, or, asymptotically, the energy due to extreme stretching. Critical points of Dirichlet energy are called *harmonic maps*, and any harmonic map between topological spheres is necessarily holomorphic or anti-holomorphic [Eells and Wood 1976]. We hence find a connection to conformal geometry:

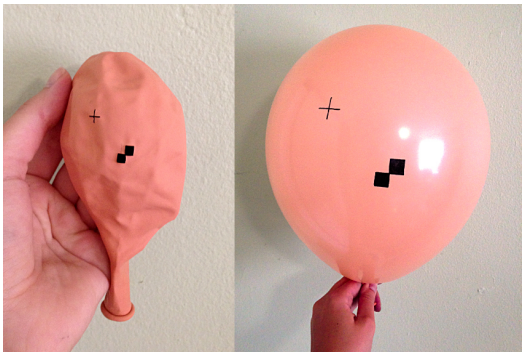

Figure 4.2 – When inflated, rubber balloons exhibit near-conformal deformation (indicated by the preservation of right angles), further motivating our use of an auxetic design space for inflatable structures.

Theorem 1. *Consider a surface* (M, g_0) *of spherical topology. Among all embeddings* $f : M \to \mathbb{R}^3$ *of fixed enclosed volume* $\mathrm{vol}(f) = c$*, any embedding minimizing the membrane energy* E_D *is conformal,* i.e.*, the induced metric* $g := df \otimes df$ *is conformally equivalent to* g_0*.*

Proof. Let $\tilde{f}$ be a *non*-conformal embedding with volume c, and let $\Sigma := \tilde{f}(M) \subset \mathbb{R}^3$ denote the image of $\tilde{f}$. We know that a map minimizing Dirichlet energy over all orientation-preserving embeddings $f : (M, g_0) \to \Sigma$ is holomorphic (and in particular, conformal since it is injective and orientation-preserving). Therefore, because $\tilde{f}$ is not conformal, we can find an embedding f^* mapping to Σ with smaller Dirichlet energy. This f^* still has volume c, but lower E_D, so $\tilde{f}$ is not minimal. □

Due to the rather simplistic model of membrane energy, one might wonder whether this theorem provides any useful information about real physical balloons or our auxetic mechanisms (which allow an area scaling of at most 4). However, Dirichlet energy will still tend to dominate more realistic nonlinear models of elasticity in the limit of large stretching. Consider for instance the elastic energy described by Chao et al. [2010], $E(f) := \int_M |df - R_f|^2 \, dA$, where R_f denotes the rotation closest to df. In the limit of large strain, the quadratic (*i.e.*, Dirichlet) term of the expansion $|df|^2 - 2\langle df, R_f\rangle + |R_f|^2$ dominates, and we are left with the same picture as before. Moreover, the nonlinear terms drop off rather quickly, suggesting that one should observe conformal behavior even for moderate stretching—as supported by physical experiments such as the one pictured in Figure 4.2. This observation further motivates our use of auxetic materials with bounded scale factors for inflatable structures.

4.2.3 Gravitational Deployment

Gravity is an even simpler mechanism for shape deployment: just suspend a sheet of material by its boundary and let gravity pull it into the target shape. This approach is most suitable for surfaces with simple boundary curves like in Figure 4.9. In fact, to simplify the fabrication process, we require that the initial surface spanning the boundary curves be a height field; otherwise attaching the flat material to the boundary curves would require a complicated manual deformation. The height field property also guarantees that the downward gravitational force has a positive component along the surface's normal direction, ensuring that it can pull the surface open analogously to the inflation setup.

When fabricated from our idealized material (characterized by having zero stiffness until an upper area bound is reached), we observe that height-field-initialized surfaces will remain height fields during the deployment. This follows from the fact that only two types of forces act on interior points during the deployment: gravity and the material stresses enforcing the area bound. Gravity pushes points in the material straight downward, decreasing height values but preserving the height field property. Stresses enforcing the area stretch bound always take the form of tensile forces: regions of material that have reached their stretching bound pull uniformly inward against the surrounding material (tangentially to the surface). Unlike

expansive forces, these tensile forces act to straighten out the material and will not cause the sheet to fold over itself to violate the height field property.

We now characterize the space of height field surfaces deployable by gravity, again ignoring questions of dynamics. For consistency with the inflation setup, we orient the surface's height axis vertically (parallel to gravity) and choose the surface orientation so that normals point downward. The gravitational deployment process is formulated as minimizing the immersion f's gravitational potential energy:

$$U(f) := \int_M f \cdot z \, dA,$$

where z is the height axis vector oriented opposite gravity and scaled by the gravitational acceleration constant. Note that dA is the area element induced by an isometric immersion of M (for which we assume the material density is 1) and is independent of the particular immersion f.

Proposition 2. *A height field surface represented as a smooth immersion $f : M \to \mathbb{R}^3$ that locally minimizes the gravitational potential energy $U(f)$ over all smooth immersions satisfying $dA_f \leq dA^+$ and Dirichlet conditions $f = f_{tgt}$ on ∂M, must (i) have strictly positive mean curvature $H > 0$ and (ii) achieve the upper area bound ($dA_f = dA^+$).*

Proof. Suppose there exists a region $R \in M$ on which $H \leq 0$ or $dA_f < dA^+$. We can construct a smooth, positive bump function u compactly supported on R so that the positive normal variation $\dot{f} := uN$ decreases gravitational potential to first order:

$$\tfrac{d}{dt} U(f + tuN)|_{t=0} = \int_R uN \cdot z \, dA < 0,$$

because $N \cdot z < 0$ by the height field property. Furthermore, this variation does not violate the upper bound on area. If $dA_f < dA^+$, no bound is active in R, and the variation must be admissible. If $H \leq 0$, the area measure changes by

$$d\dot{A}_f = 2uH dA_f < 0$$

for all points in R and the variation is admissible. Therefore, f does not locally minimize gravitational potential energy. □

4.2.4 Projection to Feasible Surfaces

If the surface violates the positive mean curvature requirement, we must modify it for compatibility with our deployment mechanisms. However, we wish to keep the design as similar to the input surface as possible. Accordingly, we change the surface only where needed, leaving the regions of positive mean curvature untouched. In the regions violating the requirement,

we make the smallest change necessary in mean curvature space.

We propose the following repair process to achieve these goals: apply mean curvature flow $\dot{f} = -HN$ to each region of negative mean curvature, terminating when mean curvature reaches zero. Then, to ensure $H \geq \varepsilon > 0$, an arbitrarily small, smooth normal variation can be applied, computed, *e.g.*, by solving 4.1 with $\dot{H} = 1$ and zero Dirichlet boundary conditions.

Our repair process indeed produces the closest admissible surface in the sense of minimizing pointwise curvature distance $|H - H_0|$ almost everywhere in M (where H_0 is the mean curvature of the initial immersion): it preserves mean curvature in the positive regions and minimally adjusts each non-positive value. Curvature-based distance metrics like this are often considered good models of perceptual distance [Kim et al. 2002]. However, for the examples we tried, we can make an additional observation: the repair process also locally minimizes pointwise distances to the original surface.

We formalize the repair process as follows. For a smooth initial immersion $f_0 : M \to \mathbb{R}^3$, the regions $R_i \subset M$ on which $H < 0$ are always bounded by well-defined curves ∂R_i. The repair process cuts away each $f_0(R_i)$ and replaces it with a minimal surface $f(R_i)$ spanning the same immersed boundary curve. This viewpoint corresponds to the limit $\varepsilon \to 0$.

First, we consider the space of admissible variations one might apply to the repaired surface when attempting to move it closer to the original. We consider an arbitrary suitably regular variation $\dot{f} := R_i \to \mathbb{R}^3$ and define normal velocity $u := \dot{f} \cdot N$ for convenience. We observe that $u = 0$ on ∂R_i since the perturbed surface must still fill the same boundary curve.

The corresponding first-order change in mean curvature is [Doğan and Nochetto 2012]:

$$2\dot{H} = -\triangle_f u - (\kappa_1^2 + \kappa_2^2)u + 2\dot{f} \cdot \nabla_f H = -\triangle_f u - 2|K|u, \tag{4.1}$$

where $\kappa_1 = -\kappa_2$ are the minimal surface patch's principal curvatures. The term involving $\dot{f}$ vanishes because $H \equiv 0$, and we applied the simplification $\kappa_1^2 + \kappa_2^2 = 2|\kappa_1\kappa_2| = 2|K|$. Preserving non-negative mean curvature requires:

$$\dot{H} \geq 0 \quad \Longrightarrow \quad \triangle_f u + 2|K|u \leq 0.$$

For small $|K|$ (mildly curved repaired patches), we expect the Laplacian term to dominate and force the normal velocity to achieve its minimum on the boundary ∂R_i (*superharmonic* functions obey a minimum principle). But $u = 0$ there, forcing $u \geq 0$ inside R_i.

Furthermore, in our experiments, closest points on the original surface always lie to the negative side of the repaired patch in that, $\forall p \in f(R_i)$ and nearest original points on the surface $p^* = \operatorname{argmin}_{\tilde{p} \in f_0(R_i)} \left\| \tilde{p} - p \right\|$, we have $N \cdot (p^* - p) \leq 0$. This should be expected for moderate edits, as the curvature flow process converging to the minimal surface moves points only in the *positive* normal direction. In these cases, moving any point on our repaired surface

closer to the original surface requires a motion in the negative normal direction which, for small $|K|$, violates the non-negative mean curvature constraint.

4.3 Material Design

Our goal is to design a mechanism that deforms from an initial flat configuration into a doubly-curved target surface when actuated by inflation or gravity. The regular auxetic linkages that we study in Chapter 3 have two key obstacles to overcome when it comes to rapidly deployable structures, namely (i) a perfectly regular lattice encodes no information about the target shape, necessitating some kind of "scaffolding" such as a 3D print to guide assembly, and (ii) there is no clear way to *actuate* such a surface, which must be laboriously pointwise-aligned to the mold and deformed by hand. These observations motivate us to (i) encode the target shape into the linkage by considering a *spatially varying* pattern rather than a regular one, and (ii) consider geometries that can be rapidly deployed via inflation or gravity, as studied in Section 4.2.

Discrete Conformal Geometry

A key motivation for starting with the Kagome lattice is that, as discussed in Chapter 3, deformations of this lattice behave at the large scale like conformal mappings with bounded scale factor. This loose analogy is made a bit more precise by making a connection to the Cauchy-Riemann equations: for both conformal maps and the lattice, infinitesimal planar motions are determined by real degrees of freedom at the boundary. Another connection recently made by Lam [2017] is that infinitesimal rotations of the lattice can be described as discrete harmonic functions (in the usual sense of the cotangent Laplacian), mirroring the fact that for the logarithmic derivative $\log(z') = u + \imath\theta$ of a holomorphic map z, the two components u, θ describing scaling and rotation (resp.) are conjugate harmonic. To date, however, there is still no complete discrete theory of conformal maps based on the Kagome lattice that includes finite deformations, nor conformal immersions in $\mathbb{R}^3$. Nonetheless, adopting the conformal point of view allows us to leverage well-developed tools from computational conformal geometry for the purpose of designing deployable mechanisms.

Mechanical Properties

From a mechanical point of view, linkages based on the Kagome lattice are flexible enough to produce a wide variety of curved surfaces and already have a locking mechanism built-in: stretching the material to four times its original area fully opens the linkage, blocking further expansion. In fact, one can easily show that the linkage is rigid (albeit unstable) in its fully open configuration; additional forces such as gravity or air pressure help to stabilize the fully open state. We take advantage of these mechanical properties to aid deployment. In particular, we adapt the pattern to achieve a spatially varying (rather than constant) maximum bound on

expansion across the surface. When deployed, the varying expansion leads to out-of-plane buckling; thus the linkage must assume a curved configuration.

The geometric and mechanical pictures can of course be linked: the bound on expansion in the discrete linkage can be modeled by a bound on the conformal scale factor e^u of a smooth conformal map, and the buckling exhibited by the deployed linkage is approximately determined by the *Yamabe equation* $\Delta u = e^{2u}K$ relating the logarithm of the scale factor to the Gaussian curvature K of a smooth surface approximating the target geometry. To explore designs for our mechanical linkage, we therefore adopt a strategy based on geometry: first, we compute a conformal map from the plane to the target surface, and read off the scale factors $\lambda_{\text{tgt}} := e^u$. We then use these factors to design or "program" a spatially-graded pattern that approximately matches the corresponding maximum expansion at each point. When fully expanded, a mechanism based on this pattern should approximate the desired target shape. Below we first consider the uniqueness of the deployed configuration, before detailing how to program the desired maximal expansion factor into our discrete triangular linkage.

4.3.1 Uniqueness

The spatially varying maximal extension factor uniquely determines the fully expanded linkage's metric. In other words, the deployed shape is completely determined up to isometric deformation. Does this mean that the metamaterial uniquely encodes the target shape? In general, the answer is no. For instance, the material alone cannot distinguish between "bumps" with negative or positive mean curvature since both produce the same metric distortion. However, in this case our specific deployment methods provide additional regularization: they always produce surfaces of positive mean curvature, eliminating this ambiguity.

Convex surfaces are known to be unique up to global rigid transformations. Surprisingly, the question of whether smooth closed surfaces can be *flexible* in $\mathbb{R}^3$ (*i.e.*, admit infinitesimal deformations preserving the metric) remains an open problem in differential geometry [Ghomi 2017]. So far, no counterexamples have been found, and in practice, all of our examples deployed to their proper target configurations.

4.3.2 Auxetic Linkages with Locally-Controlled Stretching

We now consider how to adapt the regular triangle auxetic linkage structure to impose a spatially-varying upper scaling bound tailored to the conformal scale factor λ_{tgt}. We begin with the following observation: taking the standard linkage pattern (with length stretch factor λ in the range $1 \leq \lambda \leq 2$) and pre-stretching by $2/\lambda_{\text{tgt}}$ yields a new material with the stretching bounds $\lambda_{\text{tgt}}/2 \leq \lambda \leq \lambda_{\text{tgt}}$. Effectively, this pre-stretching limits the amount of additional expansion possible until the fully opened configuration is reached (see Figure 4.3). This reduces our problem to producing a linkage with a spatially-varying pre-stretch in its flat configuration. The challenge now is to piece together patches with different pre-stretch. As illustrated in

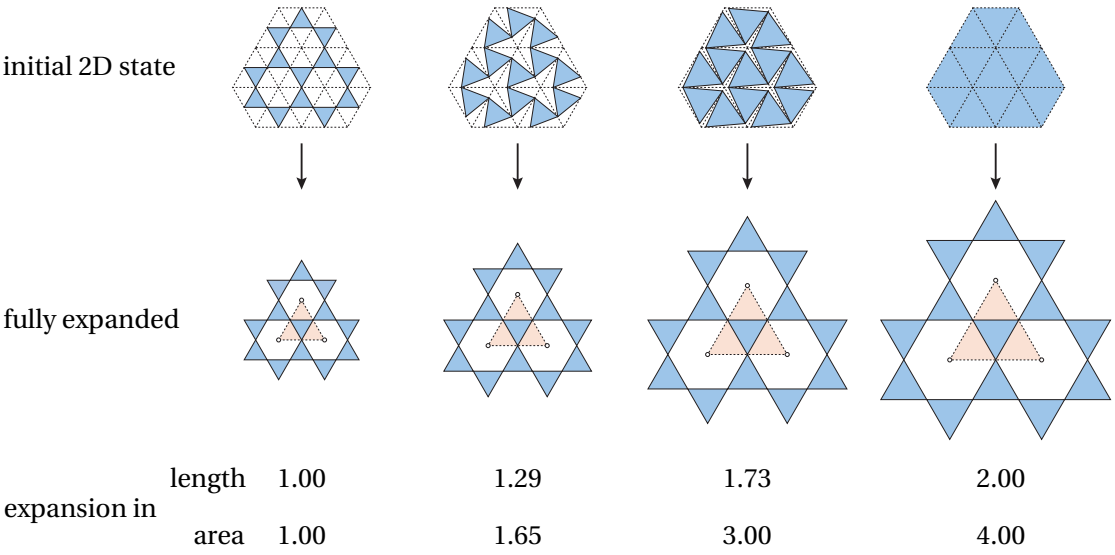

Figure 4.3 – Spatially variable maximal expansion of the linkage can be achieved by scaling and rotating the linkage triangles in the initial 2D state. When already fully opened (left), no more expansion is possible. When fully closed (right), the linkage can expand to increase by a factor two in length (or a factor of four in area). Partially opening the initial configuration allows varying the scale factor, indicated by the size of the orange triangles connecting the barycenters of the openings.

Figure 4.3, this can only be done by scaling the triangles, as will be detailed below.

Figure 4.4 shows an example and provides a comparison between our spatially graded auxetic linkage and the regular pattern from Chapter 3. Note that the nonuniform linkage structure no longer fully opens *or closes* in the plane like the regular auxetic linkage could; once any region (hexagonal opening) in the pattern fully opens or fully closes, further expansion/contraction requires spatially varying the stretch factors, inducing curvature that forces the structure into 3D.

4.4 Material Optimization

In this section, we describe our computational workflow and the optimization algorithm for computing the deployable auxetic linkage for a given design surface.

4.4.1 Preprocessing

Our first step is to analyze the input surface to ensure that it satisfies the positive mean curvature requirement. As discussed in Section 4.2.4, we correct infeasible surfaces by applying

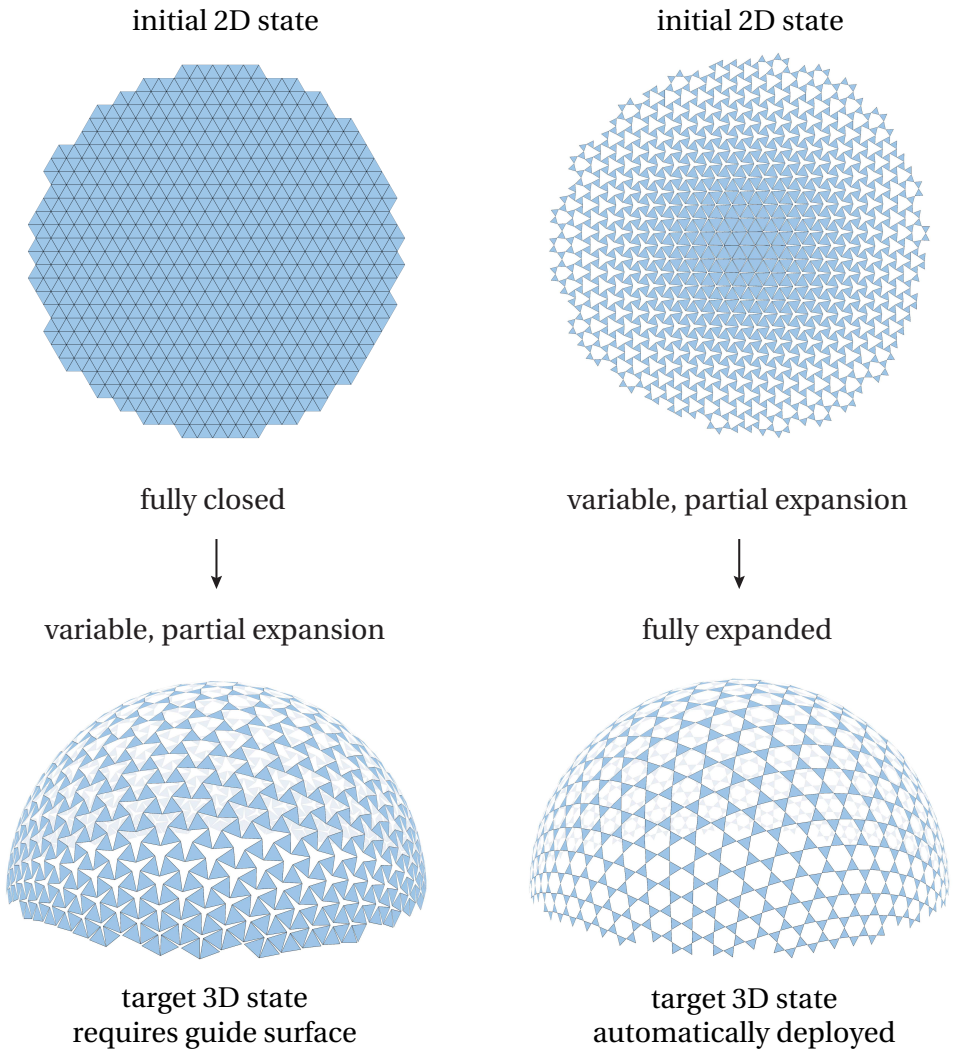

Figure 4.4 – The method in Chapter 3 (left) uses a uniform, fully closed initial 2D state and achieves its target state with variable partial openings. Proper deployment thus requires a guide surface and precise manual alignment. In contrast, our spatially varying initial openings in the 2D state allow encoding the target surface in the flat configuration, facilitating automatic deployment by maximal expansion without the need of any guide surface (right).

mean curvature flow adapted to operate only on regions of non-positive mean curvature(see also Figure 4.6). We use implicit integration for the flow as proposed by Desbrun et al. [1999]:

$$(M^t + hL^t)\mathbf{x}^{t+1} = M^t\mathbf{x}^t,$$

where M is the mass matrix, h is the step size, L is the positive semidefinite cotan Laplace matrix, $\mathbf{x}$ is a matrix of vertex positions (one row per input surface vertex), and the superscripts indicate the iteration number. We run this flow until convergence updating only the positions of vertices with non-positive mean curvature.

Given the corrected input surface S, our goal now is to find the 2D layout of the triangular linkage that, when deployed to maximal expansion, approximates S as closely as possible. Figure 4.5 illustrates the main steps of our algorithm.

4.4.2 Conformal Flattening and Remeshing

We first compute a conformal map $f : S \to \Omega$ from the target surface S to a planar domain $\Omega \subset \mathbb{R}^2$ using the methods of Sawhney and Crane [2017]. We check if the conformal scale factors are within the bounds prescribed by the linkage mechanism, and, if necessary, introduce cone singularities at user-selected locations to reduce scale distortion as described below. Next, we sample the parametric domain Ω with a regular equilateral triangle mesh M_{2D} that defines the base structure of our linkage. The user selects the resolution and orientation of this mesh to match her design intent. Lifting M_{2D} onto S by the inverse map f^{-1} yields M_{3D}.

4.4.3 3D Linkage Optimization

We now obtain an initial guess for the fully-opened linkage structure by constructing the medial triangle for each triangle in M_{3D} (*i.e.*, inscribing a triangle by connecting edge midpoints; see 4.5). While this initialization is already close to the desired target configuration, the discrete nature of the lifting function introduces inaccuracies that necessitate further optimization. In particular, we need to ensure that the linkage triangles remain equilateral and are maximally expanded everywhere while staying close to the target surface. Fortunately, these objectives can be formulated easily in the context of the projective approach of Bouaziz et al. [2012]. Specifically, to obtain the linkage's curved target configuration L_{3D} we minimize an energy function E_{L3D} defined as the sum of three different objective terms over the vertex positions $\mathbf{x}$,

$$E_{L3D}(\mathbf{x}) = \omega_1 E_{\text{expand}}(\mathbf{x}) + \omega_2 E_{\text{equi}}(\mathbf{x}) + \omega_3 E_{\text{design}}(\mathbf{x}), \tag{4.2}$$

with weights ω_i. Each term can be formulated as a sum of constraint proximity functions of the form $\phi(\mathbf{x}_c) = \|\mathbf{x}_c - P(\mathbf{x}_c)\|_2^2$, where $\mathbf{x}_c$ is the vertex set involved in the specific constraint, and P denotes the projection operator to the constraint set, as detailed below.

We observe that in the fully expanded state, the hexagonal openings formed by the linkage must attain maximum area. By Cramer's theorem [Niven 1981, p. 236], this maximum is achieved when all vertices of the opening lie on a circle.

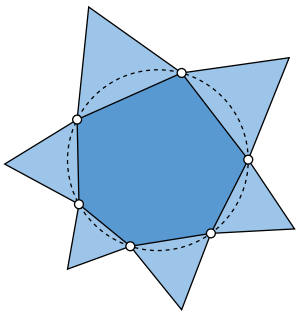

We thus introduce the expansion term

$$E_{\text{expand}} = \sum_{h \in H} \|\mathbf{x}_h - P_C(\mathbf{x}_h)\|_2^2,$$

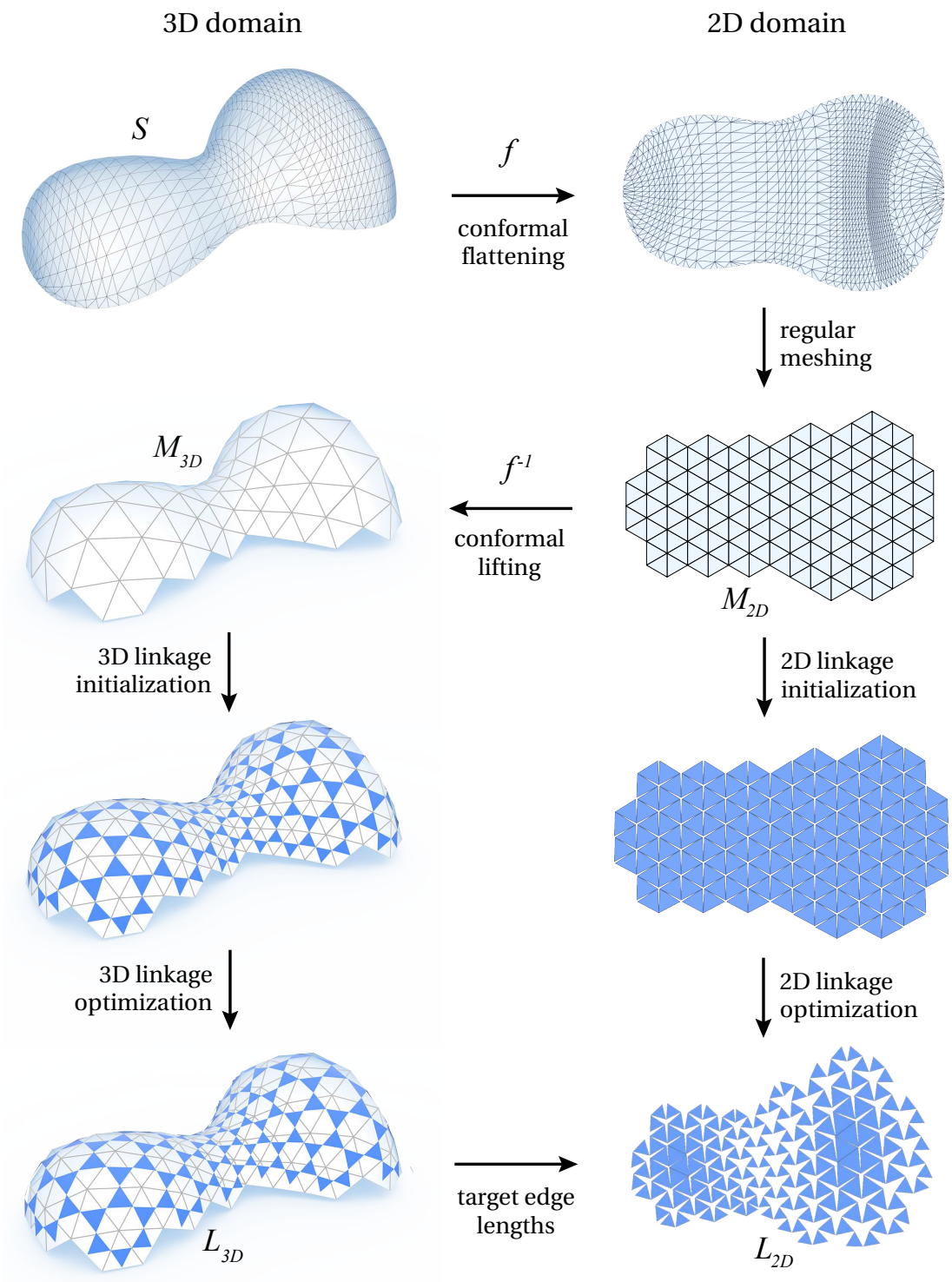

Figure 4.5 – Sketch of the optimization algorithm for computing the spatially graded auxetic linkage for a given input surface S.

where h is an index set of vertices in a particular hexagonal opening, and H is the collection of all such index sets in the linkage. $P_C(\mathbf{x}_h)$ defines the projection to the circle closest to the vertices of $\mathbf{x}_h$ computed as described in [Bouaziz et al. 2012].

Contrary to the uniform pattern used in Chapter 3, the linkage triangles need to vary in scale to introduce spatially varying maximal expansion. In order to let triangles scale freely but keep their equilateral shape, we introduce the energy

$$E_{\text{equi}} = \sum_{t \in T} \|\mathbf{x}_t - P_T(\mathbf{x_t})\|_2^2,$$

where t is the index set of the vertices of a triangle, T is the set of all linkage triangles, and P_T is the projection to the closest equilateral triangle, computed using shape matching as described in [Umeyama 1991].

Finally, to keep the linkage close to the design surface, we apply positional constraints of the form

$$E_{\text{design}} = \sum_{v \in V} \|\mathbf{x}_v - P_S(\mathbf{x}_v)\|_2^2,$$

where v is a vertex index, V is the set of all linkage vertices, and P_S defines the projection to the closest point on S.

The minimization of E_{L3D} then follows the typical local/global iteration strategy (see also [Sorkine and Alexa 2007]): the local step computes all the constraint projections involved in the objective terms for the fixed current vertex positions; the global step subsequently solves for the optimal vertex positions keeping the constraint projections fixed. Details on the precise definitions of the projection operators and the corresponding numerical solver implementations can be found in [Bouaziz et al. 2012] and [Deuss et al. 2015].

4.4.4 2D Linkage Optimization

The 3D optimization provides us with the curved target configuration L_{3D} of the linkage in its fully opened state. Now we need to find the contracted linkage in the plane that defines the material rest state to be fabricated. We formulate this problem as a second projective optimization. We first apply the necessary topological cuts to convert M_{2D} into a regular triangular linkage L_{2D} with uniform triangle sizes (Figure 4.5). Note that this flat linkage has a one-to-one vertex correspondence with the deployed linkage L_{3D}. Next, we optimize the 2D vertex coordinates $\mathbf{u}$ of L_{2D} so that the triangles assume the edge lengths of L_{3D}. This is again easily implemented using a projective edge length constraint of the form

$$E_{\text{edge}} = \sum_{(i,j) \in E} \|(\mathbf{u}_i - \mathbf{u}_j) - P_E(\mathbf{u}_i, \mathbf{u}_j)\|_2^2,$$

where (i, j) denotes the vertex indices of an edge and E is the set of edges of the linkage. The operator

$$P_E(\mathbf{u}_i, \mathbf{u}_j) = \frac{\|\mathbf{x}_i - \mathbf{x}_j\|}{\|\mathbf{u}_i - \mathbf{u}_j\|}(\mathbf{u}_i - \mathbf{u}_j)$$

projects to the closest edge with target length $\|\mathbf{x}_i - \mathbf{x}_j\|$ of the corresponding edge in the 3D linkage L_{3D}. We also add the non-penetration constraint proposed in Section 3.3.2 to avoid collisions in the 2D state. The final optimized linkage L_{2D} then defines the flat auxetic surface material that deploys to the desired target state.

4.4.5 Algorithm Parameters

Our implementation of the projective constraint solver is based on the open-source library provided by Deuss et al. [2015]. We set the weights in (4.2) to $\omega_1 = \omega_2 = 100$ and $\omega_3 = 1$ and apply between 100 to 600 iterations, depending on the mesh resolution. Total computation time for 3D and 2D optimization for a linkage with 8k triangles is 1.8 minutes on a standard desktop computer with 4.2 GHz computed on a single core.

4.4.6 Cone Singularities for Programmable Auxetics

When the conformal scale factors exceed the maximal expansion limits of the auxetic linkage, we need to insert cone singularities in the conformal map to reduce scale distortion. Singularities can also be mandated by the input surface's topology (to satisfy the Gauss-Bonnet theorem). These singularities correspond to boundary vertices of M_{2D} where the incident boundary curves (seams) close up when lifted to M_{3D} by the conformal map.

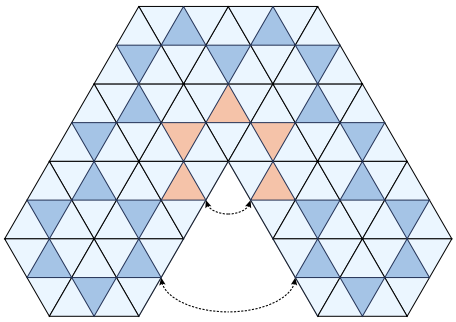

Because conformal maps preserve angles, for the surface to close up and form a regular equilateral triangle mesh when lifted to M_{3D}, the sum of triangle angles around the singular vertex in M_{2D}—referred to as the *cone angle*—must be an integer multiple of $\frac{\pi}{3}$. In the inset figure, we show an example with cone angle $\frac{5\pi}{3}$ and see how the equilateral triangle mesh (and an inscribed linkage) will properly stitch together when lifted to M_{3D}. Figure 4.7 shows examples with singularities of cone angle $\frac{4\pi}{3}$ and $\frac{5\pi}{3}$. Note the difference with the regular auxetic linkage singularities, where only even multiples of $\frac{\pi}{3}$ are feasible (Section 3.2.2). Singularities with odd multiples of $\frac{\pi}{3}$ are unable to connect in the closed configuration while preserving the linkage topology (see Figure 4.13).

4.4.7 In-plane Opening

In case the computed scale factors do not fully cover the maximal admissible range, the resulting 2D linkage can still be expanded in the plane until one hexagonal opening is fully opened—or contracted until one opening is fully closed—as shown in the inset.

We leverage this property for the fabrication result in Figure 4.1 to reduce the material stresses at the triangle joints during inflation by pre-opening the linkage as much as possible; this minimizes the rotation necessary to achieve the fully expanded configuration. In the optimization, we add an additional angle constraint [Deng et al. 2015] with a low weight that either tries to expand or contract the linkage in the flat configuration, depending on the user's preference.

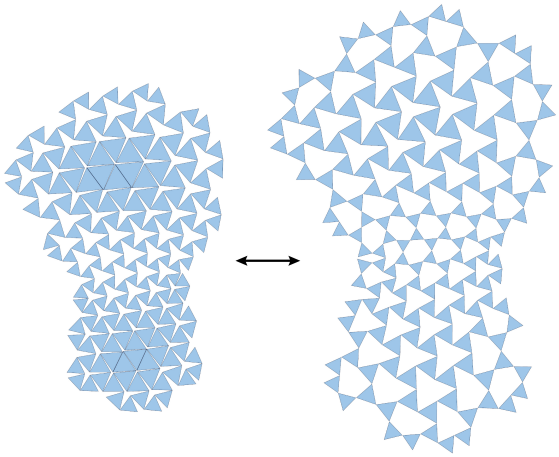

4.4.8 Filling in the Surface

If the user desires a deployed surface without holes, the hexagonal openings in the fully expanded linkage can be filled in by layering four sheets offset from each other:

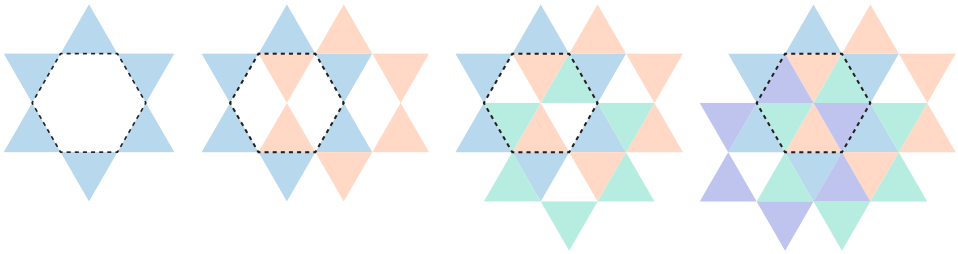

However, simply creating copies of the optimized linkage L_{3D} and shifting them does not work: this would effectively translate the deployed surface itself and also would lead to triangles imperfectly fitting the hexagonal holes due to the varying scale factors. Instead, these sheets must be designed by offsetting copies of M_{2D} in the parametric domain and lifting/optimizing them in 3D. Figure 4.12 shows an example of a surface filled in with this method.

4.4.9 Verification by Simulation.

Recall that the above optimization maximizes surface expansion of the linkage on a target surface of positive mean curvature. In the smooth setting, our analysis in Section 4.2 shows that this defines a deployable target surface under inflation or gravity. To verify that this observation also holds in the discrete case, and that the computed linkage does indeed define

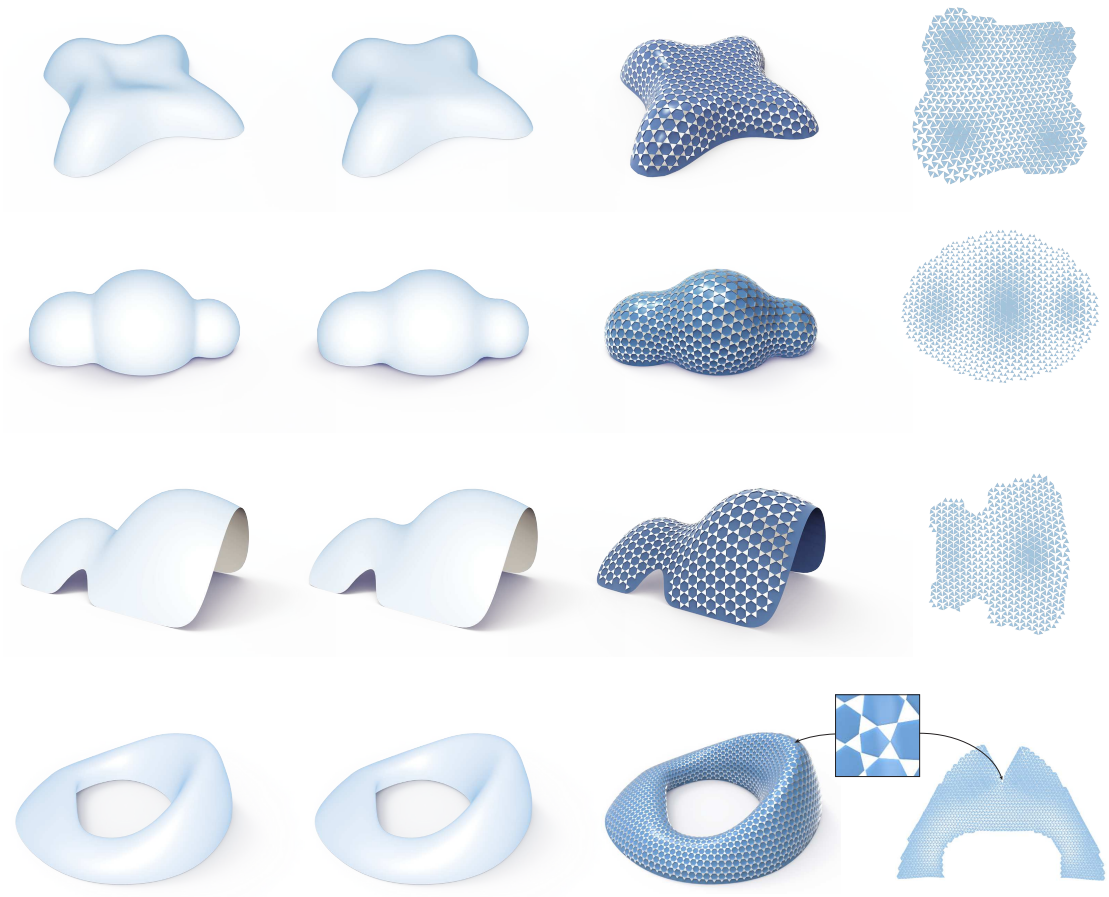

Figure 4.6 – From left to right: input design surface, modified surface with positive mean curvature everywhere, optimized linkage in deployed state, 2D rest state of flat-fabricatable material. In the bottom row, a singularity of cone angle $\frac{5\pi}{3}$ is introduced to bring the conformal scale factors to lie within the admissible range.

a steady state under inflation or gravitational loading, we apply a physics-based simulation. We use the same projective approach as we did for linkage design, using only edge length constraints to keep triangles rigid and positional constraints to fix the boundary. We augment this optimization with dynamics as proposed in [Bouaziz et al. 2014] by applying forces on the linkage vertices. For inflation, the force vectors are oriented along the surface normal, for gravity along the fixed negative vertical axis.

Our experiments confirm that the linkages properly deploy, reaching an equilibrium configuration very close to L_{3D}. For each of our examples, we compute the maximal distance between vertices in L_{3D} and their corresponding pairs in the equilibrium linkage. We then compute a maximum relative vertex deviation for each model by dividing this distance by the length of the bounding box diagonal. The model with the worst relative deviation has a maximal vertex distance of 0.0513 and a bounding box diagonal of 28.5, giving a relative deviation of 0.0018. In all cases, the differences are nearly imperceptible.

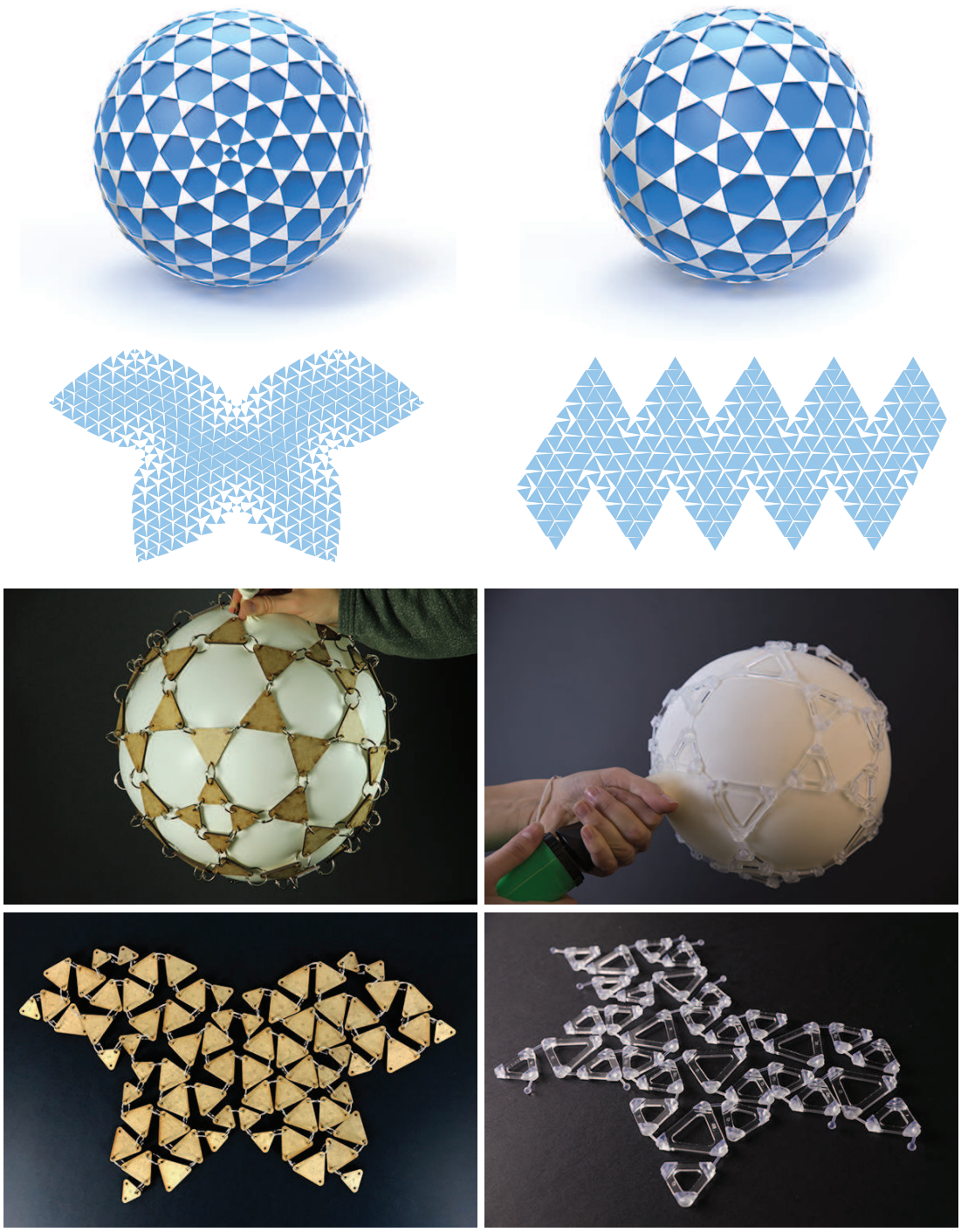

Figure 4.7 – Cone singularities are required when modeling closed surfaces such as the sphere. The simulated models at the top depict examples with cone angles of $4\pi/3$ and $5\pi/3$, respectively. At the bottom, lower-resolution fabricated prototypes with cone angles of $4\pi/3$ are shown, one fabricated by laser cutting with triangles connected by rings, one 3D printed with ball joint connections. The surfaces have been closed manually along the boundary elements prior to inflation.

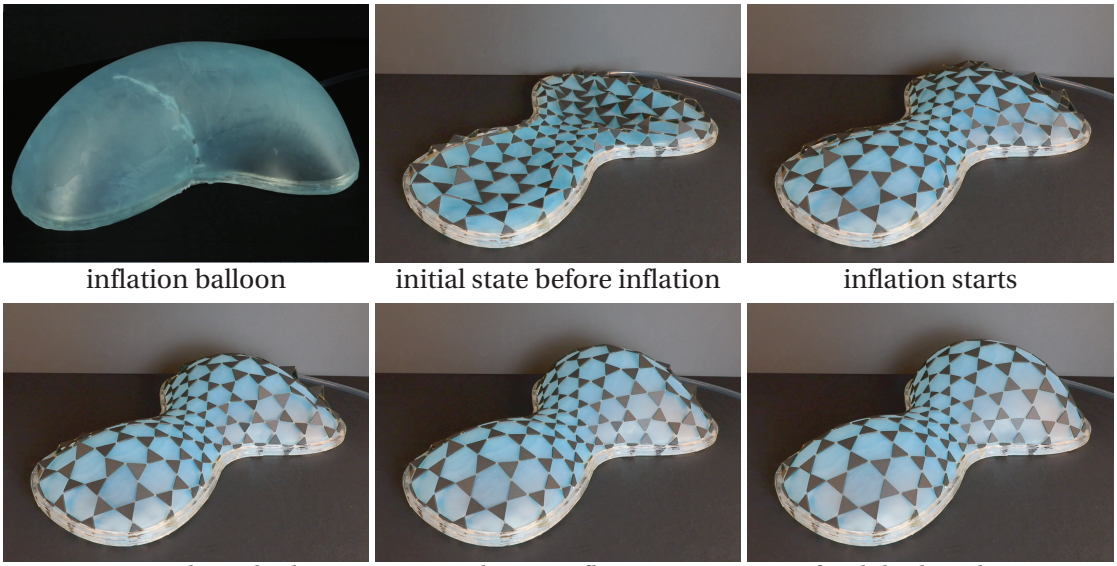

Figure 4.8 – Deployment via inflation. A generic rubber ballon is attached to a support frame. When inflated, the balloon has no information about the target shape. The linkage blocks further inflation when it reaches the fully expanded state, forming the encoded target shape.

4.5 Results

We verify our material design and optimization approach with a number of numerical and physical experiments, illustrating a range of potential application fields with different materials and usage domains. Figure 4.6 shows several examples of our deployable auxetic surfaces computed with the optimization algorithm described in Section 4.4.

4.5.1 Fabricated Prototypes

Figure 4.1 shows how one can deploy a doubly-curved freeform surface from a single flat sheet of material. The expansive forces for deployment are created by a generic rubber balloon that is inflated against the support plane. As the balloon is pumped with air, it presses against and deforms the linkage until the target shape is reached at maximal stretch (Figure 4.8). The balloon has no information about the target shape, which is solely encoded in the linkage pattern computed by our algorithm. Note that while the inflated surface has positive *mean* curvature everywhere as required by our analysis, both positive and negative Gaussian curvature are present in the target shape.

Figure 4.7 shows how cone singularities are introduced when inflating closed surfaces. In contrast to regular auxetic linkage (see Figure 3.7), our spatially-varying auxetic pattern can approximate a sphere with cone angles of both even and odd multiples of $2\pi/3$.

The structure of Figure 4.9 illustrates how gravitational forces can be used to deploy the target

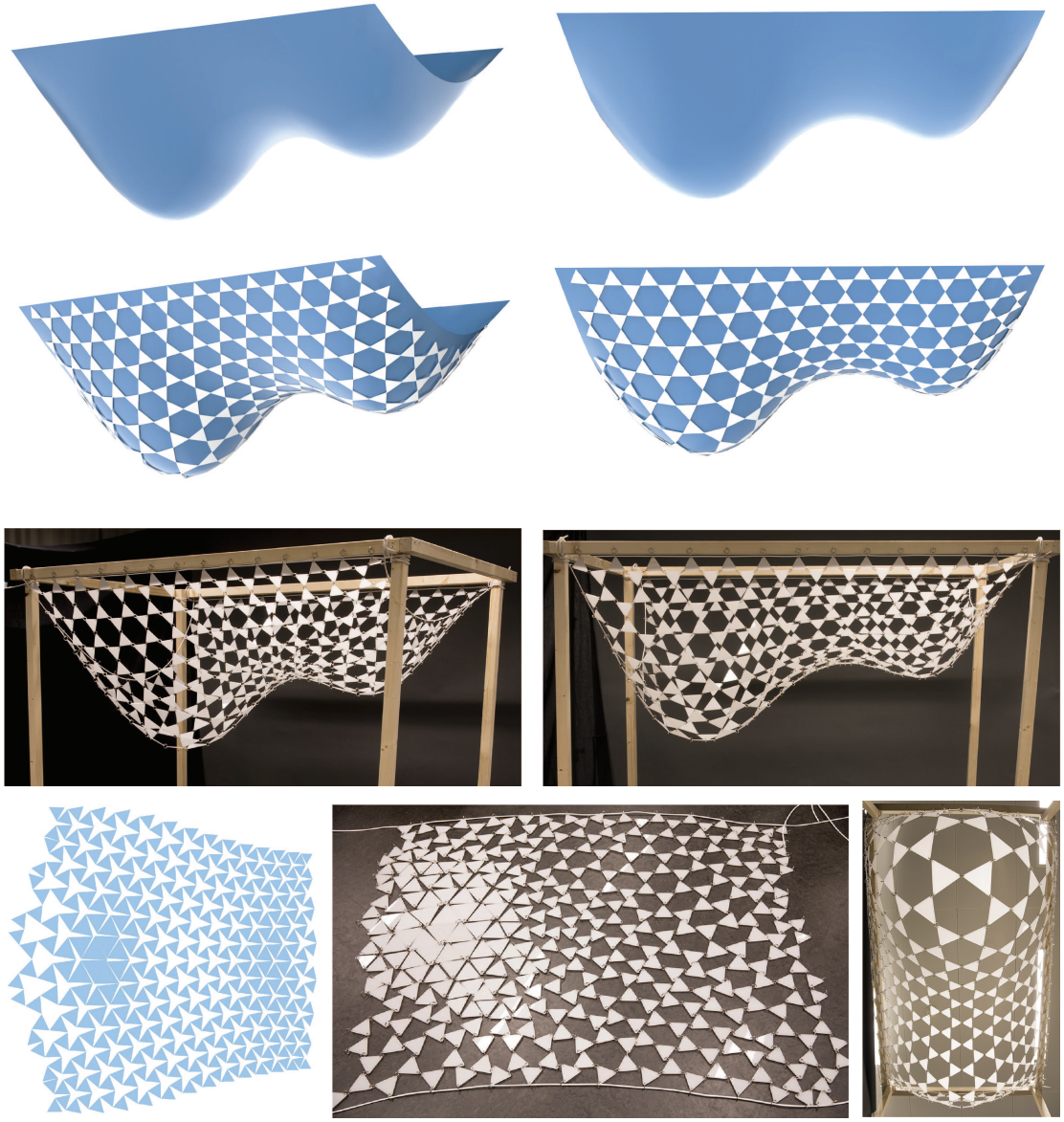

Figure 4.9 – Deployment via gravity. The auxetic linkage shown on the bottom left has been optimized to match the input design surface in the top row. The structure has been assembled in the flat state (bottom middle) from individually laser-cut triangles that are connected by metallic rings to enable the rotational motion of the linkage triangles. When lifted onto the rectangular support, the surface automatically deploys into its target shape. The linkage is in maximal expansion everywhere (bottom right). Note that boundary vertices are fixed along the long edges of the support rectangle, and connected with strings on the short edges.

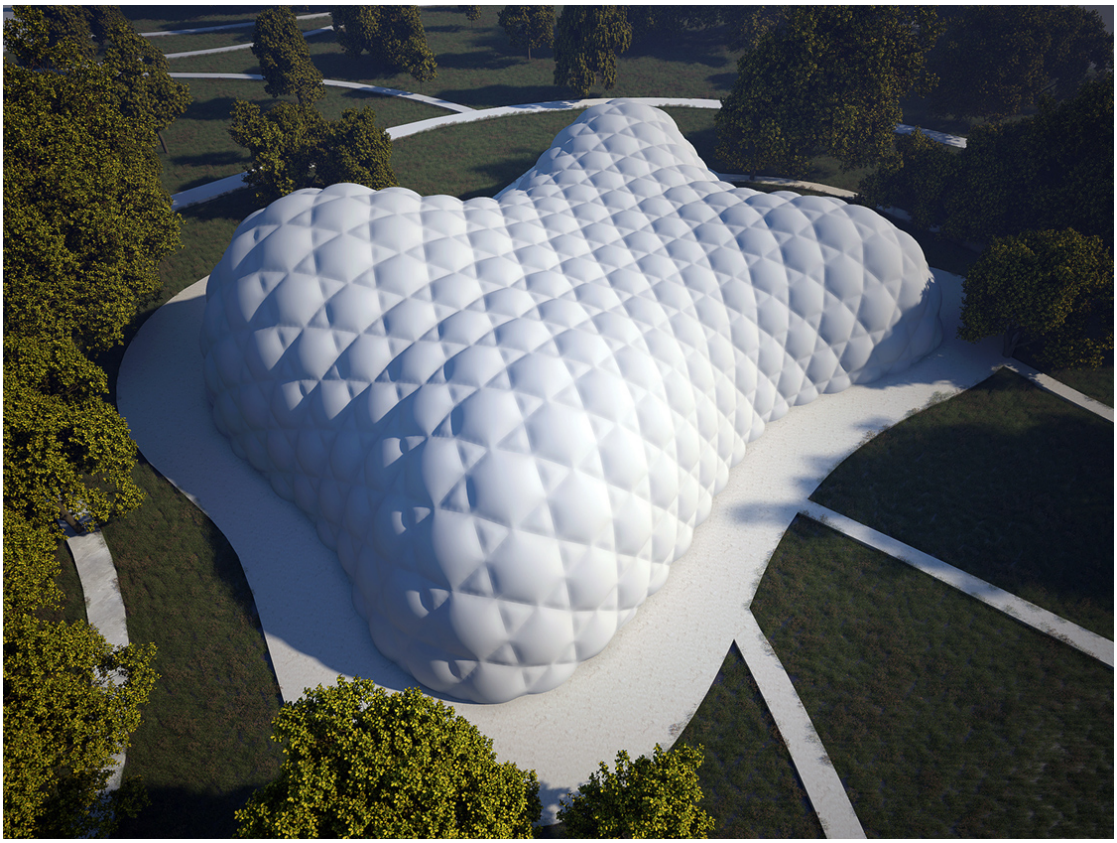

Figure 4.10 – Design study of deployable architecture. The freeform inflatable dome can be used as a semi-permanent, relocatable space.

shape from the flat rest configuration. The resulting structure is in tension everywhere and can thus be used for physical form-finding of self-supporting structures in analogy to the famous approach of Antoni Gaudi [Fernández 2006].

4.5.2 Application Case Studies

Figure 4.10 highlights an application in deployable architecture to construct a relocatable, semi-permanent structure. Compared to the simple geometries of existing inflatable structures, our approach supports a broader class of freeform shapes, which allows adapting the structure to the design-specific interior space requirements.

Figure 4.11 illustrates an application in personalized medicine, where a deployable freeform coronary stent can be customized to a specific patient. The stent is fabricated as a flat structure, then rolled into a thin cylinder. When inflated, the stent adopts the desired freeform shape to best advance blood flow in the critical artery.

Figure 4.12 illustrates how multiple layers of our programmable auxetic material combine to create the approximately closed surfaces of a freeform chair (deployed by gravity).

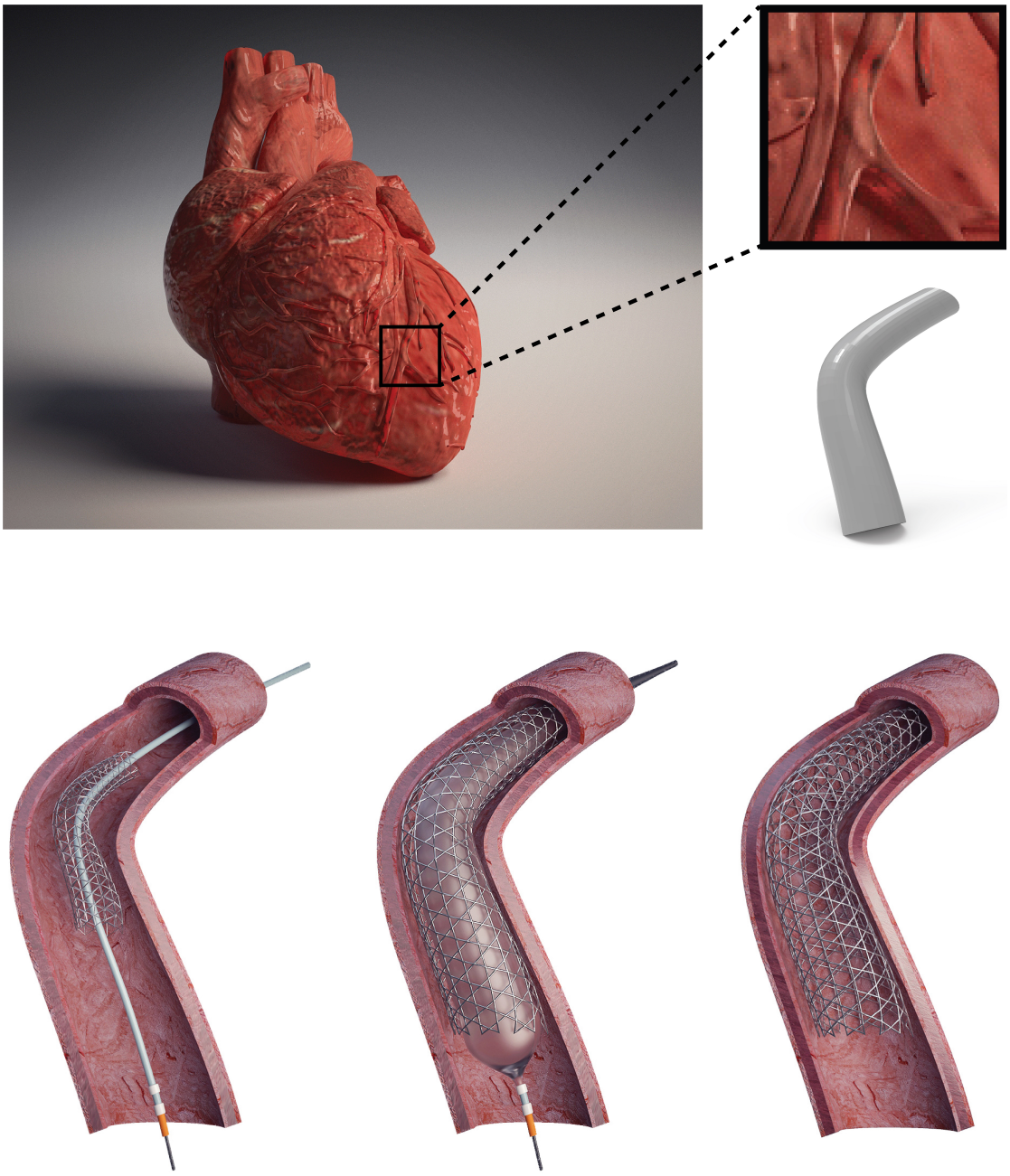

Figure 4.11 – Conventional heart stents are straight and typically chosen by the surgeon from a set of standard sizes. Recent research has shown the benefits of curved stents [Tomita et al. 2015]. Our method can be used to create freeform curved heart stents that can be adapted to the specific geometry of the patients' blood vessels. Top row shows a zoom on the target vessel region and its 3D model reconstruction to approximate with our programmable auxetics. The stent is administered with a catheter to the correct position (bottom left) and inflated to its target geometry (bottom middle, right).

Figure 4.12 – Design study of a freeform chair realized using four layers of spatially graded auxetic material to fully cover the surface (see Section 4.4 for details).

4.6 Additions and Remarks

Our current deployment strategies using inflation or gravity can only actuate a subset of the surfaces realizable with a graded auxetic linkage: those with positive mean curvature. Adding additional constraints—for example, in the form of strings connecting certain vertices and thus preventing expansion towards positive mean curvature—can enlarge the space of deployable shapes. It is an interesting question for future work to find a minimal set of such constraints for a given target surface. One potential example is shown in Figure 4.14 in the case of inflatable sofa.

For closed surfaces and surfaces requiring singularities, we must introduce cuts to flatten the material to the plane (see Figure 4.7 and bottom row of Figure 4.6). While this retains the benefits of planar fabrication, the deployment becomes more complex, as the material has to be re-connected along the cut seam prior to actuation (also see Figure 4.13).

Our results confirm that we obtain a close approximation of the target shape even for relatively coarse resolutions of the linkage. However, although we have observed several connections to conformal mapping theory that inform our optimization algorithms, we currently do not have

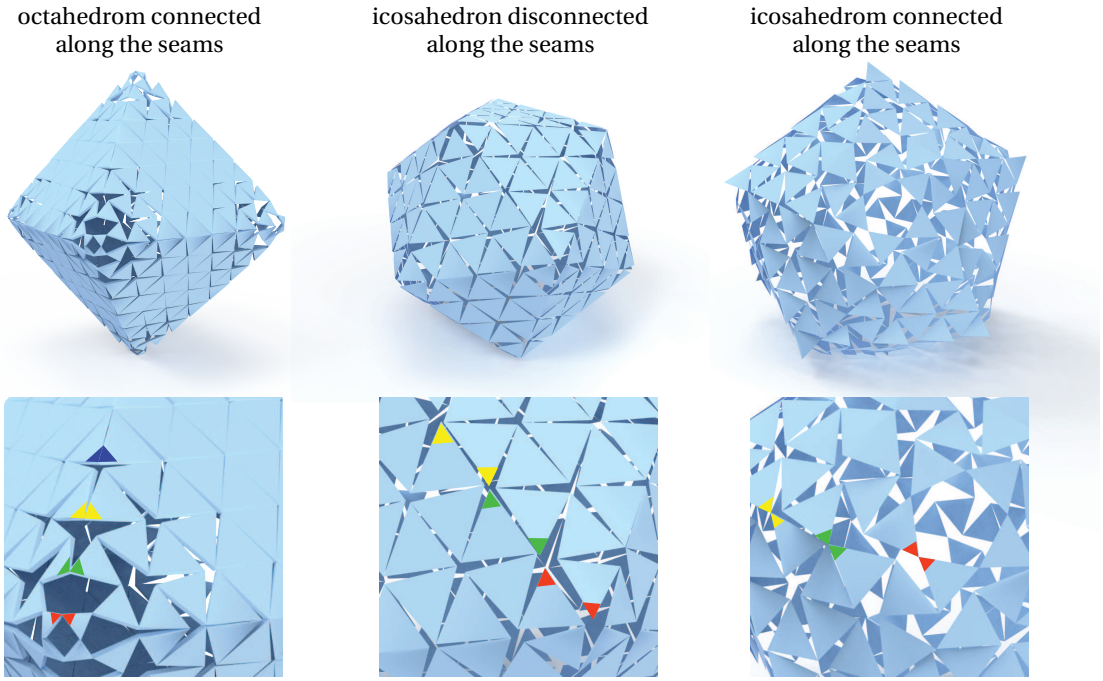

Figure 4.13 – Singularities with cone angles of even multiple of $\pi/3$ are easier to connect along the seams. The correct linkage topology can be obtained even when the linkage is in the maximally closed configuration. Here we show closing of the linkage along the seams of two sphere examples from Figure 4.7. In order to preserve the linkage topology, the same color vertices need to be connected. Odd multiple of $\pi/3$ singularities can be connected only in the fully opened configuration, hence the icosahedron needs to deform to obtain a completely closed linkage.

a *discrete* theory for the geometry of graded auxetic linkages. Developing such a theory in the context of discrete differential geometry is an exciting avenue for future work.

While our fabricated prototypes provide a proof-of-concept for the physical realizability of our designs, we do not address important fabrication-related issues at different scales. In particular, it is crucial for robust deployment to optimize the joints connecting the linkage triangles. It also would be interesting to test techniques for permanently rigidifying the deployed structure. We hope that our work can stimulate new research in material science, mechanical engineering, and architectural construction to study these questions in more detail.

4.7 Discussion

Numerous physical objects, such as ship or airplane hulls, building facades, clothing, and many consumer products are fabricated by shaping thin, initially planar materials. The shaping process typically involves bending, stretching, or otherwise deforming the material

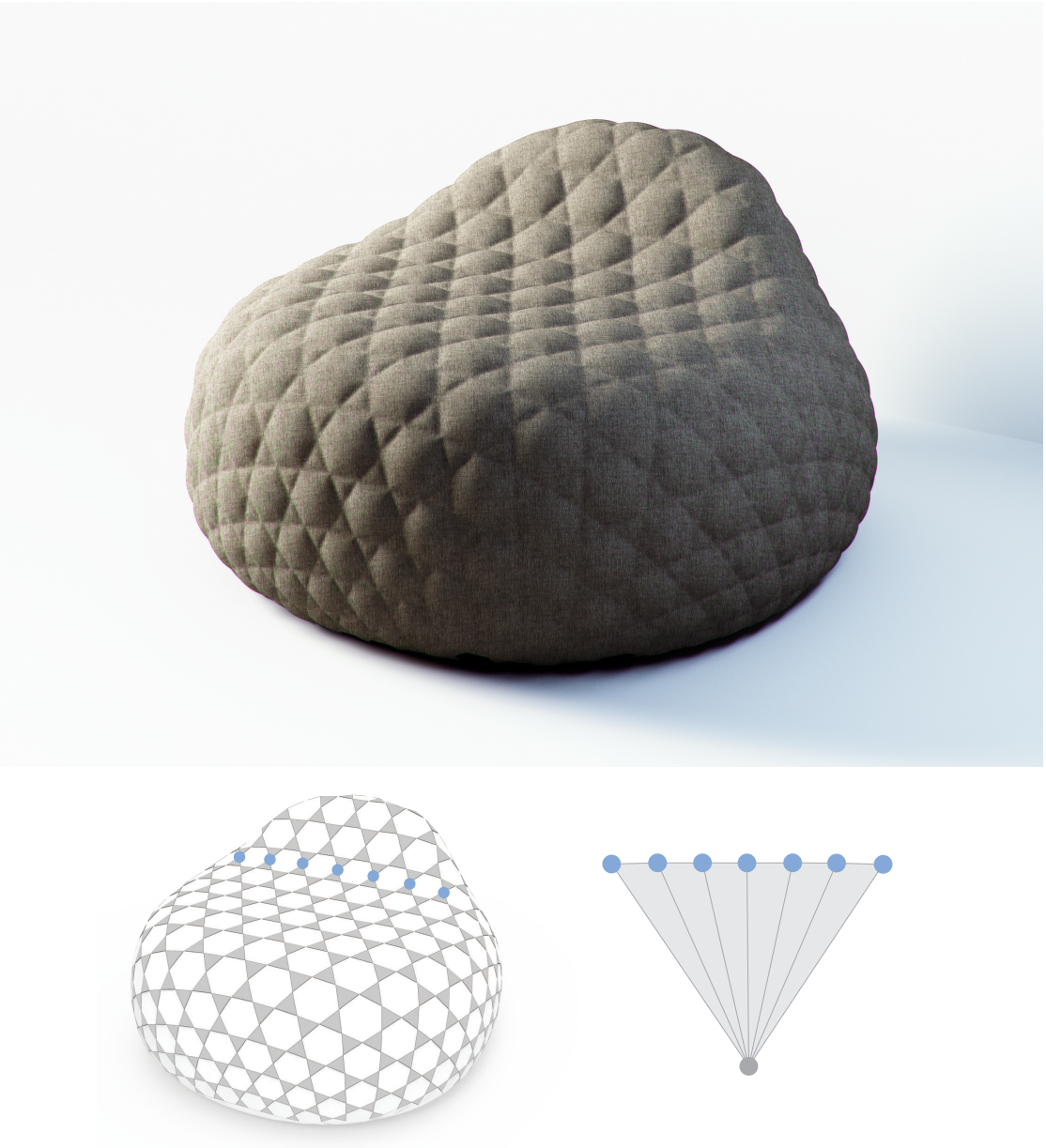

Figure 4.14 – Example of inflatable furniture with a negative mean curvature region. To prevent the middle region from inflating outwards, a few linkage vertices in the negative mean curvature region could be fixed with internal connection such as strings or material patches similar to [Skouras et al. 2014].

using a mold or scaffold to guide the deformation towards the desired 3D shape. Deployable structures provide an alternative where the shaping process and resulting target geometry are implicitly encoded in the structure itself. We have shown that spatially graded auxetics are well suited to implement deployable surface structures. Instead of rationalizing a 3D design surface for a given homogeneous material, we spatially optimize the material itself.

By carefully controlling the expansion behavior of the material, we directly program the target surface geometry into the flat 2D rest state. Inflation or gravitational loading then automatically deploys the rest state towards the target, which is assumed when the material cannot expand any further. As a consequence, we can leverage the efficiency of 2D digital fabrication technologies without requiring any additional 3D guide surface. Our deployment strategy is robust and reversible, which supports efficient storage and transport and enables new applications for semi-permanent structures.

The combination of limited-expansion auxetic material with a deployment via inflation or gravity imposes limits on the space of realizable shapes. Our analysis clearly delimits this space and directly informs our computational solution, providing designers with an effective tool to realize new deployable structures not possible before. Further improvements are possible by introducing internal connections, although this could complicate the fabrication process.

Note

This chapter is mainly based on the following publication:

> Mina Konaković-Luković, Julian Panetta, Keenan Crane, and Mark Pauly. Rapid Deployment of Curved Surfaces via Programmable Auxetics. *ACM Transactions on Graphics (Proceedings of SIGGRAPH), 2018*.

The candidate contributed most of the scientific developments and implementation of this publication.

5 Forward Design of Deployable Auxetic Shells

This chapter proposes an interactive computational design method for deployable auxetic shells. We realize deployable auxetics as triangular linkages that can be actuated with simple expansive mechanisms to assume a desired freeform target shape. The core feature of these structures is that the target shape is directly and uniquely encoded in the 2D linkage layout. As a consequence, the structure can be fabricated and assembled in the plane and automatically deployed to its 3D target configuration without the need for any scaffold, formwork, or other temporary support structure. We focus on automatic deployment via inflation or gravitational loading for which a rigorous theoretical analysis has been given in Chapter 4. This chapter builds upon these results and presents optimization-based direct manipulation tools to edit and adapt an auxetic linkage structure to effectively explore design alternatives. In addition, our solution enables simulation-based form-finding, where the desired target surface is interactively constructed using the deployment mechanism as a form-finding force. We present several design case studies that demonstrate the effectiveness of our approach and highlight potential applications in architecture.

5.1 Introduction

Architectural structures are commonly composed of multiple elements that are assembled on-site. Construction is executed by incrementally placing components at their target 3D location, using scaffolding or other support mechanisms to guide element positioning and maintain structural stability during intermediated stages of the assembly. Especially for intricate free-form geometry, the complexities of this process can pose severe challenges.

Deployable structures offer an interesting alternative for construction. They typically can be assembled in a significantly simpler state and then deform to the desired target shape. A prominent example is elastic grid shells that can be assembled on the ground and mounted into a double-curved form, see [Lienhard 2014] .

We propose a computational design system for a new type of deployable structure based on

a triangular auxetic linkage. Our structures can be fabricated and assembled in the plane and deployed to their target position using either inflation or gravity. No additional guiding scaffold is required because the target shape is *directly encoded* in the planar assembly. The key concept is a spatially graded auxetic pattern, where individual triangular elements are scaled to *program* the maximal local expansion factor required to achieve the global target shape. Paired with an area-expanding deployment, such as air-inflated cushions or gravitational loading, this yields a simple and robust way to realize double-curved surface structures.

Deployable auxetics offer a number of benefits:

- Form-defining deployment: The double-curved target shape is automatically achieved via expansive deployment from a planar configuration. Inflation or gravitational loading (for height field geometry) can be used to maximally stretch the material everywhere, which then constrains the surface to the desired target configuration.

- Simple fabrication: The geometric simplicity of the auxetic linkage directly transfers to fabrication. Variable-sized triangles can easily be cut using CNC fabrication technology from a wide variety of approximately inextensible base materials, such as fabrics, wood, metals, or plastics. Mass fabrication of joints is possible since all node connections are identical.

- Rich geometry: Deployable auxetics admit a rich and well-defined design space, enabling new forms beyond the existing classes of structures deployable from planar rest states.

This chapter complements the work from Chapter 4 where we proposed a post-rationalization process to find a deployable auxetic linkage for a fixed input design surface. While post-rationalization is an important design tool, it offers limited support for evaluating design alternatives or engaging in material- and construction-aware exploration. The functional and aesthetic properties of the resulting auxetic linkage are difficult to anticipate when designing the required reference geometry. In particular, the sizing of triangles and specific boundary alignment result from a global optimization that does not necessarily yield easily foreseeable results. It is therefore beneficial to provide direct manipulation tools to further edit and adapt the optimized structure to better meet the design goals. Our work introduces such direct editing operations. The presented computation-assisted design system allows for effective design space exploration of deployable auxetic structures and gives the designer full control of the final deployed surface geometry. In addition, our approach provides tools for computational form-finding, where the desired target surface is interactively constructed using the deployment mechanism as a form-finding force.

scale factor	boundary	dynamics	2D rest state	3D top view	3D side view
prescribe	free	collisions			
fixed	fixed	gravity			
fixed	free	expand			
smoothing	free	expand			
fixed	set to circle	gravity			

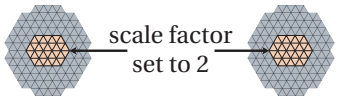

Figure 5.1 – A simple form-finding example to illustrate our atomic editing operators and their effect on the auxetic structure. After prescribing scale factors, we resolve collisions which expands the material in the plane. Applying gravity forces pushes the linkage to a deployed state. However, when applying full expansion, we observe that the surface cannot be realized as a height field, mainly due to the sharp transition in scale factors. After smoothing the scale factors and letting the boundary evolve freely, we obtain a consistent height field surface. Finally, we show how to constrain the boundary onto a circle curve.

5.2 Design Space Exploration and Form-Finding

As discussed above, the desired target shape in the deployed state can be programmed into the auxetic structure by optimizing for suitable maximal expansion factors across the linkage, which in turn determine the spatial layout and sizing of linkage triangles. The post-rationalization method is highly efficient when a designer has a clearly defined target surface and a good intuition of how the material behaves. Nevertheless, the indirect nature of this method provides only limited support for exploring design alternatives or discovering new forms that are directly informed by the material and deployment mechanism. More direct manipulation is required to offer interactive design control in a tight feedback loop.

However, trying to manipulate the deployed geometry by directly displacing linkage vertices is not appropriate since the consistency of the design cannot be easily maintained. Linkage vertices would need to be moved in a coordinated way to respect the complex global coupling imposed by the material structure and deployment mechanism, which becomes virtually impossible without computational support.

This is why we propose interactive, optimization-assisted design operators. Specifically, we allow the designer to directly modify the maximal scale factors of the linkage and impose design-specific geometric constraints. We then apply optimization to jointly determine the 2D rest shape and the 3D deployed shape. Since this optimization can be executed at interactive rates, the designer gets immediate feedback on her edits, while being freed of the complexities of maintaining consistency of the structure.

We found that the following editing operators yield an effective toolbox for design space exploration:

- *Prescribing scale factors:* We provide a painting interface where the designer can directly prescribe the desired maximal scale factors in the allowable range [1,2]. Increasing scale factors allows the material to stretch more under deployment, while reducing scale factors locally shrinks the deployed surface.

- *Smoothing scale factors:* Sharp transitions in scale factors can lead to non-smooth surface appearance and, in extreme cases, surface wrinkles. Spatially averaging the scale factors evens out these variations and generally leads to smoother deployed surfaces. Controlling the amount of scale factor smoothing yields different design alternatives.

- *Boundary control:* The user can directly edit the 3D boundary curves of the design and control the behavior of boundary linkage vertices, which can slide along boundary curves. Since the boundary has a strong influence on the overall shape of the deployed surface, we also allow boundary linkage triangles to deviate from equilateral shape, which can improve the overall surface quality.

- *Geometric constraints:* The user can further control the geometry of the deployed surface by imposing additional geometric constraints, for example on the planarity of certain edge curves, symmetry of selected vertices, or smoothness of the surface.

We also provide a separate form-finding optimization for the boundary curves. This can be helpful when the total area of the chosen linkage is not well-suited for the imposed boundary curve, e.g., when there is too much material or too little for the surface to conform to the boundary. In such cases, we apply an expansion force on the linkage to fully expand the hexagonal openings and let the boundary vertices move freely to their preferred positions.

Figure 5.1 illustrates how these design operators can be employed in an interactive form-finding design.

5.2.1 Algorithm

Our interactive design system runs a constraint-based optimization algorithm to provide direct visual feedback on the flat and deployed state of the auxetic linkage. This optimization is based on the projective approach of [Bouaziz et al. 2014; Deuss et al. 2015] that allows combining different geometric constraints to model the material behavior and the dynamics of the deployment mechanism.

Painting or smoothing scale factors provides constraint targets for the triangle edge lengths. We apply point-to-curve constraints to limit the movement of boundary vertices to the boundary curves. When optimizing for the boundary, we apply circle constraints on the hexagonal openings to expand the surface, as the maximal area is achieved when all hexagon vertices lie on a circle, see [Niven 1981], page 236 (also in Section 4.4). We also use non-penetration constraint proposed in Section 3.3.2 to prevent the inter-penetration of neighboring triangles.

Additional geometric constraints, e.g., planarity of user-selected edge curves in the deployed state, can easily be formulated on the linkage vertices. Gravitational deployment is modeled with a constant downward force, while inflation is approximated by outward-pointing normal forces. These forces are converted into geometric constraints in an implicit time integration solver as discussed in [Bouaziz et al. 2014].

We found it helpful in some editing situations to introduce an additional regularizing constraint to prevent triangles from twisting. This is achieved by adding a planarity constraint with very small weights with respect to the other active constraints on the vertices $\mathbf{v}_{i_0}, \ldots \mathbf{v}_{i_4}$ for each pair of neighboring triangles (see inset figure). This basically penalizes the angle between the normals $\mathbf{n}_{i_1}$ and $\mathbf{n}_{i_2}$.

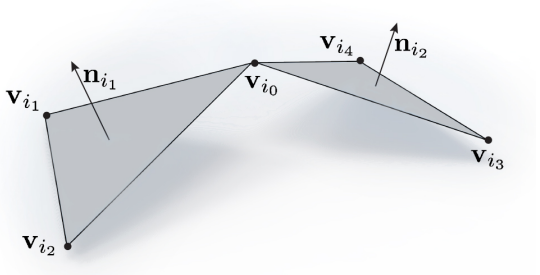

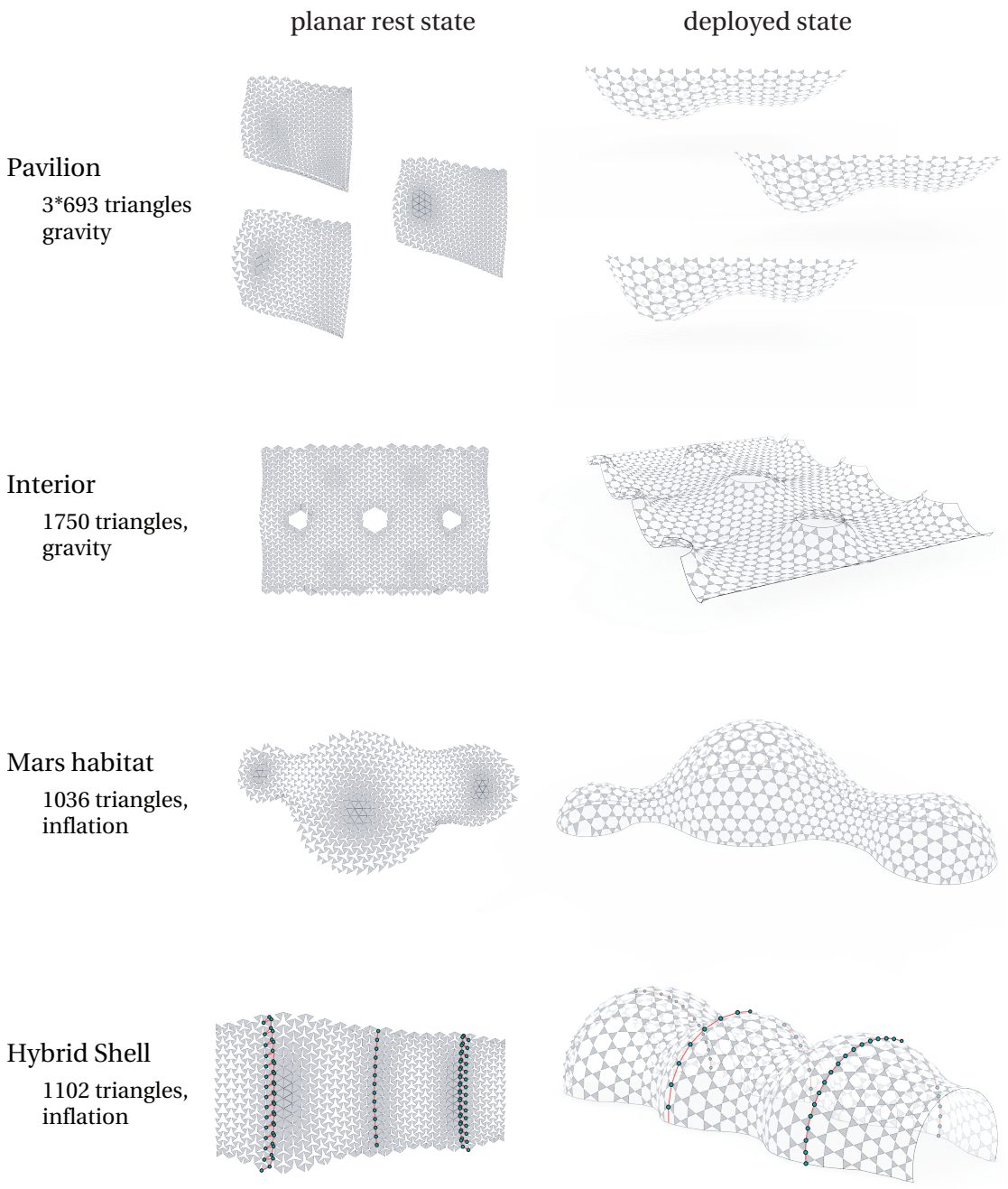

Figure 5.2 – Four design examples shown in planar rest configuration and final deployed state. The number of auxetic linkage triangles and deployment method is indicated. In the bottom row, the highlighting shows three sets of vertices and edges that are each constrained to lie on a plane in the deployed 3D model to create planar support beams. See Figures 5.4 to 5.5 for detailed renderings.

Figure 5.3 – Interior decorative cladding. This hanging structure has been optimized to align with the boundary constraints imposed by the ambient space. The designer controls the shape by interactively modifying scale factors while allowing the triangles to slide along the boundary curves.

During editing, the constraint-based optimization solves for the linkage vertex positions in the flat 2D state and the deployed 3D state to provide immediate visual feedback on the performed edits. For more implementation details and an open-source library of the projection-based solver, we refer to www.shapeop.org.

5.3 Application Case Studies

We illustrate the potential of our computational design approach with a number of application case studies for deployable auxetic structures. The design process starts with an initial 2D triangular linkage, either obtained by the post-rationalization process from Chapter 4 or simply created as a uniform triangle pattern when designing from scratch. We then apply a series of editing operations as described above to explore design alternatives. The final output of this interactive form-finding process is a specific triangular linkage with spatially varying triangles that can be fabricated and assembled in the plane and deployed automatically to the desired target shape. Four example designs are summarized in Figure 5.2 and described in more detail below.

Figure 5.3 shows a gravity-deployed structure in an interior space, with potential use cases of acoustic dampening or decoratively masking of functional components such as AC pipes, wirings or insulation. This example shows how directly prescribing scale factors and smooth-

Figure 5.4 – Multi-layer shading pavilion deployed by gravity.

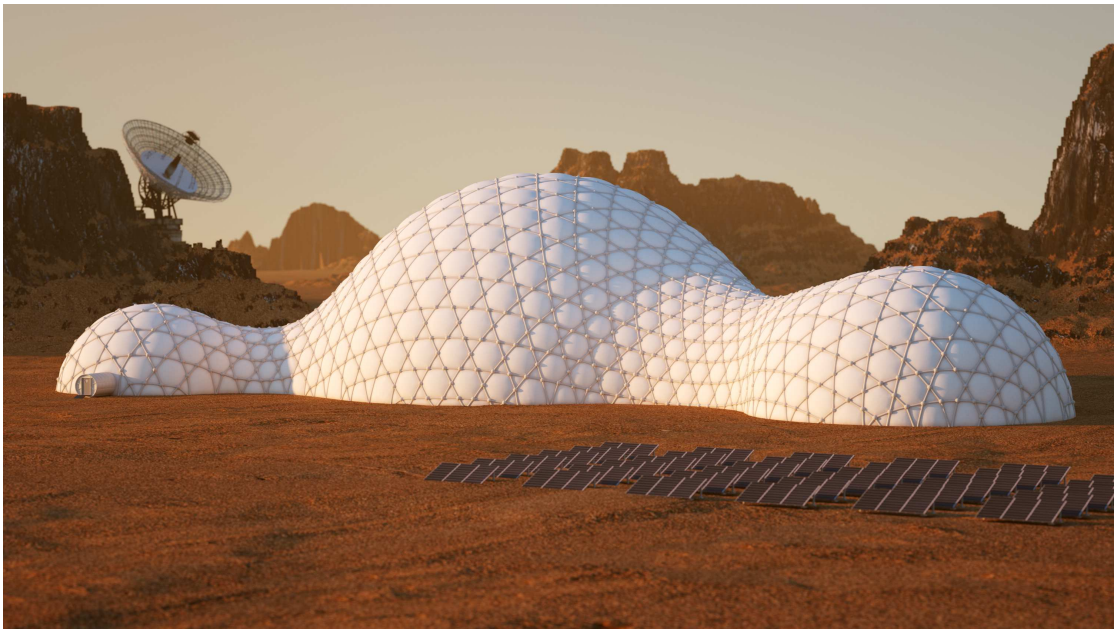

Figure 5.5 – Inflatable freeform dome for a potential Mars habitat.

ing them in combination with detailed boundary control offers effective ways to integrate a deployable auxetic structure into an existing space with precisely defined boundary constraints.

Figure 5.4 shows a design study of a shading pavilion, realized as a linkage of inextensible fabric triangles that are connected with ring joints at the triangle vertices. As a hanging structure, the surface deploys under gravity to its desired double-curved target state. This design has been created in an interactive form-finding process from a uniform auxetic linkage that is subsequently manipulated using our design operators to create three design variations. These are combined in a multi-layer structure, which allows designing spatially varying opacity to optimize the shading performance of the structure for the anticipated use case.

In Figure 5.6, we demonstrate how we can incorporate additional geometric constraints to optimize the design. In this example, we impose planarity constraints on selected edge and vertex curves of the auxetic linkage to form structural arches that can reinforce the inflated shell. The planarity of these arches significantly simplifies their fabrication. The arches can be mounted after deploying the linkage.

Figures 5.5 and 5.7 show a speculative design study for habitats on Mars. Since the atmospheric pressure on Mars is 100 times lower than Earth's, the interior must be pressurized. This motivates the use of inflatable structures that can be efficiently erected from flat configurations, offering the additional benefits of low weight and compact storage. Our deployable auxetics offer a rich design shape space, so we can optimize the shape of the freeform domes to match interior space objectives.

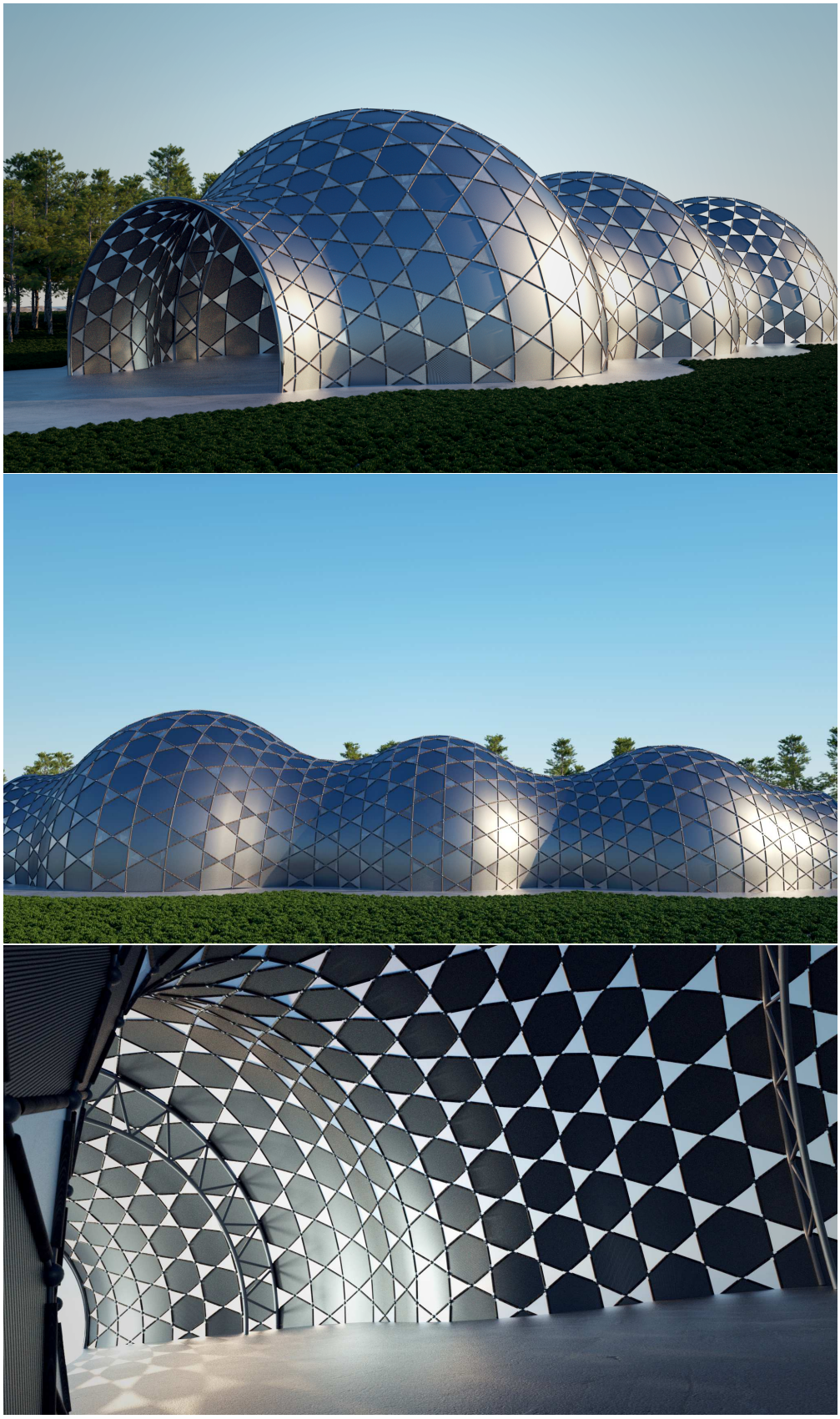

Figure 5.6 – A hybrid shell structure integrates planar support arches in the interior into a deployable auxetic surface.

Figure 5.7 – Another example of an inflatable dome for a potential Mars habitat with different interior space objectives.

5.4 Discussion

We have shown how optimization-assisted shape exploration yields an effective method for designing deployable structures based on auxetic triangular linkages. By directly manipulating the form-defining geometric properties, i.e., the material scaling and the surface boundary, the designer obtains full control of the deployed shape while being shielded from the complexity of maintaining consistency between the 2D assembly state and the 3D deployed state. Automatic deployment via inflation or gravity allows transforming compact flat assemblies into freeform surfaces without the need of any supporting structures or complex construction process. Fabrication requires only 2D technologies such as sawing or laser cutting to produce the triangular panels. Despite this inherent simplicity, expressive freeform surfaces can be realized for a variety of different use cases.

Our approach is not limited to linkages with triangular panels. After obtaining the final linkage configuration from the form-finding system, we can easily change the shape of each triangle element as long as the connecting points between elements remain fixed. The behavior of our linkage is completely determined by the arrangements of joints, and the distance between them. It does not depend on the panel shape. Hence, any collection of panel shapes that partition the plane and meet at the vertices of a regular grid can be used as a deployable linkage. Some examples are shown in Figure 5.8.

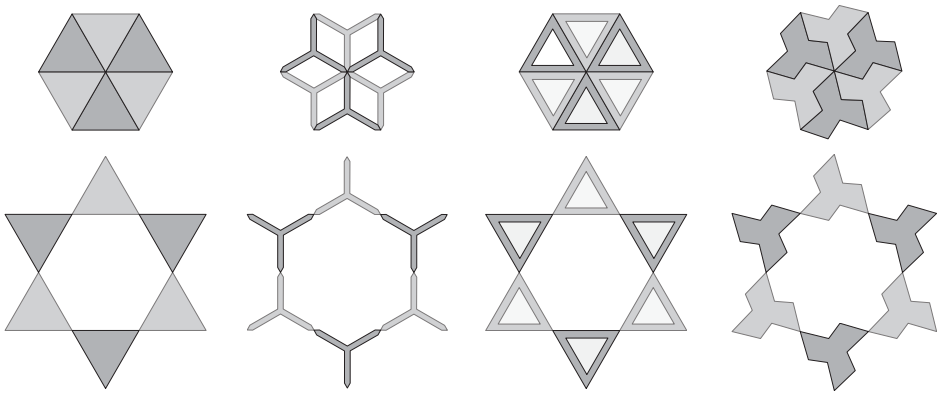

Figure 5.8 – Our method can be used with any pattern that tiles the plane and keeps the location and distance of joints the same as in the triangular pattern.

Other panels that do not partition the plane but use the same arrangement of joints can also work with our method. However, depending on the scale factor of the panels, they may not be able to assemble flat without some overlap. For some applications and choice of physical panels and joints this is not an issue. For example, relatively thin plates connected with ring joints would permit small overlap of the neighboring panels by lifting one panel on top of the other. In Figure 5.9 we use hexagonal panels to increase the shadow area covered by a single linkage layer. We can control the amount of light that passes through the linkage by controlling the shape of the panels (see Appendix D). We leave exploration of other panel shapes for future work.

A number of open questions offer numerous opportunities for future work. So far, we did not address questions of structural integrity in a systematic way, nor did we incorporate performative objectives into the optimization. For example, light transmission of the shading pavilion or the acoustic dampening for the interior cladding design study could be directly integrated into the form-finding method to yield a more informative shape exploration process. Finally, we see interesting research potential in exploring other expansive deployment mechanisms, for example based on material swelling, motorization, or pre-stressing.

Note

This chapter is mainly based on the following publication:

> Mina Konaković-Luković, Pavle Konaković, and Mark Pauly. Computational Design of Deployable Auxetic Shells. *Advances in Architectural Geometry, 2018*.

The candidate contributed most of the scientific developments and implementation of this publication.

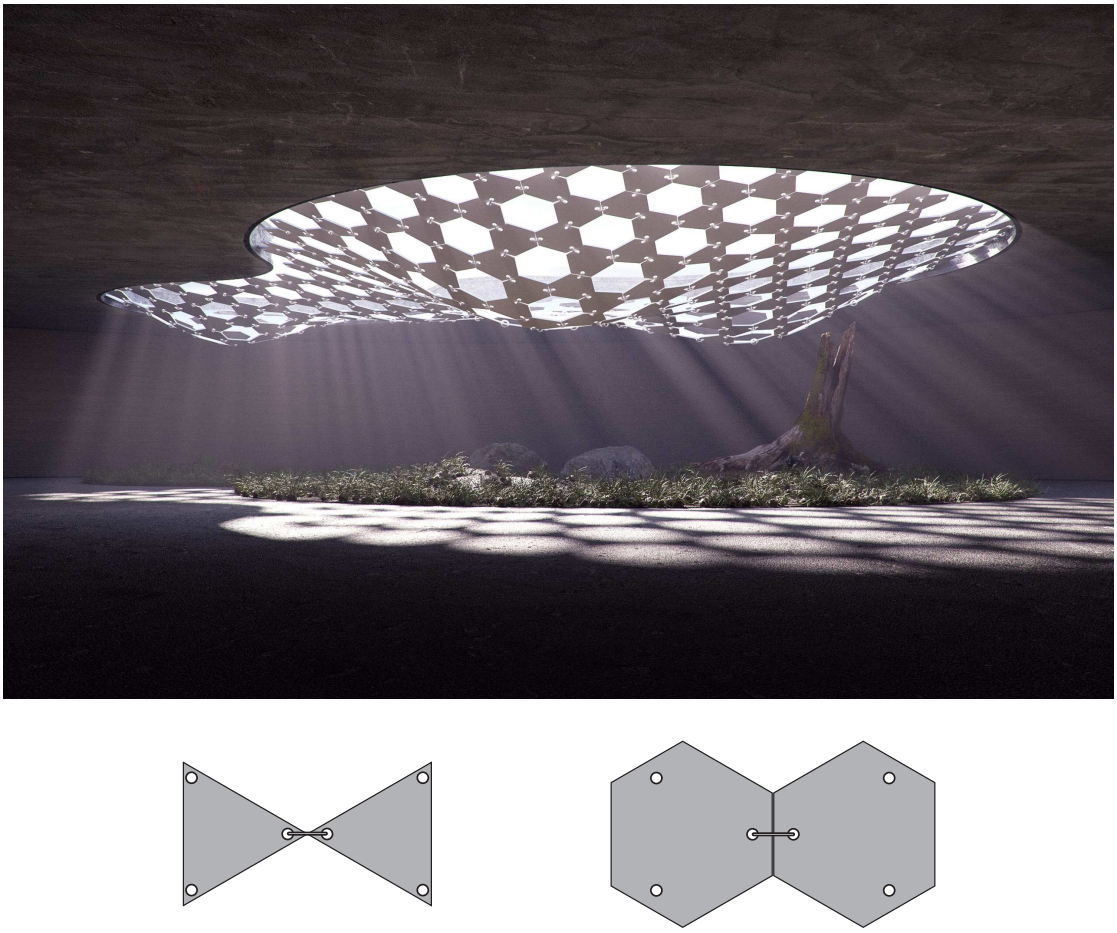

Figure 5.9 – A shading pavilion deployed by gravity demonstrating how we can control the area covered with shadow by changing the shape of the linkage elements. Here we use hexagonal panels to create more shadow than with a single layer of triangular elements. Each hexagonal panel preserves the location of the three connection points as in the triangular case.

6 Conclusion

Auxetic materials appear in various application domains. They have been used for product design, architecture, car designs, soft robots, prosthetics, sensing skins, high-performance textiles, fashion, art, etc. However, these applications were limited to very simple geometric shapes. Due to the complexity of the deformation behavior that this material exhibits, it is difficult to manually anticipate how to align and deform it to achieve the desired shape. The work of this thesis addresses this problem with computational design tools.

This thesis presented a computational method for design and fabrication via auxetic materials. We have shown that conformal geometry is a key ingredient in understanding and modeling auxetic designs. More specifically, conformal mapping is used to initialize a non-linear constraint-based optimization system for surface approximation. Conformal maps allow us to have global control over the material alignment and handle non-local dependencies inherent in the auxetic linkage. We have developed an optimization-based interactive design tool to find the final linkage configuration that closely approximates a target 3D surface. Our computational approach enables designs not possible before. A series of physical prototypes and design studies demonstrate that we can approximate arbitrary curved surfaces with an auxetic linkage.

In addition, this thesis introduced the design of programmable auxetic materials via spatially graded triangular linkages. The sizing of the triangular elements is related to the curvature of a target surface and is optimized to control the maximal local stretching of the material. The linkage can be fabricated flat and easily deployed to its final 3D configuration through expansive forces of inflation or gravitational loading. It reaches its target configuration when it cannot expand any further. This way a given 3D surface is directly encoded into the 2D pattern layout. We have shown that only surfaces of positive mean curvature everywhere can be deployed in this manner. Furthermore, a surface adaptation algorithm is proposed for surfaces that include negative mean curvature regions. Our method then finds a surface approximation and computes a 2D linkage layout with conformal mapping and constraint-based optimization. A physics-based simulation and physical prototypes validate our approach.

Finally, to complete the design process, we have developed a forward design tool for programmable auxetic materials. A designer obtains full control over the deployed shape by directly manipulating the form-defining geometric properties while being supported by the form-finding simulation based on the deployment mechanisms. We have demonstrated the effectiveness of this approach in exploring design alternatives and interactively constructing deployable linkages.

One benefit of this thesis is that the presented computational methods are scale independent. Our approach relays on a geometric abstraction of the auxetic linkages that has no limitations on the linkage size or properties of the material used for linkage elements as long as the elements remain approximately rigid. Hence our method is applicable to micro- and macro-scale designs of various base materials.

6.1 Future Work

Our work inspired a series of research papers and case studies in computer graphics, material science, product design, and architecture. For example, it is used for orthopedic casts [Rao et al. 2019], inflatable cars [Eguchi et al. 2019], and some art products. The work is still in development with scientific and industry collaborators.

6.1.1 EPFL Shading Pavilion

One of the outputs of the research presented in this thesis is the EPFL Shading Pavilion Project. We work in collaboration with architects from the EPFL ALICE laboratory and with the support of INGENI structural engineering to develop a deployable auxetic canopy (see Figure 6.1). The canopy is created with methods from Chapters 4 and 5 (see also Figure 5.9 and Appendix D). It is designed as a double-layer auxetic linkage, mounted on a circular ring and separated by a single compression pole. The two layers are aligned to create a maximal shadow area at noon during the summertime. The structure is composed of hexagonal aluminum panels connected with steel cable rings for simple and cost-efficient manufacturing. The panels can be assembled on the ground and then mounted onto the support frame to assume the target configuration. The project is planned to be constructed in early 2020 on EPFL Campus, next to the Rolex Learning Center.

6.1.2 Open Problems

A number of open problems offer numerous opportunities for future work. This thesis focuses on auxetic linkages with triangular patterns. Two-dimensional auxetic linkages with a similar deformation behavior exist in a combination of various polygonal shapes, such as quads, hexagons, octagons, or with irregular shape tilings of the plane. These patterns can also be modeled with conformal maps, but with a different scaling factor. Depending on the pattern

Figure 6.1 – Left: A side and a top view of the EPFL Shading Pavilion linkage structure. Right: A fabricated prototype of the 4 linkage elements, made from 1mm thick aluminum panels connected with uniform steel cable rings.

combination, the material can stretch less or more than the scale factor of 2 that a regular triangular linkage exhibits. Furthermore, hierarchical auxetic patterns can offer additional flexibility in surface design. Developing a general framework for auxetic patterns would be a valuable contribution.

We empirically observed that our geometric abstraction of auxetic materials based on linkages of rigid elements well approximates the behavior of the cut surface material. However, we do not model the physical behavior of the exact linkage connectors. For each material this behavior is different. It is important to conduct in-depth tests for structural performance of different cutting lines shapes, as well as the hinge and material thicknesses. We have only used "Y" shape and straight lines for cutting. Vachicouras et al. [2017] explore a variety of geometries and densities of cutting motifs for multilayer thin films of non-elastic materials, e.g., plastics, metals, ceramics. They show how rounded cutting corners reduce the mechanical failure of the material. Integrating a finite-element simulation into the design process to adapt the shape of connectors is an interesting problem.

For some applications, it is necessary to use mechanical joints to connect linkage elements. Programmable auxetics would benefit from joints that can lock in the target configuration. When the structure is deployed by inflation, the joints should be mechanically blocked in the final state. This would prevent the structure from collapsing after the pressure is lost or if it is necessary to remove the material used to inflate the auxetic linkage. For regular auxetic linkages, it would be useful to have joints with motors to control the openings. Another open question is how to optimize for a minimal number of actuators needed to transform the linkage.

So far, we have discussed sheet auxetic materials and 2D patterns. Auxetic behavior also appears in three-dimensional structures. One of the first engineered auxetic materials were 3D foams. Developing a computational method to work with volumetric auxetic patterns is an exciting avenue for future research.

Another possible research direction would be to incorporate performative objectives into the optimization system of the design method. For example, one could control the amount and the shape of the shadow generated by the pattern by adapting the linkage configuration. An interesting question is how to optimize the auxetic shape to generate a given shadow image on the ground. A fascinating effect of caustics could also be accomplished with curved auxetic surfaces. In addition, a dynamic shading system could take into consideration the sun path and change the openings in the structure accordingly.

Finally, we have not developed a discrete theory for the geometry of regular nor graded auxetic linkages. A discrete notion of Gaussian curvature, Laplace operator, etc., defined directly on the linkage could provide more insights into the geometry of the linkage surfaces for performative design. Such theory would potentially enable algorithms for general auxetic structures.

With the advances in manufacturing techniques, improvements in auxetic materials will certainly come. This thesis enables exploration of new applications of auxetic structures and hopefully inspires similar research on material design and surface approximation. Moreover, creating a global framework for design and modeling with general deformable materials is an exciting open problem. We hope that our work can stimulate new research in mechanical engineering, material science, biomedical engineering, and architecture construction to study these questions in more detail.

A Degrees of Freedom for a Trihexagonal Linkage

We here show that the number of degrees of freedom for a planar linkage is equal to the number of boundary vertices of degree 2, up to rigid motions. The basic idea is to start with the configuration space of each individual hexagon, then subtract the shared degrees of freedom. The rest is a rather tedious counting argument. Our main claim has also been validated via numerical experiment.

To begin, consider a disk-like subset of the trihexagonal tiling of the plane such that no boundary edge is contained in a hexagon—the collection of triangular faces in this subset corresponds to one of our linkages. Let V, E, and F denote the number of vertices, edges, and faces, and let $H := 2E$ denote the number of oriented edges or *halfedges*. Also let I and B denote the number of interior and boundary vertices (respectively), so that $V = I + B$, and let B_k denote the number of boundary vertices of degree k. Likewise, let F_k denote the number of faces of degree k, so that $F = F_3 + F_6$. The number of halfedges can then be expressed as $H = 3F_3 + 6F_6 + B$, i.e., we can associate three halfedges to each triangle, six to each hexagon, plus one more for each boundary edge.

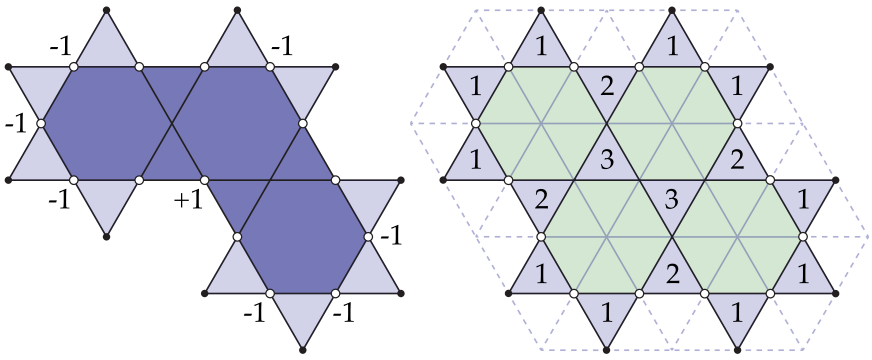

Lemma 1. *The number of degree-2 and degree-4 boundary vertices is related by* $B_4 = 2B_2 - 6$.

Proof. For brevity, we will call degree-2 boundary vertices "black" and degree-4 boundary vertices "white." Each black vertex can be uniquely identified with its two white neighbors

$(+2B_2)$, except where the polygon formed by the white vertices has a corner: at each convex corner one of the white vertices is shared (-1) and at each concave corner there is an additional white vertex $(+1)$. Since the curve turns by $\pi/3$ at each corner and by 2π in total, the overall parity must be -6. □

Lemma 2. *The number of hexagons can be expressed as* $F_6 = \frac{1}{2}F_3 - \frac{1}{3}B_2 - \frac{1}{12}(B_4 - 6)$.

Proof. Triangulate each hexagon by inserting a vertex at its centroid; call original triangles "blue" and new triangles "green." Each blue triangle is now adjacent to three green triangles $(+3F_3/6)$, except along the boundary where blue triangles with a black vertex are adjacent to only one green triangle $(-2B_2/6)$, and triangles with two white vertices are adjacent to only two green triangles $((-B_4/2)/6)$, modulo an adjustment -6 which arises for the same reason as in Lemma 1. □

Lemma 3. $3F_6 - I = B_2 - 3$.

Proof. Recalling that $V = I + B$ we have $3F_6 - I = 3F_6 - V + B$, and applying Euler's formula $V - E + F = 1$ for a disk, plus the fact that $H = 2E$ yields $3F_6 - (1 + E - F) + B = 3F_6 - 1 - H/2 + F + B$. Applying our earlier expression for H, this sum becomes $F_6 - \frac{1}{2}F_3 + \frac{1}{2}B_4 + \frac{1}{2}B_2 - 1$. Applying Lemma 2 then yields $\frac{5}{12}B_4 + \frac{1}{6}B_2 - 1/2$, and applying Lemma 1 gives $B_2 - 3$, as desired. □

Consider now that the motion of each hexagon can (independent of the rest of the linkage) be parameterized by its six exterior angles. Six quadratic constraints on edge length become 6 linear constraints on variations in position, leaving us with 3 angular degrees of freedom per hexagon (since angles specify a polygon only up to rigid motions). But since the angles around any interior vertex must sum to 2π, the linkage itself has only $3F_6 - I$ degrees of freedom—which we know from Lemma 3 is the same as $B_2 - 3$, i.e., a scalar value per degree-2 boundary vertex, up to a global rigid motion.

B Inscribing Regular Linkage Triangles into Conformally Lifted Tiling Grid

We use conformal mapping to lift the regular triangular tiling from 2D domain onto a target 3D surface. Once lifted, the tiling triangles uniformly scale with respect to the conformal scaling factor. The linkage triangles, however, have to remain rigid, *i.e.* preserve their edge lengths. Hence, the linkage triangles rotate and open to achieve the necessary scaling in area. Here we show inscription of linkage triangles (depicted in blue) into scaled tiling grid triangles (depicted in green), where the scaling factor increases from 1 on the left to 2 on the right.

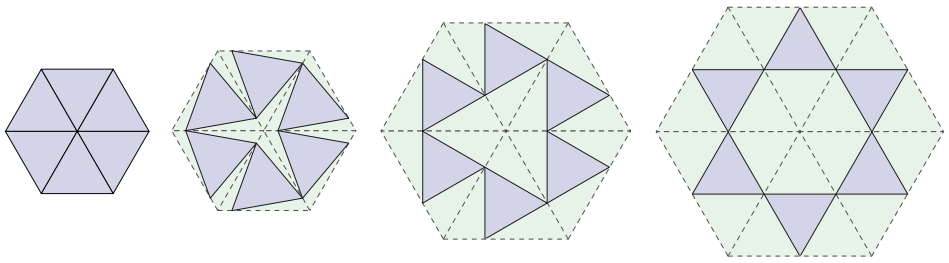

The rotation of a single linkage triangle can be computed from the difference between the area of a linkage triangle and a lifted tiling triangle.

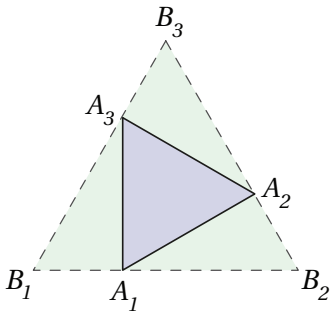

Let $a = A_1A_2 = A_2A_3 = A_3A_1$ and $b = B_1B_2 = B_2B_3 = B_3B_1$. Let $x = B_1A_1 = B_2A_2 = B_3A_3$. The area of the linkage triangle is then

$$\text{Area}(\triangle A_1A_2A_3) = \frac{a^2\sqrt{3}}{4}.$$

The area of the lifted tiling triangle is

$$\begin{aligned}\text{Area}(\triangle B_1B_2B_3) &= \frac{b^2\sqrt{3}}{4} \\ &= \text{Area}(\triangle A_1A_2A_3) + \text{Area}(\triangle A_1B_2A_2) + \text{Area}(\triangle A_2B_3A_3) + \text{Area}(\triangle A_3B_1A_1).\end{aligned}$$

Since

$$\text{Area}(\triangle A_1B_2A_2) = \text{Area}(\triangle A_2B_3A_3) = \text{Area}(\triangle A_3B_1A_1) = \frac{x(b-x)\sqrt{3}}{4},$$

finally we have

$$x = \frac{b-\sqrt{\frac{3}{4}a^2-\frac{1}{3}b^2}}{2}.$$

We use the length x to initialize the location of each linkage triangle inside the lifted tiling grid.

C Code for Non-penetration Constraint

Our numerical solver extends the open source implementation available at www.shapeop.org with the projection operator for the non-penetration constraint

$$P_{\text{collision}}([\mathbf{v}_1,\mathbf{v}_2,\mathbf{v}_3]) = \begin{cases} [\mathbf{v}_1,\mathbf{v}_2,\mathbf{v}_3] & \text{if } (\mathbf{v}_1\times\mathbf{v}_2)\cdot(\mathbf{v}_2\times\mathbf{v}_3)\geq 0 \\ [\mathbf{v}_1,\mathbf{h}(\mathbf{h}\cdot\mathbf{v}_2),\mathbf{h}(\mathbf{h}\cdot\mathbf{v}_3)] & \text{otherwise} \end{cases},$$

where

$$\mathbf{v}_1 = \mathbf{x}_{i_1} - \mathbf{x}_{i_0}, \quad \mathbf{v}_2 = \mathbf{x}_{i_2} - \mathbf{x}_{i_0}, \quad \mathbf{v}_3 = \mathbf{x}_{i_3} - \mathbf{x}_{i_0},$$

and $\mathbf{h}$ is the left singular vector of matrix $[\mathbf{v}_2,\mathbf{v}_3] \in \mathbb{R}^{3\times 2}$ for the largest singular value. Below is the code of our C++ implementation.

```
void NonPenetrationConstraint::project(
  const Matrix3X &positions, Matrix3X &projections
  ) const
{
  // Vertex indices
  int i0 = idI_[0], i1 = idI_[1],
      i2 = idI_[2], i3 = idI_[0];

  // Compute vectors v1, v2, v3
  Vector3 v1 = positions.col(i1) - positions.col(i0),
    v2 = positions.col(i2) - positions.col(i0),
    v3 = positions.col(i3) - positions.col(i0);

  // Compute the projections
  Vector3 proj1, proj2, proj3;
```

```
  // Verify the constraint
  if(v1.cross(v2).dot(v2.cross(v3)) < 0)
  {
    // Perform SVD to compute vector h
    Matrix32 M;
    M.col(0) = v2;  M.col(1) = v3;
    JacobiSVD<Matrix32> jsvd(M,  ComputeFullU);
    Vector3 h = jsvd.matrixU().col(0);

    proj1 = v1;
    proj2 = h * h.dot(v2);
    proj3 = h * h.dot(v3);
  }
  else
  {
    proj1 = v1;   proj2 = v2;   proj3 = v3;
  }

  // Output the projection
  projections.col(id0_) = proj1;
  projections.col(id0_ + 1) = proj2;
  projections.col(id0_ + 2) = proj3;
}
```

D Increasing Area Covered with Linkage

We can control the amount of surface area covered with the linkage by controlling the shape and size of the panels. If we use regular hexagonal panels the area increases from 25% up to 66.67%.

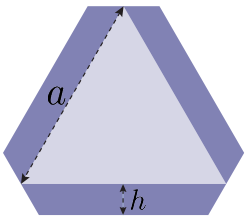

$$\text{Triangle Area} = \frac{a^2\sqrt{3}}{4}$$

$$\text{Hexagon Area} = \frac{a^2\sqrt{3}}{4} + \underbrace{3ah - h^2\sqrt{3}}_{\text{area increase}}$$

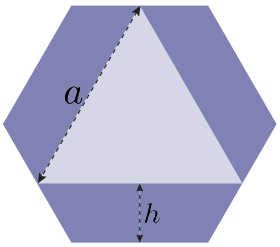

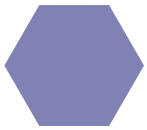

$$\text{for} \quad h = \frac{a\sqrt{3}}{6}$$

$$\text{Hexagon Area} = \frac{8}{3} \cdot \frac{a^2\sqrt{3}}{4}$$

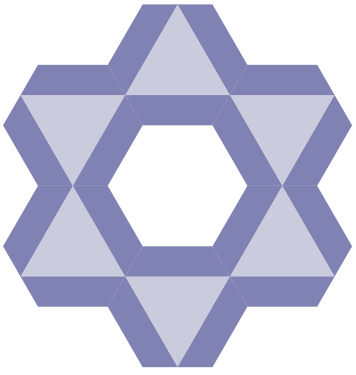

covers 66.67% of total surface area

covers 25% of total surface area

E Abstracts of Other Published Work

Here we include abstracts of publications that were not explicitly discussed in this thesis, but were produced during the same period.

- Julian Panetta, Mina Konaković-Luković, Florin Isvoranu, Etienne Bouleau, and Mark Pauly. X-Shells: A new class of deployable beam structures. *ACM Transactions on Graphics (Proceedings of SIGGRAPH), 2019*.

  Abstract. We present X-shells, a new class of deployable structures formed by an ensemble of elastically deforming beams coupled through rotational joints. An X-shell can be assembled conveniently in a flat configuration from standard elastic beam elements and then deployed through force actuation into the desired 3D target state. During deployment, the coupling imposed by the joints will force the beams to twist and buckle out of plane to maintain a state of static equilibrium. This complex interaction of discrete joints and continuously deforming beams allows interesting 3D forms to emerge. Simulating X-shells is challenging, however, due to unstable equilibria at the onset of beam buckling. We propose an optimization-based simulation framework building on a discrete rod model that robustly handles such difficult scenarios by analyzing and appropriately modifying the elastic energy Hessian. This real-time simulation method forms the basis of a computational design tool for X-shells that enables interactive design space exploration by varying and optimizing design parameters to achieve a specific design intent. We jointly optimize the assembly state and the deployed configuration to ensure the geometric and structural integrity of the deployable X-shell. Once a design is finalized, we also optimize for a sparse distribution of actuation forces to efficiently deploy it from its flat assembly state to its 3D target state. We demonstrate the effectiveness of our design approach with a number of design studies that highlight the richness of the X-shell design space, enabling new forms not possible with existing approaches. We validate our computational model with several physical prototypes that show excellent agreement with the optimized digital models.

- Christopher Robeller, Mina Konaković, Mira Dedijer, Mark Pauly, and Yves Weinand. Double-layered timber plate shell. *International Journal of Space Structures, 2017*.

  Abstract. This article presents a new lightweight construction system for doubly curved shells made from timber plates, inspired by the masonry vaults of Eladio Dieste. The system was developed for a specific case-study project, and general applications to other freeform surfaces are being discussed. The shells are built from two interconnected layers of structural wood veneer plates, using integral through-tenon joints for a fast, precise, and simple assembly. This allows for the construction of a series of differently shaped vaults without a costly mold or support structure. Instead, inclined joints cut with a 5-axis computer numerical controlled milling machine embed the correct location and angle between plates into the shape of the parts. This constrains the relative motions between joined parts to one assembly path. To take advantage of the benefits of such connectors, the constrained assembly paths must be considered in the fundamental design of the system, allowing for the insertion of each plate. This imposes additional constraints in the segmentation process of doubly curved shells. In order to meet the requirements and resolve the multi-constraint system, we use a global, nonlinear optimization approach. Developed as a close collaboration between architects, computer scientists and structural engineers, this article includes an experimental analysis of the influence of parametric modifications in the shape of connectors on their load-bearing performance.

- Christopher Robeller, Mina Konaković, Mira Dedijer, Mark Pauly, and Yves Weinand. A Double-layered Timber Plate Shell – Computational Methods for Assembly, Prefabrication and Structural Design. *Advances in Architectural Geometry, 2016*.

  Abstract. This paper presents a new lightweight construction system for doubly-curved shells, built from two interconnected layers of structural wood veneer plates. The system uses integral through-tenon joints for a fast, precise, and simple assembly, allowing for the construction of a series of differently shaped shells without a costly mould or support structure. Instead, inclined joints cut with a 5-axis CNC milling machine embed the correct location and angle between plates into the shape of the parts. This constrains the relative motions between joined parts to one assembly path.

  To take advantage of the benefits of such connectors, the constrained assembly paths must be considered in the fundamental design of the system, allowing for the insertion of each plate. This imposes additional constraints in the segmentation process of doubly-curved shells. In order to meet the requirements and resolve the multi-constraint system, we use a global, nonlinear optimization approach.

  Developed as a close collaboration between architects, computer scientists and structural engineers, the paper includes an experimental analysis of the influence of parametric modifications in the shape of connectors on their load-bearing performance.

Bibliography

Yonathan Aflalo, Ron Kimmel, and Michael Zibulevsky. Conformal mapping with as uniform as possible conformal factor. *SIAM Journal on Imaging Sciences*, 6(1):78–101, 2013. doi: 10.1137/110845860.

Marco Attene, Marco Livesu, Sylvain Lefebvre, Thomas Funkhouser, Szymon Rusinkiewicz, Stefano Ellero, Jonas Martinez, and Amit Haim Bermano. *Design, Representations, and Processing for Additive Manufacturing*, volume 10. Morgan & Claypool Publishers, June 2018. ISBN 1681733552, 9781681733555. URL https://hal.inria.fr/hal-01836525.

Thierry Aubin. *Some Nonlinear Problems in Riemannian Geometry*. Springer Monographs in Mathematics. Springer Berlin Heidelberg, 2013. ISBN 9783662130063. URL https://books.google.ch/books?id=iM7uCAAAQBAJ.

Changyeob Baek, Andrew O. Sageman-Furnas, Mohammad K. Jawed, and Pedro M. Reis. Form finding in elastic gridshells. *Proceedings of the National Academy of Sciences*, 2017. doi: 10.1073/pnas.1713841115.

Martin Z. Bazant and Darren Crowdy. Conformal Mapping Methods for Interfacial Dynamics. In *Handbook of Materials Modeling*, pages 1417–1451. Springer, Dordrecht, 2005. doi: 10.1007/978-1-4020-3286-8_71.

Mirela Ben-Chen and Craig Gotsman. Characterizing shape using conformal factors. In *Proceedings of the 1st Eurographics Conference on 3D Object Retrieval*, 3DOR '08, pages 1–8, 2008. ISBN 978-3-905674-05-7.

Mirela Ben-Chen, Craig Gotsman, and Guy Bunin. Conformal flattening by curvature prescription and metric scaling. *Computer Graphics Forum*, 27(2):449–458, 2008. ISSN 1467-8659. doi: 10.1111/j.1467-8659.2008.01142.x. URL http://dx.doi.org/10.1111/j.1467-8659.2008.01142.x.

Amit H. Bermano, Thomas Funkhouser, and Szymon Rusinkiewicz. State of the art in methods and representations for fabrication-aware design. *Comput. Graph. Forum*, 36(2):509–535, May 2017. ISSN 0167-7055. URL https://doi.org/10.1111/cgf.13146.

Bernd Bickel, Moritz Bächer, Miguel A. Otaduy, Hyunho Richard Lee, Hanspeter Pfister, Markus Gross, and Wojciech Matusik. Design and fabrication of materials with desired deformation behavior. *ACM Trans. Graph.*, 29(4):63:1–63:10, July 2010. ISSN 0730-0301.

Bernd Bickel, Paolo Cignoni, Luigi Malomo, and Nico Pietroni. State of the Art on Stylized Fabrication. *Computer Graphics Forum*, 2018. ISSN 1467-8659. doi: 10.1111/cgf.13327.

Sofien Bouaziz, Mario Deuss, Yuliy Schwartzburg, Thibaut Weise, and Mark Pauly. Shape-up: Shaping discrete geometry with projections. *Comput. Graph. Forum*, 31(5):1657–1667, 2012.

Sofien Bouaziz, Sebastian Martin, Tiantian Liu, Ladislav Kavan, and Mark Pauly. Projective dynamics: Fusing constraint projections for fast simulation. *ACM Trans. Graph.*, 33(4): 154:1–154:11, July 2014. ISSN 0730-0301.

Luca Caneparo. *Digital Fabrication in Architecture, Engineering and Construction*. Springer Publishing Company, Incorporated, 1st edition, 2016. ISBN 9401779937, 9789401779937.

Paolo Celli, Connor McMahan, Brian Ramirez, Anton Bauhofer, Christina Naify, Douglas Hofmann, Basile Audoly, and Chiara Daraio. Shape-morphing architected sheets with non-periodic cut patterns. *Soft Matter*, 14:9744–9749, 2018. doi: 10.1039/C8SM02082E. URL http://dx.doi.org/10.1039/C8SM02082E.

Isaac Chao, Ulrich Pinkall, Patrick Sanan, and Peter Schröder. A simple geometric model for elastic deformations. *ACM Trans. Graph.*, 29(4):38:1–38:6, July 2010. ISSN 0730-0301.

Tian Chen, Jochen Mueller, and Kristina Shea. Integrated design and simulation of tunable, multi-state structures fabricated monolithically with multi-material 3d printing. *Scientific Reports*, 7:45671 EP –, 03 2017. URL https://doi.org/10.1038/srep45671.

Xiang Chen, Changxi Zheng, Weiwei Xu, and Kun Zhou. An asymptotic numerical method for inverse elastic shape design. *ACM Trans. Graph.*, 33(4):95:1–95:11, July 2014. ISSN 0730-0301.

Yigil Cho, Joong-Ho Shin, Avelino Costa, Tae Ann Kim, Valentin Kunin, Ju Li, Su Yeon Lee, Shu Yang, Heung Nam Han, In-Suk Choi, and David J. Srolovitz. Engineering the shape and structure of materials by fractal cut. *Proceedings of the National Academy of Sciences*, 111 (49):17390–17395, 2014. doi: 10.1073/pnas.1417276111. URL http://www.pnas.org/content/111/49/17390.

Paolo Cignoni, Nico Pietroni, Luigi Malomo, and Roberto Scopigno. Field-aligned mesh joinery. *ACM Trans. Graph.*, 33(1):11:1–11:12, February 2014. ISSN 0730-0301. doi: 10.1145/2537852. URL http://doi.acm.org/10.1145/2537852.

Fionnuala Connolly, Conor J. Walsh, and Katia Bertoldi. Automatic design of fiber-reinforced soft actuators for trajectory matching. *Proceedings of the National Academy of Sciences*, 114 (1):51–56, 2017.

Corentin Coulais, Eial Teomy, Koen de Reus, Yair Shokef, and Martin van Hecke. Combinatorial design of textured mechanical metamaterials. *Nature*, 535:529 EP –, 07 2016. URL https://doi.org/10.1038/nature18960.

Keenan Crane, Ulrich Pinkall, and Peter Schröder. Spin transformations of discrete surfaces. *ACM Trans. Graph.*, 30(4):104:1–104:10, July 2011. doi: 10.1145/2010324.1964999. URL http://doi.acm.org/10.1145/2010324.1964999.

Keenan Crane, Ulrich Pinkall, and Peter Schröder. Robust fairing via conformal curvature flow. *ACM Trans. Graph.*, 32(4):61:1–61:10, July 2013. ISSN 0730-0301. doi: 10.1145/2461912.2461986. URL http://doi.acm.org/10.1145/2461912.2461986.

Bailin Deng, Sofien Bouaziz, Mario Deuss, Alexandre Kaspar, Yuliy Schwartzburg, and Mark Pauly. Interactive design exploration for constrained meshes. *Computer-Aided Design*, 61: 13–23, 2015.

Mathieu Desbrun, Mark Meyer, Peter Schröder, and Alan H. Barr. Implicit fairing of irregular meshes using diffusion and curvature flow. In *Proceedings of the 26th Annual Conference on Computer Graphics and Interactive Techniques*, SIGGRAPH '99, pages 317–324, New York, NY, USA, 1999. ACM Press/Addison-Wesley Publishing Co. ISBN 0-201-48560-5.

Mathieu Desbrun, Mark Meyer, and Pierre Alliez. Intrinsic parameterizations of surface meshes. *Computer Graphics Forum*, 21(3):209–218, 2002. ISSN 1467-8659. doi: 10.1111/1467-8659.00580. URL http://dx.doi.org/10.1111/1467-8659.00580.

Mario Deuss, AndersHolden Deleuran, Sofien Bouaziz, Bailin Deng, Daniel Piker, and Mark Pauly. ShapeOp – a robust and extensible geometric modelling paradigm. In *Modelling Behaviour*, pages 505–515. Springer International Publishing, 2015. URL http://dx.doi.org/10.1007/978-3-319-24208-8_42.

Günay Doğan and Ricardo H. Nochetto. First variation of the general curvature-dependent surface energy. *ESAIM: Mathematical Modelling and Numerical Analysis*, 46(1):59–79, 2012.

Lionel Du Peloux. *Modeling of bending-torsion couplings in active-bending structures. Application to the design of elastic gridshells.* PhD thesis, Université Paris Est, École des Ponts Paris Tech, 2017.

Levi H. Dudte, Etienne Vouga, Tomohiro Tachi, and L. Mahadevan. Programming curvature using origami tessellations. *Nature Materials*, 15(5):583–588, 2016.

K E. Evans and Andrew Alderson. Auxetic materials: Functional materials and structures from lateral thinking! *Advanced Materials - ADVAN MATER*, 12:617–628, 05 2000. doi: 10.1002/(SICI)1521-4095(200005)12:93.0.CO;2-3.

J. Eells and J.C. Wood. Restrictions on harmonic maps of surfaces. *Topology*, 15(3):263 – 266, 1976. ISSN 0040-9383. doi: https://doi.org/10.1016/0040-9383(76)90042-2. URL http://www.sciencedirect.com/science/article/pii/0040938376900422.

Soya Eguchi, Ryoma Takamori, Ryohei Yuasa, and Hiroya Tanaka. Morphing design for socially interactive autonomous car by multi-material 3d-printing. In *Extended Abstracts of the 2019 CHI Conference on Human Factors in Computing Systems*, CHI EA '19, pages LBW1310:1–LBW1310:6, New York, NY, USA, 2019. ACM. ISBN 978-1-4503-5971-9. doi: 10.1145/3290607.3312939. URL http://doi.acm.org/10.1145/3290607.3312939.

Timothy G. Feeman. *Portraits of the Earth: A Mathematician Looks at Maps.* American Mathematical Society, 2002.

Santiago Fernández. Structural design in the work of gaudí. *Architectural Science Review*, 49:324–339, 12 2006. doi: 10.3763/asre.2006.4943.

Jan Friedrich, Sven Pfeiffer, and Christoph Gengnagel. Locally varied auxetic structures for doubly-curved shapes. In Klaas De Rycke, Christoph Gengnagel, Olivier Baverel, Jane Burry, Caitlin Mueller, Minh Man Nguyen, Philippe Rahm, and Mette Ramsgaard Thomsen,

editors, *Humanizing Digital Reality: Design Modelling Symposium Paris 2017*, pages 323–336. Springer Singapore, Singapore, 2018. ISBN 978-981-10-6611-5.

C.J. Gantes. *Deployable Structures: Analysis and Design*. High performance structures and materials. WIT Press, 2001. ISBN 9781853126604. URL https://books.google.ch/books?id=Har0nQEACAAJ.

Akash Garg, Andrew O. Sageman-Furnas, Bailin Deng, Yonghao Yue, Eitan Grinspun, Mark Pauly, and Max Wardetzky. Wire mesh design. *ACM Trans. Graph.*, 33(4):66:1–66:12, July 2014. ISSN 0730-0301.

Ruben Gatt, Luke Mizzi, Joseph I Azzopardi, Keith M Azzopardi, Daphne Attard, Aaron Casha, Joseph Briffa, and Joseph N Grima. Hierarchical auxetic mechanical metamaterials. *Scientific Reports*, 5, 2015.

Mohammad Ghomi. Open problems in geometry of curves and surfaces. http://people.math.gatech.edu/~ghomi/Papers/op.pdf, October 2017. Accessed: 2017-12-12.

Ian Gibson, David Rosen, and Brent Stucker. *Additive Manufacturing Technologies: 3D Printing, Rapid Prototyping, and Direct Digital Manufacturing*. Springer, 2nd edition, 2015.

Xianfeng Gu and Shing-Tung Yau. Global conformal surface parameterization. In *Proceedings of the 2003 Eurographics/ACM SIGGRAPH Symposium on Geometry Processing*, SGP '03, pages 127–137, Aire-la-Ville, Switzerland, Switzerland, 2003. Eurographics Association. ISBN 1-58113-687-0. URL http://dl.acm.org/citation.cfm?id=882370.882388.

Xianfeng David Gu and Shing-Tung Yau. *Computational conformal geometry*. International Press of Boston, Inc., 2008.

Ren Guo. Local rigidity of inversive distance circle packing. *Transactions of the American Mathematical Society*, 363(9):4757–4776, 2011.

Ruslan Guseinov, Eder Miguel, and Bernd Bickel. Curveups: Shaping objects from flat plates with tension-actuated curvature. *ACM Trans. Graph.*, 36(4):64:1–64:12, July 2017. ISSN 0730-0301.

Philippe Hannequart, Michael Peigney, Jean-François Caron, Olivier Baverel, and Emmanuel

Viglino. The potential of shape memory alloys in deployable systems—a design and experimental approach. *Humanizing Digital Reality: Design Modelling Symposium Paris 2017*, pages 237–246, 2018.

Kristian Hildebrand, Bernd Bickel, and Marc Alexa. crdbrd: Shape fabrication by sliding planar slices. *Computer Graphics Forum*, 31(2):583–592, 2012. ISSN 1467-8659. doi: 10.1111/j.1467-8659.2012.03037.x. URL http://dx.doi.org/10.1111/j.1467-8659.2012.03037.x.

Emmanuel Iarussi, Wilmot Li, and Adrien Bousseau. Wrapit: Computer-assisted crafting of wire wrapped jewelry. *ACM Trans. Graph.*, 34(6):221:1–221:8, October 2015. ISSN 0730-0301. doi: 10.1145/2816795.2818118. URL http://doi.acm.org/10.1145/2816795.2818118.

Yuki Igarashi, Takeo Igarashi, and Jun Mitani. Beady: Interactive beadwork design and construction. *ACM Trans. Graph.*, 31(4):49:1–49:9, July 2012. ISSN 0730-0301. doi: 10.1145/2185520.2185545. URL http://doi.acm.org/10.1145/2185520.2185545.

Alexandra Ion, Johannes Frohnhofen, Ludwig Wall, Robert Kovacs, Mirela Alistar, Jack Lindsay, Pedro Lopes, Hsiang-Ting Chen, and Patrick Baudisch. Metamaterial mechanisms. In *Proceedings of the 29th Annual Symposium on User Interface Software and Technology*, UIST '16, pages 529–539, New York, NY, USA, 2016. ACM. ISBN 978-1-4503-4189-9. doi: 10.1145/2984511.2984540. URL http://doi.acm.org/10.1145/2984511.2984540.

Caigui Jiang, Chengcheng Tang, Amir Vaxman, Peter Wonka, and Helmut Pottmann. Polyhedral patterns. *ACM Trans. Graph.*, 34(6):172:1–172:12, October 2015. ISSN 0730-0301. doi: 10.1145/2816795.2818077. URL http://doi.acm.org/10.1145/2816795.2818077.

Liliya Kharevych, Boris Springborn, and Peter Schröder. Discrete conformal mappings via circle patterns. *ACM Trans. Graph.*, 25(2):412–438, April 2006. ISSN 0730-0301. doi: 10.1145/1138450.1138461. URL http://doi.acm.org/10.1145/1138450.1138461.

Martin Kilian, Simon Flöry, Zhonggui Chen, Niloy J. Mitra, Alla Sheffer, and Helmut Pottmann. Curved folding. *ACM Trans. Graph.*, 27(3):75:1–75:9, August 2008. ISSN 0730-0301. doi: 10.1145/1360612.1360674. URL http://doi.acm.org/10.1145/1360612.1360674.

Martin Kilian, Aron Monszpart, and Niloy J. Mitra. String actuated curved folded surfaces. *ACM Trans. Graph.*, 36(4), May 2017. ISSN 0730-0301. doi: 10.1145/3072959.3015460. URL http://doi.acm.org/10.1145/3072959.3015460.

Jungwook Kim, James A. Hanna, Myunghwan Byun, Christian D. Santangelo, and Ryan C. Hayward. Designing responsive buckled surfaces by halftone gel lithography. *Science*, 335 (6073):1201–1205, March 2012. ISSN 1095-9203. doi: 10.1126/science.1215309.

Sun-Jeong Kim, Soo-Kyun Kim, and Chang-Hun Kim. Discrete differential error metric for surface simplification. In *10th Pacific Conference on Computer Graphics and Applications, 2002. Proceedings.*, pages 276–283, 2002.

Mina Konaković, Keenan Crane, Bailin Deng, Sofien Bouaziz, Daniel Piker, and Mark Pauly. Beyond developable: Computational design and fabrication with auxetic materials. *ACM Trans. Graph.*, 35(4):89:1–89:11, July 2016. ISSN 0730-0301.

Mina Konaković-Luković, Pavle Konaković, and Mark Pauly. Computational design of deployable auxetic shells. In *Advances in Architectural Geometry 2018*, pages 94–111. Klein Publishing GMBH, 2018a. ISBN 978-3-903015-13-5.

Mina Konaković-Luković, Julian Panetta, Keenan Crane, and Mark Pauly. Rapid deployment of curved surfaces via programmable auxetics. *ACM Trans. Graph.*, 37(4):106:1–106:13, July 2018b. ISSN 0730-0301. doi: 10.1145/3197517.3201373. URL http://doi.acm.org/10.1145/3197517.3201373.

W. Y. Lam. Minimal surfaces from infinitesimal deformations of circle packings. *ArXiv e-prints*, December 2017.

Bruno Lévy, Sylvain Petitjean, Nicolas Ray, and Jérome Maillot. Least squares conformal maps for automatic texture atlas generation. *ACM Trans. Graph.*, 21(3):362–371, July 2002. ISSN 0730-0301. doi: 10.1145/566654.566590. URL http://doi.acm.org/10.1145/566654.566590.

Hao Li, Bart Adams, Leonidas J. Guibas, and Mark Pauly. Robust single-view geometry and motion reconstruction. *ACM Trans. Graph.*, 28(5):175:1–175:10, December 2009. ISSN 0730-0301. doi: 10.1145/1618452.1618521. URL http://doi.acm.org/10.1145/1618452.1618521.

Siming Li, Wei Zeng, Dengpan Zhou, Xianfeng David Gu, and Jie Gao. Compact conformal map for greedy routing in wireless mobile sensor networks. In *INFOCOM*, pages 2409–2417. IEEE, 2013.

Julian Lienhard. *Bending-Active Structures: Form-finding Strategies Using Elastic Deformation in Static and Kinetic Systems and the Structural Potentials Therein.* Forschungsberichte aus

dem Institut für Tragkonstruktionen und konstruktives Entwerfen der Universität Stuttgart. Universität Stuttgart Inst. f. Tragkonstr., 2014. ISBN 9783922302360.

Yaron Lipman. Bounded distortion mapping spaces for triangular meshes. *ACM Trans. Graph.*, 31(4):108:1–108:13, July 2012.

Yaron Lipman and Thomas Funkhouser. Möbius voting for surface correspondence. *ACM Trans. Graph.*, 28(3):72:1–72:12, July 2009. ISSN 0730-0301.

Yang Liu, Helmut Pottmann, Johannes Wallner, Yong-Liang Yang, and Wenping Wang. Geometric modeling with conical meshes and developable surfaces. *ACM Trans. Graph.*, 25(3):681–689, July 2006. ISSN 0730-0301. doi: 10.1145/1141911.1141941. URL http://doi.acm.org/10.1145/1141911.1141941.

Ying Liu, Brandi Shaw, Michael D. Dickey, and Jan Genzer. Sequential self-folding of polymer sheets. *Science Advances*, 3(3), 2017.

Alessandro Liuti, Alberto Pugnale, and Sofia Colabella. The airshell prototype: a timber gridshell erected through a pneumatic formwork. In *Proceedings of the IASS Annual Symposium 2017*, September 2017.

Sheng-Jie Luo, Yonghao Yue, Chun-Kai Huang, Yu-Huan Chung, Sei Imai, Tomoyuki Nishita, and Bing-Yu Chen. Legolization: Optimizing lego designs. *ACM Trans. Graph.*, 34(6): 222:1–222:12, October 2015. ISSN 0730-0301. doi: 10.1145/2816795.2818091. URL http://doi.acm.org/10.1145/2816795.2818091.

Li-Ke Ma, Yizhong Zhang, Yang Liu, Kun Zhou, and Xin Tong. Computational design and fabrication of soft pneumatic objects with desired deformations. *ACM Trans. Graph.*, 36(6): 239:1–239:12, November 2017. ISSN 0730-0301.

Roberto Naboni and Stefano Sortori Pezzi. Embedding auxetic properties in designing active-bending gridshells. *XX Congress of the Iberoamerican Society of Digital Graphics*, 2016.

Tuan Ngo, Alireza Kashani, Gabriele Imbalzano, Kate Nguyen, and David Hui. Additive manufacturing (3d printing): A review of materials, methods, applications and challenges. *Composites Part B Engineering*, 143, 02 2018. doi: 10.1016/j.compositesb.2018.02.012.

Ivan Niven. *Maxima and Minima Without Calculus*. Number v. 6 in Dolciani Mathematical Expositions. Mathematical Association of America, 1981. ISBN 9780883853061.

Jifei Ou, Mélina Skouras, Nikolaos Vlavianos, Felix Heibeck, Chin-Yi Cheng, Jannik Peters, and Hiroshi Ishii. aeromorph - heat-sealing inflatable shape-change materials for interaction design. In *Proceedings of the 29th Annual Symposium on User Interface Software and Technology*, UIST '16, pages 121–132, New York, NY, USA, 2016. ACM. ISBN 978-1-4503-4189-9.

Johannes Overvelde, Twan A De Jong, Yanina Shevchenko, Sergio A Becerra, George M Whitesides, James Weaver, Chuck Hoberman, and Katia Bertoldi. A three-dimensional actuated origami-inspired transformable metamaterial with multiple degrees of freedom. *Nature Communications*, 7, 03 2016. doi: 10.1038/ncomms10929.

Julian Panetta, Qingnan Zhou, Luigi Malomo, Nico Pietroni, Paolo Cignoni, and Denis Zorin. Elastic textures for additive fabrication. *ACM Trans. Graph.*, 34(4):135:1–135:12, July 2015. ISSN 0730-0301.

Julian Panetta, Mina Konaković-Luković, Florin Isvoranu, Etienne Bouleau, and Mark Pauly. X-shells: A new class of deployable beam structures. *ACM Trans. Graph.*, 38(4), July 2019.

Jesús Pérez, Bernhard Thomaszewski, Stelian Coros, Bernd Bickel, José A. Canabal, Robert Sumner, and Miguel A. Otaduy. Design and fabrication of flexible rod meshes. *ACM Trans. Graph.*, 34(4):138:1–138:12, July 2015. ISSN 0730-0301.

Jesús Pérez, Miguel A. Otaduy, and Bernhard Thomaszewski. Computational design and automated fabrication of kirchhoff-plateau surfaces. *ACM Trans. Graph.*, 36(4):62:1–62:12, July 2017. ISSN 0730-0301.

Helmut Pottmann, Michael Eigensatz, Amir Vaxman, and Johannes Wallner. Architectural geometry. *Comput. Graph.*, 47(C):145–164, April 2015. ISSN 0097-8493. doi: 10.1016/j.cag.2014.11.002. URL http://dx.doi.org/10.1016/j.cag.2014.11.002.

Gregory Charles Quinn and Christoph Gengnagel. A review of elastic grid shells, their erection methods and the potential use of pneumatic formwork. *Mob Rapidly Assem Struct IV*, 136: 129–143, 2014.

Michael Rabinovich, Tim Hoffmann, and Olga Sorkine-Hornung. Discrete geodesic nets for

modeling developable surfaces. *ACM Trans. Graph.*, 37(2):16:1–16:17, February 2018. ISSN 0730-0301. doi: 10.1145/3180494. URL http://doi.acm.org/10.1145/3180494.

Ahmad Rafsanjani and Damiano Pasini. Multistable compliant auxetic metamaterials inspired by geometric patterns in Islamic arts. APS March Meeting, 2016a.

Ahmad Rafsanjani and Damiano Pasini. Bistable auxetic mechanical metamaterials inspired by ancient geometric motifs. *Extreme Mechanics Letters*, 9:291 – 296, 2016b. ISSN 2352-4316.

Cong Rao, Lihao Tian, Dong-Ming Yan, Shenghui Liao, Oliver Deussen, and Lin Lu. Consistently fitting orthopedic casts. *Computer Aided Geometric Design*, 71:130 – 141, 2019. ISSN 0167-8396. doi: https://doi.org/10.1016/j.cagd.2019.04.018. URL http://www.sciencedirect.com/science/article/pii/S0167839619300342.

Dan Raviv, Wei Zhao, Carrie Lee McKnelly, Athina Papadopoulou, Achuta Kadambi, Boxin Shi, Shai Hirsch, Daniel Dikovsky, Michael Zyracki, Carlos Olguin, Ramesh Raskar, and Skylar Tibbits. Active printed materials for complex self- evolving deformations. *Scientific reports*, 4:7422, 12 2014. doi: 10.1038/srep07422.

Ronald D. Resch. The topological design of sculptural and architectural systems. In *Proceedings of the June 4-8, 1973, National Computer Conference and Exposition*, AFIPS '73, pages 643–650, New York, NY, USA, 1973. ACM. doi: 10.1145/1499586.1499744. URL http://doi.acm.org/10.1145/1499586.1499744.

Christopher Robeller, Mina Konaković, Mira Dedijer, Mark Pauly, and Yves Weinand. A double-layered timber plate shell - computational methods for assembly, prefabrication and structural design. In *Advances in Architectural Geometry 2016*, pages 104–123. vdf Hochschulverlag AG, an der ETH Zurich, 2016.

Christopher Robeller, Mina Konaković, Mira Dedijer, Mark Pauly, and Yves Weinand. Double-layered timber plate shell. *International Journal of Space Structures*, 32(3-4):160–175, 2017. doi: 10.1177/0266351117742853. URL https://doi.org/10.1177/0266351117742853.

Thilo Röhrig, Stefan Sechelmann, Agata Kycia, and Moritz Fleischmann. Surface panelization using periodic conformal maps. In *Advances in Architectural Geometry 2014*, pages 199–214. Springer International Publishing, 2014. ISBN 978-3-319-11417-0. doi: 10.1007/978-3-319-11418-7_13. URL http://dx.doi.org/10.1007/978-3-319-11418-7_13.

Rohan Sawhney and Keenan Crane. Boundary first flattening. *ACM Trans. Graph.*, 37(1): 5:1–5:14, December 2017. ISSN 0730-0301.

Krishna Kumar Saxena, Raj Das, and Emilio P. Calius. Three decades of auxetics research - materials with negative poisson's ratio: A review. *Advanced Engineering Materials*, 18(11): 1847–1870, 2016. ISSN 1527-2648.

Alexander Schiftner, Mathias Höbinger, Johannes Wallner, and Helmut Pottmann. Packing circles and spheres on surfaces. *ACM Trans. Graph.*, 28(5):139:1–139:8, December 2009a. ISSN 0730-0301.

Alexander Schiftner, Mathias Höbinger, Johannes Wallner, and Helmut Pottmann. Packing circles and spheres on surfaces. *ACM Trans. Graph.*, 28(5):139:1–139:8, December 2009b. ISSN 0730-0301. doi: 10.1145/1618452.1618485. URL http://doi.acm.org/10.1145/1618452.1618485.

Christian Schumacher, Bernd Bickel, Jan Rys, Steve Marschner, Chiara Daraio, and Markus Gross. Microstructures to control elasticity in 3d printing. *ACM Trans. Graph.*, 34(4):136:1–136:13, July 2015. ISSN 0730-0301.

Yuliy Schwartzburg and Mark Pauly. Fabrication-aware design with intersecting planar pieces. *Computer Graphics Forum*, 32(2):317–326, 2013. ISSN 1467-8659. doi: 10.1111/cgf.12051. URL http://dx.doi.org/10.1111/cgf.12051.

Mélina Skouras, Bernhard Thomaszewski, Bernd Bickel, and Markus Gross. Computational design of rubber balloons. *Comput. Graph. Forum*, 31(2pt4):835–844, May 2012. ISSN 0167-7055.

Mélina Skouras, Bernhard Thomaszewski, Peter Kaufmann, Akash Garg, Bernd Bickel, Eitan Grinspun, and Markus Gross. Designing inflatable structures. *ACM Trans. Graph.*, 33(4): 63:1–63:10, July 2014. ISSN 0730-0301.

Yousuf Soliman, Dejan Slepčev, and Keenan Crane. Optimal cone singularities for conformal flattening. *ACM Trans. Graph.*, 37(4):105:1–105:17, July 2018. ISSN 0730-0301. doi: 10.1145/3197517.3201367. URL http://doi.acm.org/10.1145/3197517.3201367.

Justin Solomon, Etienne Vouga, Max Wardetzky, and Eitan Grinspun. Flexible developable surfaces. *Comput. Graph. Forum*, 31(5):1567–1576, August 2012. ISSN 0167-7055. doi: 10.

1111/j.1467-8659.2012.03162.x. URL http://dx.doi.org/10.1111/j.1467-8659.2012.03162.x.

Peng Song, Chi-Wing Fu, Prashant Goswami, Jianmin Zheng, Niloy J. Mitra, and Daniel Cohen-Or. Reciprocal frame structures made easy. *ACM Trans. Graph.*, 32(4):94:1–94:13, July 2013. ISSN 0730-0301. doi: 10.1145/2461912.2461915. URL http://doi.acm.org/10.1145/2461912.2461915.

Olga Sorkine and Marc Alexa. As-rigid-as-possible surface modeling. In *Proceedings of the Fifth Eurographics Symposium on Geometry Processing*, SGP '07, pages 109–116. Eurographics Association, 2007. ISBN 978-3-905673-46-3.

Boris Springborn, Peter Schröder, and Ulrich Pinkall. Conformal equivalence of triangle meshes. *ACM Trans. Graph.*, 27(3):77:1–77:11, August 2008. ISSN 0730-0301.

Oded Stein, Eitan Grinspun, and Keenan Crane. Developability of triangle meshes. *ACM Trans. Graph.*, 37(4):77:1–77:14, July 2018. ISSN 0730-0301. doi: 10.1145/3197517.3201303. URL http://doi.acm.org/10.1145/3197517.3201303.

Kenneth Stephenson. Circle packing: a mathematical tale. *Notices of the AMS*, 50(11):1376–1388, 2003.

John M. Sullivan. Conformal tiling on a torus. In Reza Sarhangi and Carlo H. Séquin, editors, *Proceedings of Bridges 2011: Mathematics, Music, Art, Architecture, Culture*, pages 593–596. Tessellations Publishing, 2011. ISBN 978-0-9846042-6-5.

Tomohiro Tachi. Origamizing polyhedral surfaces. *IEEE Trans. Vis. Comput. Graph.*, 16(2): 298–311, 2010. URL http://dblp.uni-trier.de/db/journals/tvcg/tvcg16.html#Tachi10.

Tomohiro Tachi. Composite rigid-foldable curved origami structure. In *Proceedings of Transformables*, 2013a.

Tomohiro Tachi. Freeform origami tessellations by generalizing Resch's patterns. *Journal of Mechanical Design*, 135(11), 2013b. ISSN 1050-0472. URL http://www.researchgate.net/publication/267644436_Freeform_Origami_Tessellations_by_Generalizing_Reschs_Patterns.

Chengcheng Tang, Pengbo Bo, Johannes Wallner, and Helmut Pottmann. Interactive design of

developable surfaces. *ACM Trans. Graph.*, 35(2):12:1–12:12, January 2016. ISSN 0730-0301. doi: 10.1145/2832906. URL http://doi.acm.org/10.1145/2832906.

Yunlong Tang and Yaoyao Zhao. A survey of the design methods for additive manufacturing to improve functional performance. *Rapid Prototyping Journal*, 22:569–590, 01 2016. doi: 10.1108/RPJ-01-2015-0011.

Romain Testuz, Yuliy Schwartzburg, and Mark Pauly. Automatic Generation of Constructable Brick Sculptures. In M.-A. Otaduy and O. Sorkine, editors, *Eurographics 2013 - Short Papers*. The Eurographics Association, 2013. doi: 10.2312/conf/EG2013/short/081-084.

Hideshi Tomita, Takashi Higaki, Toshiki Kobayashi, Takanari Fujii, and Kazuto Fujimoto. Stenting for curved lesions using a novel curved balloon: Preliminary experimental study. *Journal of Cardiology*, 66(2):120 – 124, August 2015. ISSN 0914-5087.

Shinji Umeyama. Least-squares estimation of transformation parameters between two point patterns. *IEEE Trans. Pattern Anal. Mach. Intell.*, 13(4):376–380, 1991.

Nicolas Vachicouras, Christina M. Tringides, Philippe B. Campiche, and Stéphanie P. Lacour. Engineering reversible elasticity in ductile and brittle thin films supported by a plastic foil. *Extreme Mechanics Letters*, 15:63 – 69, 2017. ISSN 2352-4316.

Amir Vaxman, Christian Müller, and Ofir Weber. Conformal mesh deformations with Möbius transformations. *ACM Trans. Graph.*, 34(4):55:1–55:11, July 2015. ISSN 0730-0301. doi: 10.1145/2766915. URL http://doi.acm.org/10.1145/2766915.

Amir Vaxman, Christian Müller, and Ofir Weber. Regular meshes from polygonal patterns. *ACM Trans. Graph.*, 36(4):113:1–113:15, July 2017. ISSN 0730-0301. doi: 10.1145/3072959.3073593. URL http://doi.acm.org/10.1145/3072959.3073593.

Marius Wagner, Tian Chen, and Kristina Shea. Large shape transforming 4d auxetic structures. *3D Printing and Additive Manufacturing*, 4(3):133–142, 2017. doi: 10.1089/3dp.2017.0027. URL https://doi.org/10.1089/3dp.2017.0027.

Ofir Weber, Ashish Myles, and Denis Zorin. Computing extremal quasiconformal maps. *Comput. Graph. Forum*, 31(5):1679–1689, August 2012. ISSN 0167-7055. doi: 10.1111/j.1467-8659.2012.03173.x. URL http://dx.doi.org/10.1111/j.1467-8659.2012.03173.x.

Changxi Zheng, Timothy Sun, and Xiang Chen. Deployable 3d linkages with collision avoidance. In *Proceedings of the ACM SIGGRAPH/Eurographics Symposium on Computer Animation*, SCA '16, pages 179–188, Aire-la-Ville, Switzerland, Switzerland, 2016. Eurographics Association. ISBN 978-3-905674-61-3.

Bo Zhu, Mélina Skouras, Desai Chen, and Wojciech Matusik. Two-scale topology optimization with microstructures. *ACM Trans. Graph.*, 36(4), July 2017. ISSN 0730-0301. doi: 10.1145/3072959.3095815. URL http://doi.acm.org/10.1145/3072959.3095815.

Henrik Zimmer and Leif Kobbelt. Zometool rationalization of freeform surfaces. *Visualization and Computer Graphics, IEEE Transactions on*, 20(10):1461–1473, Oct 2014. ISSN 1077-2626. doi: 10.1109/TVCG.2014.2307885.

Mina Konaković Luković

EPFL IC BC 349 Station 14, 1015 Lausanne, Switzerland
+41 21 69 36865 | mina.konakovic.lukovic@gmail.com | https://lgg.epfl.ch/∼mina

Education

- Sep 2014 - Jul 2019 — **Swiss Federal Institute of Technology Lausanne (EPFL), Switzerland**
  PhD in Computer Science
  Computer Graphics and Geometry Laboratory (LGG)
  PhD thesis: *Computational Design of Auxetic Shells*
  Advisor: *Prof. Dr. Mark Pauly*
- Sep 2013 - Aug 2014 — **Faculty of Mathematics, University of Belgrade, Serbia**
  MSc in Mathematics, module Computer Science and Informatics
  First Class Honor, GPA: **10.00/10.00**
  Master thesis: *Stochastic context free grammars and applications*
  Advisor: *Prof. Dr. Gordana Pavlović-Lažetić*
- Sep 2009 - Jul 2013 — **Faculty of Mathematics, University of Belgrade, Serbia**
  BSc in Mathematics, module Computer Science and Informatics
  First Class Honor, GPA: **10.00/10.00**
- Sep 2005 - Jun 2009 — **Mathematics High School, Belgrade, Serbia**
  Special track for gifted students
  GPA: 5.00/5.00

Publications

- J. Panneta, **M. Konaković-Luković**, F. Isvoranu, E. Bouleau, M. Pauly, *"X-Shells: A new class of deployable beam structures"*, ACM Transactions on Graphics (Proceedings of SIGGRAPH) 2019.
- **M. Konaković-Luković**, J. Panneta, K. Crane, M. Pauly, *"Rapid Deployment of Curved Surfaces via Programmable Auxetics"*, ACM Transactions on Graphics (Proceedings of SIGGRAPH) 2018.
- **M. Konaković-Luković**, P. Konaković, M. Pauly, *"Computational Design of Deployable Auxetic Shells"*, Advances in Architectural Geometry 2018.
- C. Robeller, **M. Konaković**, M. Dedijer, M. Pauly, Y. Weinand, *"Double-layered Timber Plate Shell"*, International Journal of Space Structures (Special Issue Advanced Geometry in Structures) 2017.
- C. Robeller, **M. Konaković**, M. Dedijer, M. Pauly, Y. Weinand, *"A Double-layered Timber Plate Shell - Computational Methods for Assembly, Prefabrication and Structural Design"*, Advances in Architectural Geometry 2016.
- **M. Konaković**, K. Crane, B. Deng, S. Bouaziz, D. Piker, M. Pauly, *"Beyond Developable: Computational Design and Fabrication with Auxetic Materials"*, ACM Transactions on Graphics (Proceedings of SIGGRAPH) 2016.

Patents

- **Method of encoding a 3D shape into a 2D surface.** US Patent Application No. 16/186,901

Professional Experience

- Jul 2018 - Oct 2018 **Research Intern, Adobe Research, Seattle, WA, USA**
  Mentor: *Dr. Danny Kaufman*
- Jun 2017 - Sep 2017 **Visiting Researcher, Carnegie Mellon University, PA, USA**
  Host: *Prof. Dr. Keenan Crane*
  Worked on topics in (Discrete) Differential Geometry
- Aug 2016 - Sep 2016 **Visiting Researcher, Carnegie Mellon University, PA, USA**
  Host: *Prof. Dr. Keenan Crane*
  Worked on topics in Conformal Geometry Processing
- Sep 2015 - Aug 2019 **Teaching Assistant, EPFL, Switzerland**
  CS-341 Introduction to Computer Graphics (Spring 2016, 2017, 2018)
  CS-446 Digital 3D Geometry Processing (Autumn 2016, 2017, 2018)
  MATH-111 Linear Algebra (Autumn 2015)
- Sep 2015 - Aug 2019 **Student Supervision (semester projects), EPFL, Switzerland**
  Didier Bieler (2019), Antoine Hoffmann (2018), Gaspard Zoss (2017), Malcom Malo Drougard (2017), Hao Sun (2016), Vincent de Marignac (2015)
- Aug 2015 - Aug 2018 **PhD Researcher, Swiss National Centre of Competence in Research Digital Fabrication (NCCR dfab), ETH, Switzerland**
  Project: Integral Mechanical Attachment for Timber Plate Structures
- Feb 2015 - Aug 2019 **Research Assistant, Computer Graphics and Geometry Laboratory (LGG), EPFL, Switzerland**
  Project: Geometry Optimization for Digital Fabrication and Architectural Design
- Review Services **SIGGRAPH 2019** - technical papers
  SIGGRAPH ASIA 2019 - technical papers
  Graphics Interface 2019 (program committee) - technical papers

Honors and Awards

- **Schmidt Science Fellowship** (In partnership with the Rhodes Trust)
  For the postdoctoral studies in 2019/20, awarded to 20 researchers worldwide across all areas of science
- **The Government of Serbia Fund for Young Talents scholarship**
  For the best students from Serbia studying abroad in 2015, 2016, 2017, 2018, 2019
- **EPFL EDIC Fellowship**
  For the first year of PhD studies in 2014/2015
- **Crown of Success award**
  For the best female student of the University of Belgrade, graduating in 2013
- **City of Belgrade scholarship**
  For the best students in the city of Belgrade in 2011, 2012, and 2013
- **Faculty of Mathematics excellence award**
  For outstanding academic performance and the best students in 2011, 2012, and 2013

Selected Talks and Workshops

- **Physics-based Modeling for Computational Fabrication and Robotics Course, May 2019, ETH, Zurich, Switzerland**
  Invited speaker
- **SIGGRAPH Doctoral Consortium, August 2018, Vancouver, Canada**
  Selected participant as 1 of 8 best graduating PhD students from the field of computer graphics
- **ACM SIGGRAPH, August 2018, Vancouver, Canada**
  Technical paper presenter
- **International Geometry Workshop, September 2017, Obergurgl, Austria**
  Invited participant
- **ACM Symposium on Computational Fabrication, June 2017, MIT, Boston, USA**
  Selected presenter
- **SIGCHI Summer School: Computational Fabrication and Smart Matter, June 2017, MIT, Boston, USA**
  Selected participant
- **ACM SIGGRAPH, July 2016, Anaheim, USA**
  Technical paper presenter

Selected Press Coverage

- **WIRED**: A Freaky Anti-Rubber Is Still Weirding Scientists Out
- **The Weather Channel**: Most Contrary Material on Planet?
- **TechChurch**: New technique lets you fold flat metal or plastic into a 3D shape
- **Business Standard**: New method to create everyday objects in a 3D shape
- **EPFL**: Creating 3D objects from inextensible sheet materials
- **CMU**: Computational design tool transforms flat materials into 3-D shapes
- **Phys.org**: Creating 3-D objects from inextensible sheet materials
- **The Times of India**: Researchers devise method to create everyday objects in a 3D shape
- **Design Engineering**: New computational design tool turns flat sheets into complex 3D shapes
- **EUREKA**: Computational design tool transforms flat materials into 3D shapes
- **3ders.org**: New 3D design tool turns flat 2D sheets of metal or plastic into complex 3D shapes
- **Space Daily**: Computational design tool transforms flat materials into 3-D shapes
- **Swissinfo.ch**: Damenschuh im "Löcher-Look": Schlitze machen Blech beliebig formbar